

AD-A071 055

PRATT AND WHITNEY AIRCRAFT GROUP WEST PALM BEACH FL 0--ETC F/G 21/5
MARINE GAS TURBINE HOT CORROSION DEPENDENCE ON INGESTED SALT LE--ETC(U)
APR 79 R H BARKALOW, F S PETTIT
PWA-FR-11544 N00173-77-C-0206
NL

UNCLASSIFIED

1 OF 2
AD
A071055



ADA071055

LEVEL II

2
C

MARINE GAS TURBINE HOT CORROSION
DEPENDENCE ON INGESTED SALT LEVELS

DDC FILE COPY.



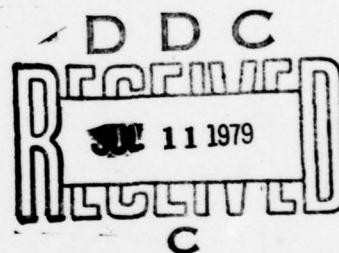
Report No. FR-11544

Contract N00173-77-C-0206

MARINE GAS TURBINE HOT CORROSION
DEPENDENCE ON INGESTED SALT LEVELS



R.H. Barkalow and F.S. Pettit
United Technologies Corporation
Pratt & Whitney Aircraft Group
Government Products Division
West Palm Beach, FL 33402



16 April 1979

Final Report: 29 July 1977 to 31 Oct 1978

Approved for public release; distribution unlimited

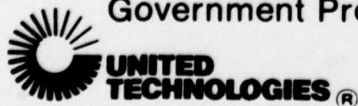
Prepared for:

Naval Research Laboratory
Washington, DC 20375

PRATT & WHITNEY AIRCRAFT GROUP

Government Products Division

P. O. Box 2691
West Palm Beach, Florida 33402



UNCLASSIFIED

SECURITY CLASSIFICATION OF THIS PAGE (When Data Entered)

REPORT DOCUMENTATION PAGE		READ INSTRUCTIONS BEFORE COMPLETING FORM
1. REPORT NUMBER	2. GOVT ACCESSION NO.	3. RECIPIENT'S CATALOG NUMBER
4. TITLE (and Subtitle) <u>MARINE GAS TURBINE HOT CORROSION DEPENDENCE ON INGESTED SALT LEVELS.</u>		5. TYPE OF REPORT & PERIOD COVERED Final Technical Report, 29 Jul. 1977 - 31 Oct 1978
7. AUTHOR(s) R. H. Barkalow and F. S. Pettit		6. PERFORMING ORG. REPORT NUMBER FR-11544
9. PERFORMING ORGANIZATION NAME AND ADDRESS United Technologies Corporation Pratt & Whitney Aircraft Group Government Products Division West Palm Beach, Florida 33402		8. CONTRACT OR GRANT NUMBER(s) N00173-77-C-0206/new
11. CONTROLLING OFFICE NAME AND ADDRESS Naval Research Laboratory Washington, DC 20375		10. PROGRAM ELEMENT, PROJECT, TASK AREA & WORK UNIT NUMBERS
14. MONITORING AGENCY NAME & ADDRESS (if different from Controlling Office) 12 110p		12. REPORT DATE 16 Apr 1979
		13. NUMBER OF PAGES 98
		15. SECURITY CLASS. (of this report) UNCLASSIFIED
		15a. DECLASSIFICATION/DOWNGRADING SCHEDULE
16. DISTRIBUTION STATEMENT (of this Report) Approved for public release; distribution unlimited		
17. DISTRIBUTION STATEMENT (of the abstract entered in Block 20, if different from Report)		
18. SUPPLEMENTARY NOTES		
19. KEY WORDS (Continue on reverse side if necessary and identify by block number) Hot Corrosion Sulfur Trioxide Salt Ingestion NaCl - SO ₃ Interactions Salt Deposition		
20. ABSTRACT (Continue on reverse side if necessary and identify by block number) Turbine section hardware in marine engines is susceptible to hot corrosion attack induced by salt deposition. In attempting to control this type of materials degradation, it is necessary to examine the dependence of hot corrosion on ingested salt level and to determine the deposition rate below which hot corrosion attack will be negligible. In this program, test specimens (uncoated and aluminized Mar-M509 and IN 792, CoCrAlY-coated IN 792) were exposed at 700 and 900°C in laboratory tube furnaces to conditions which induce		

UNCLASSIFIED

SECURITY CLASSIFICATION OF THIS PAGE(When Data Entered)

20. ABSTRACT (continued)

hot corrosion attack. The microstructures developed in these tests were compared with those observed in service hardware, using standard metallurgical analysis techniques (e.g. optical metallography, scanning electron microscopy, X-ray diffraction, electron probe microanalysis). A test at 700°C with a salt deposit of sodium sulfate, either pure or mixed with metallic sulfates, and a gaseous environment of oxygen with approximately 10^{-4} atm SO_3 was found to most closely duplicate the degradation microstructure most common in hardware from marine service. Burner rig tests at 700°C with SO_3 in the combustion gas were then performed on CoCrAlY-coated IN 792 at several salt deposition rates. Although decreased corrosion at low deposition rates was encountered, it was found that a deposition rate estimated to be approximately 0.01 mg/cm²/hr produced clearly discernable corrosion which cannot be considered negligible. Such results support the hypothesis that any condensed salt deposit is likely to produce unacceptable hot corrosion and hence the only safe ingestion level is that which produces no salt deposition on turbine hardware.

UNCLASSIFIED

PREFACE

This report covers the work performed under Contract N00173-77-C-0206 during the period 29 July 1977 to 31 October 1978.

The program was administered by the Government Products Division of Pratt & Whitney Aircraft Group, West Palm Beach, Florida; the experimental work was conducted by the Materials Engineering and Research Laboratory of the Commercial Products Division at Middletown, Connecticut.

The program was accomplished under the technical direction of Dr. R. L. Jones of the Chemistry Division, Code 6130, Naval Research Laboratory, Washington D.C. Dr. F. S. Pettit was the Program Manager at Pratt & Whitney.

The authors wish to acknowledge helpful discussions with Dr. G. W. Goward, Mr. J. A. Goebel, and Mr. C. S. Giggins. Technical assistance was provided by T. J. Radzavich, C. E. Londin, A. V. Karg, C. V. Prue, and S. Russo.

Accession For	
NTIS GRA&I	
DDC TAB	
Unannounced	
Justification	
By	
Distribution/	
Availability Codes	
Dist	Avail and/or special

MARINE GAS TURBINE HOT CORROSION
DEPENDENCE ON INGESTED SALT LEVELS

TABLE OF CONTENTS

	<u>Page</u>
I. INTRODUCTION AND PROGRAM PLAN	1
II. RESULTS AND DISCUSSION	6
1. EFFECT OF SO ₃ PRESSURE ON SULFATE-INDUCED HOT CORROSION	6
a. Equipment and Procedure	6
b. SO ₃ - Induced Attack at 704°C (1300°F)	7
c. SO ₃ - Induced Attack at 899°C (1650°F)	10
d. Temperature Effect at Constant SO ₃ Pressure	13
1) PWA 68 CoCrAlY Coating	13
2) Mar-M509	13
3) IN 792	13
e. Summary and Discussion of SO ₃ Effects	14
2. CHLORIDE EFFECTS AND CHLORIDE - SO ₃ INTERACTIONS	15
a. Objective and Approach	15
b. Condensed and Vaporous Chloride Effects	16
1) Effect of Chloride Vapor on Simple Oxidation	17
2) Sulfate-Induced Hot Corrosion in Clean Air	17
3) Effect of Chloride Vapor on Sulfate-Induced Corrosion .	17
4) Sulfate-Condensed Chloride Hot Corrosion	19
5) Effect of Chloride Vapor on Sulfate-Chloride Corrosion .	19
c. Chloride - SO ₃ Interactions	20
1) NaCl - SO ₃ Effects at 704°C	20
2) NaCl - SO ₃ Effects at 899°C	22

	<u>Page</u>
d. Summary and Discussion of Chloride Effects	22
e. Choice of Conditions for Mixed Sulfate Experiments	24
3. MIXED SULFATE EFFECTS AT 704°C	25
a. Introductory Remarks and Experimental Procedure	25
b. Test Results	26
1) Effect of CoSO_4 and ZnSO_4 on CoCrAlY	26
2) Salt - Cobalt Oxide Mixture	26
3) Na_2SO_4 - CoSO_4 on Ni-base Aluminide	26
4) Thick Deposit and Vapor Honing Effects	27
5) Na_2SO_4 and Mixed Sulfate Deposits on Alumina	27
c. Summary and Discussion of Mixed Sulfate Experiments	27
4. PRELIMINARY BURNER RIG TESTING	28
5. HOT CORROSION - SALT DEPOSITION DEPENDENCE TESTS	30
a. Ducted Burner Rig	30
b. Tube Furnace Test with Various Deposit Thicknesses	34
c. Summary and Discussion of Hot Corrosion-Salt Deposition ..	35
III. SUMMARY AND CONCLUSIONS	37
1. DEPENDENCE OF HOT CORROSION ATTACK ON SO_3 PRESSURE	37
2. CHLORIDE EFFECTS AND CHLORIDE- SO_3 INTERACTIONS	37
3. MIXED SULFATE EFFECTS AT 704°C	38
4. DUCTED BURNER RIG EXPERIMENTS	39
5. DEPENDENCE OF HOT CORROSION ON AMOUNT OF SALT	39
FIGURES	41 - 97
REFERENCES	98

LIST OF FIGURES

	<u>PAGE</u>
1. Flow diagram outlining experimental work performed on this program.	41
2. Schematic diagram of horizontal tube furnace for hot corrosion testing with SO_3 gas in the atmosphere.	42
3. Effect of SO_3 pressure on 704C sulfate-induced hot corrosion of CoCrAlY-coated IN 792, as shown by surface condition after 20 hours and weight change data for 100-hour cyclic exposure.	43
4. Effect of SO_3 pressure on 704C sulfate-induced hot corrosion of uncoated Mar-M509 (Co-23.4Cr-10.0Ni-0.2Ti-7.0W-3.5Ta-0.5Zr-0.6C).	44
5. Effect of SO_3 pressure on 704C sulfate-induced hot corrosion of aluminized (PWA 28) Mar-M509.	45
6. Effect of SO_3 pressure on 704C sulfate-induced hot corrosion of uncoated IN 792 (Ni-12.0Cr-9.0Co-4.5Ti-3.1Al-1.9Mo-3.8W-3.9Ta-0.12C-0.1Zr-0.02B)	46
7. Effect of SO_3 pressure on 704C sulfate-induced hot corrosion of aluminized (PWA 273) IN 792.	47
8. Effect of SO_3 pressure on 704C sulfate-induced hot corrosion of CoCrAlY and aluminide coatings, as shown by surface condition after 100-hour cyclic exposure.	48
9. Typical depth of attack and nodular morphology of corrosion front produced by cyclic exposure of PWA 68 CoCrAlY for 100 hours at 704C and $p_{\text{SO}_3} = 0.004$ atm.	49
10. Uncoated and aluminized alloys tested concurrently with the CoCrAlY coating of Fig. 9.	50
11. Typical depth of attack and nodular morphology of corrosion front produced by cyclic exposure of PWA 68 CoCrAlY for 100 hours at 704C and $p_{\text{SO}_3} = 0.0007$ atm.	51
12. Uncoated and aluminized alloys tested concurrently with the CoCrAlY coating of Fig. 11.	52
13. Typical microstructural degradation of PWA 68 CoCrAlY produced by cyclic hot corrosion testing for 100 hours at 704C and $p_{\text{SO}_3} = 0.0001$ atm.	53
14. Uncoated and aluminized alloys tested concurrently with the CoCrAlY coating of Fig. 13.	54

	<u>PAGE</u>
15. SEM photomicrographs and X-ray maps showing the structure and composition of the scale and scale/metal interface after 704C hot corrosion of PWA 68 CoCrAlY at $p_{SO_3} = 0.004$ atm.	55
16. Accumulation of Na_2SO_4 salt in developing protrusion, as shown by sodium and sulfur X-ray images of a dry polished specimen.	56
17. High magnification SEM photomicrographs of a portion of the developing protrusion illustrated in Fig. 16.	57
18. SEM photomicrographs and X-ray maps showing the structure and composition of the scale and scale/metal interface after 100 hours at 704C and $p_{SO_3} = 0.0001$ atm.	58
19. Time to penetration versus SO_3 pressure for PWA 68 CoCrAlY coating tested as described in text.	59
20. Surface condition of PWA 68 CoCrAlY coatings after 100 hours in 899C hot corrosion test at indicated SO_3 pressures.	60
21. Microstructures of PWA 68 CoCrAlY exposed 100 hours at 899C and $p_{SO_3} = 0.0001$ atm.	61
22. Back scattered electron photomicrographs of heavily corroded area in the CoCrAlY specimen of Fig. 21.	62
23. X-ray maps showing element distribution characteristic of SO_3 -induced hot corrosion of CoCrAlY coating at 899C.	63
24. Degradation and failure of PWA 273 aluminide coating by SO_3 -induced hot corrosion at 899C.	64
25. Uncoated and aluminized alloys exposed 100 hours at 899C and $p_{SO_3} = 0.0007$ atm.	65
26. Typical microstructures and depth of attack of uncoated and aluminized Mar-M509 exposed 100 hours at 899C and $p_{SO_3} = 0.0001$ atm.	66
27. Effect of SO_3 pressure on 899C hot corrosion of uncoated IN 792, as shown by depth of attack and weight change data for 100-hour exposure at 0.0007 and 0.0001 atm.	67
28. Effect of temperature on severity of attack of PWA 68 CoCrAlY coating at fixed SO_3 pressure of 0.0007 atm, as shown by surface condition after 20 hours and weight change data for 100-hour cyclic exposure.	68
29. Weight change data showing effect of temperature on severity of attack of uncoated and aluminized Mar-M509 at fixed SO_3 pressure of 0.0007 atm.	69

	<u>PAGE</u>
30. Effects of temperature and SO_3 pressure on severity of attack of uncoated IN 792, as shown by weight change data at fixed SO_3 pressure and relative magnitude of $\Delta M/A$ values at 0.0007 versus 0.0001 atm.	70
31. Typical degradation microstructures observed in CoCrAlY-coated turbine hardware from GTV Asiafreighter after approximately 4200 hours service.	71
32. Effect of chloride vapor on sulfate-induced hot corrosion of uncoated Mar-M509.	72
33. Effect of chloride vapor on sulfate-induced hot corrosion of uncoated IN 792.	73
34. Schematic diagram of horizontal tube furnace for hot corrosion testing with both SO_3 gas and NaCl vapor in the atmosphere.	74
35. Weight change data for uncoated Mar-M509 and aluminized IN 792 in SO_3 and $\text{SO}_3 + \text{NaCl}$ atmospheres.	75
36. Microstructure of PWA 68 CoCrAlY coating tested at 704C with simultaneous presence of gaseous SO_3 and NaCl vapor.	76
37. Sulfur-containing scale in area showing SO_3 -type morphology of attack front; variation in composition and morphology of scale, possibly indicating attack mechanism oscillating between SO_3 - and chloride-type corrosion.	77
38. Uncoated and aluminized alloys tested concurrently with the CoCrAlY coating of Figs. 36 and 37.	78
39. Typical microstructure, depth of attack, and element distribution of CoCrAlY coating exposed for 100 hours at 899C with $p_{\text{SO}_3} = 0.0007$ atm and 30 ppm NaCl vapor.	79
40. Uncoated and aluminized alloys tested concurrently with the CoCrAlY coating of Fig. 39.	80
41. Typical depth and microstructure of hot corrosion attack produced by 100-hour cyclic exposure of CoCrAlY at 704C with $p_{\text{SO}_3} = 0.0007$ atm and 30 ppm NaCl vapor.	81
42. Negligible microstructural degradation of CoCrAlY coating covered with a 2 mg/cm ² mixture of Na_2SO_4 and CoO and exposed for 100 hours concurrently with the specimens of Fig. 41.	82
43. Nodular attack of PWA 273 Ni-base aluminide coating produced by a salt deposit of $\text{Na}_2\text{SO}_4 - 50\text{m}\% \text{CoSO}_4$ and cyclic exposure for 100 hours at 704C, $p_{\text{SO}_3} = 0.0007$ atm, and 30 ppm NaCl vapor.	82

	<u>PAGE</u>
44. Surface condition and typical depth of attack of CoCrAlY coating produced by 5 mg/cm ² salt deposit exposed for 20 hours at 704C with P _{SO₃} = 0.0007 and 30 ppm NaCl vapor.	83
45. CoCrAlY specimen prepared by masking and vapor honing as described in text.	84
46. Deposits of 100% Na ₂ SO ₄ and Na ₂ SO ₄ - 50m%CoSO ₄ exposed 20 hours at 704C with P _{SO₃} = 0.0007 atm.	85
47. Schematic diagram of ducted burner rig and cylindrical test specimen used for hot corrosion - salt deposition rate dependence tests.	86
48. Nodular attack developed in preliminary burner rig test with ASTM sea salt and SO ₂ gas mixed with the primary air.	87
49. Salt deposit and oxide mounds on CoCrAlY specimen exposed 10.5 hours to Na ₂ SO ₄ - 50m%MgSO ₄ salt.	87
50. Depth and microstructure of pitting attack, as shown by sectioning through the sample of Fig. 49.	88
51. Weight change data showing effect of deposition rate on severity of attack of CoCrAlY coating and uncoated X-40 in 704C ducted rig hot corrosion test with ASTM sea salt and equilibrium SO ₃ pressure of 5 x 10 ⁻⁵ atm.	89
52. Depth and typical morphology of hot corrosion attack of CoCrAlY coating tested in ducted burner rig with ASTM sea salt and SO ₂ /SO ₃ gas.	90
53. Surface condition of washed CoCrAlY specimen and salt deposit formed in 19-hour exposure at 5 mg/cm ² /hr deposition rate.	91
54. Hot corrosion of CoCrAlY coating exposed 47.1 hours in ducted burner rig; environmental conditions were as described in Fig. 52 except for salt deposition rate of 5 mg/cm ² /hr.	92
55. Hot corrosion of CoCrAlY exposed 61.1 hours in ducted burner rig; environmental conditions were the same as for the specimens of Figs. 52 - 54 except for salt deposition rate of less than 0.1 mg/cm ² /hour.	93
56. Surface condition of CoCrAlY-coated specimen exposed 6 hours to salt flux of 4 mg/cm ² /hour.	94
57. Surface features observed on the leading edge of the specimen described in Fig. 56.	95
58. Metallographic cross section presumably through a small pit of the type shown in Fig. 57.	96

	<u>PAGE</u>
59. Surface photographs of CoCrAlY-coated coupons with various deposit thicknesses after 20 hours exposure in tube furnace at 704C and $p_{SO_3} = 0.0007$ atm; weight change data versus deposit thickness for 100-hour cyclic test.	97

LIST OF TABLES

I. Temperature and gas compositions used in tube furnace experiments to determine the effect of SO_3 pressure on the rate of sulfate-induced hot corrosion.	6
II. Summary of oxidation and hot corrosion tests using chloride vapor in the gaseous environment and chloride-containing salt deposits.	18
III. Conditions for hot corrosion - deposition rate dependence tests in ducted burner rig.	31

SECTION I

INTRODUCTION AND PROGRAM PLAN

The objective of this program is to estimate the amount of sea salt which can be ingested into a marine gas turbine without unacceptable rates of hot corrosion.

The objective is formidably challenging, in spite of the apparent simplicity of limiting hot corrosion variables to the amount of salt ingested into a burner rig or test engine and extrapolating the data to an ingestion rate where hot corrosion is acceptably slow. The challenge is presented by the fact that materials degradation in any experimental or marine service situation will be strongly dependent on interactions between several major environmental variables in addition to quantity of salt:

- 1) Metal temperature
- 2) Salt chemistry
 - a. Condensed chlorides
 - b. Mixed sulfates
 - c. Vanadium and/or heavy metals
- 3) Gas chemistry
 - a. SO_3 pressure
 - b. Chloride vapors

Thus the problem is not to determine hot corrosion versus ingested salt level but to select relevant environmental conditions for the experiments and to be capable of predicting the effect of deviations from these conditions (e.g. operation of the engine at higher shaft horsepower, use of higher sulfur fuel, etc.).

In principle, for example, the objective of this program could be achieved by ingesting known amounts of salt into a shipboard engine and periodically disassembling it for metallurgical inspection of the hot section components. However, the engineering data so obtained would be

applicable only to the combination of throttle settings (i.e. shaft horsepower output) and fuel chemistry which fix the component temperatures and reactive environment of the test. Different throttle settings would simultaneously alter metal temperatures, the amount and composition of the salt deposits which condense from the combustion gases and/or spall from the compressor, and the partial pressure of sulfur oxides in the gaseous environment. The resultant effect of interrelated changes in several environmental variables on the rate of hot corrosion attack is not evident. Further, the dependence of hot corrosion on ingested salt level would be expected to vary with sulfur content of the fuel, and, lastly, an effect of transient conditions during start-up or shut-down of the engine is a possible factor.

In spite of these complications, the objective of determining marine hot corrosion dependence on ingested salt level under relevant environmental conditions is amenable to scientific and engineering study. One aspect of analyzing the problem is controlled service use of marine turbine hardware, including documentation of the time-at-temperature history of blade and vane sections as a function of engine power output and the relative temperature of various portions of the airfoil (i.e. the tip, midspan, and root sections). Visual inspection and metallographic examination can then establish the nature and severity of hot corrosion attack at high versus low engine power and in the relatively hot versus relatively cool sections of the airfoils. Information of this type has been compiled by the U.S. and Royal Navies and the major engine manufacturers (Refs. 1-6). Of major significance and relevance to this program are the following observations:

- 1) Substantial hot corrosion was encountered in the relatively cool sections of turbine airfoils and in hardware from engines whose operating history had been restricted to low shaft horsepower - hence low metal temperatures where hot corrosion had previously been thought to be inconsequential.

- 2) The low temperature corrosion was typically of nodular morphology and consumed CoCrAlY-type coatings without significant preferential attack of either the α -Co or β -CoAl phase. A thin β -denuded zone with a few small sulfides was sometimes observed, but the attack front in many cases was a sharp separation between all metal and all scale with no discernable diffusion zone or internal oxidation.

The second aspect of studying marine hot corrosion is to conduct laboratory tests which reproduce the microstructural features (and by inference the attack mechanism) of service induced degradation. Testing of this type has been done by many investigators, who have independently shown that the types of coatings being used in marine gas turbines are susceptible to low temperature (approximately 650 to 750°C) attack induced by condensed sulfate salt deposits and gaseous SO_3 (Refs. 6-11). The importance of SO_3 , as well as the condensed salt, has been demonstrated by the rapid attack of coatings known to be highly resistant to salt deposits heated in sulfur-free air. Regardless of whether the SO_3 was supplied by thermal decomposition of mixed sulfates, addition of bottled gas to furnace atmospheres or burner rig air streams, or combustion of sulfur-doped fuel, microstructural features were apparently the same and essentially equivalent to those of low temperature service-induced degradation.

Conclusions and inferences from the service evaluation and laboratory test results summarized in the preceeding paragraphs were the basis of formulating the test plan for this program as outlined in Figure 1. The plan includes tube furnace experiments to provide basic data on the effects of important hot corrosion variables and burner rig testing to determine severity of hot corrosion versus ingested salt level. Implicit in both types of experiments is the assumption that the partial pressure of SO_3 in the gaseous environment is a critical parameter. Hence, except for baseline furnace experiments to compare sulfur-containing versus sulfur-free air, all testing is done at controlled values of SO_3 pressure.

The initial series of furnace experiments attempted to evaluate quantitatively (by weight change data and metallography) the effect of p_{SO_3} on the hot corrosion produced by a given salt deposit (1 mg/cm^2 of Na_2SO_4) on various materials (CoCrAlY coatings and on IN 792, uncoated and aluminized Mar-M509 and IN 792). Such data would be useful in predicting the effect of sulfur content of the fuel on the lifetime of turbine components, since this parameter would influence the value of p_{SO_3} in the combustion gas but probably have no significant effect on other hot corrosion variables. Also, for the purpose of this program, the data were used to select a value of p_{SO_3} for subsequent experiments designed to investigate possible interactions between SO_3 and other parameters which might influence hot corrosion behavior. In this respect, it is necessary to know if the characteristic features of marine hot corrosion are produced only in a relatively narrow range of SO_3 pressures, or if the corrosion mechanism and microstructural features (although not necessarily the rate of attack) are similar over a broad spectrum of p_{SO_3} values.

The experiments in block 2 were concerned with condensed and gaseous chlorides and a possible interaction of SO_3 and vaporous NaCl. A primary effect of NaCl - previously suspected to be a major factor in marine hot corrosion - has been largely discounted because the microstructural features characteristic of chloride-induced attack (pore formation, substantial dealloying and internal oxidation) are rarely observed in corroded hardware from shipboard engines. Nevertheless the ability of NaCl to aggravate sulfate-induced hot corrosion has been repeatedly demonstrated, and it is especially important to establish whether or not a synergistic effect of NaCl and SO_3 is likely to be involved in corrosion of marine engines.

The final series of tube furnace experiments, listed in block 3, was concerned with mixed sulfates. As discussed in greater detail in presenting the results, it is known that some metallic sulfates, when present in Na_2SO_4 , may affect the hot corrosion process by depression of the melting point or thermal decomposition.

Results of the furnace experiments were considered in selecting the type of salt and other environmental variables for burner rig tests which determined severity of attack versus amount of salt ingested. Gaseous sulfur oxides in the burner rig flame were provided by mixing SO_2 with the primary air. The amount and composition of salt deposited at a given ingestion rate was determined by chemical analyses of deposits from the specimens and from an inert platinum probe of identical geometry. Furnace experiments to compare burner rig and furnace hot corrosion and to determine the dependence of furnace hot corrosion on amount of applied salt were performed as considered necessary.

All specimens from furnace and burner rig testing were examined visually and by conventional metallography; more sophisticated techniques (SEM, microprobe, and XRD) were used on selected specimens. Primary emphasis was placed on characterizing the severity of attack and degradation microstructures of CoCrAlY-coated IN 792, since this coating/substrate system is widely used in marine gas turbines. The uncoated and aluminized IN 792 and Mar-M509 were examined to compare the relative performance and mechanism of attack of Ni- versus Co-base systems under various combinations of temperature and chemical environment.

Data in the following sections are presented in the order discussed above, although some of the work was done in different sequence for experimental convenience.

SECTION II

RESULTS AND DISCUSSION

1. EFFECT OF SO_3 PRESSURE ON SULFATE-INDUCED HOT CORROSION

a. Equipment and Procedure

All tests were performed in the horizontal tube furnace illustrated in Figure 2. The input gas was mixed from bottled SO_2 and O_2 with flowmeters capable of providing ratios as low as 0.0001 volume fraction SO_2 ; total flowrate was 11.5 liters/hour. A catalyst of sputtered platinum on DuPont Torvex® honeycomb alumina was maintained at the same temperature as the specimens, which were suspended on platinum wires from a ceramic tube. The specimens were coated with 1 mg/cm^2 of Na_2SO_4 , exposed for 20 hours, water washed, and recoated with fresh salt for continued testing. Total exposure time was 100 hours unless sooner terminated because of severe attack.

Test conditions are listed in Table I. The rate of attack at 704°C - of maximum relevance to the problem of low temperature marine hot corrosion - was determined at three values of SO_3 pressure, computed from data in the JANAF tables assuming equilibration of the input gas mixture at the test temperature. The input gas composition was then adjusted to provide the same equilibrated SO_3 pressure at a higher temperature, so that comparison with the 704°C results would define the effect of metal temperature on the rate and microstructural features of SO_3 -induced corrosion.

704°C (1300°F)		899°C (1650°F)	
input $\text{SO}_2:\text{O}_2$ ratio	equilibrium SO_3 pressure (atmospheres)	input $\text{SO}_2:\text{O}_2$ ratio	equilibrium SO_3 pressure (atmospheres)
0.0050	3.5×10^{-3}	-	-
0.0010	7.1×10^{-4}	0.0029	7.1×10^{-4}
0.0002	1.4×10^{-4}	0.0006	1.4×10^{-4}

TABLE I. Temperatures and gas compositions used in tube furnace experiments to determine the effect of SO_3 pressure on the rate of sulfate-induced hot corrosion.

b. SO_3 - Induced Attack at 704°C (1300°F)

Surface photographs and weight change data showing severity of attack versus SO_3 pressure are presented in Figures 3 - 8. Except for an unusually large weight loss of one of the specimens (uncoated IN 792) at the intermediate value of p_{SO_3} , all observations and $\Delta M/A$ data indicate strong and consistent dependence of severity of attack on SO_3 pressure.

The surface photographs in Figures 3 - 7 are those taken of each specimen at the initial examination after 20 hours exposure, where the difference in surface condition as a function of SO_3 pressure was most evident. The effect of SO_3 pressure on severity of attack - especially at 0.004 versus 0.0007 atm - was not well illustrated by black and white surface photographs after longer exposure times, although the difference in degradation of the coated specimens at 0.0007 versus 0.0001 atm was apparent (Figure 8).

Post-test metallography showed that the PWA 68 CoCrAlY coating tested at 0.004 atm SO_3 was penetrated or almost penetrated in numerous locations, with most areas showing general surface degradation as well as localized nodular attack (Figure 9). The uncoated alloys in the same test (Figures 10a, 10b) showed highly irregular surfaces reflecting the substantial material consumption and scale spallation inferred from visual inspection and the large weight losses; however, there was no indication of alloy depletion, sulfide precipitation, or internal oxidation in advance of the scale/metal interface. The PWA 28 aluminide coating on Mar-M509 was almost completely consumed; the heavy scale shown in Figure 10c was spalled off in most areas and substrate attack was observed. In contrast, the PWA 273 on the Ni-base IN 792 was heavily attacked but still protective (Figure 10d).

Less severe attack, especially of the Co-base coatings, at $p_{\text{SO}_3} = 0.0007$ atm is evident from comparison of Figures 11 and 12 versus Figures 9 and 10. The CoCrAlY and the Co-base aluminide both failed in the 100-hour test at 0.004 atm; at the lower SO_3 pressure, both were substantially corroded but still intact, at least over most of the area of the specimen.

Microstructural degradation of all of the test materials was substantially less at $p_{\text{SO}_3} = 0.0001$ atm (Figures 13 and 14 versus Figures 9 - 12), possibly excepting a relatively thick scale on aluminized IN 792 which was comparable to that observed at 0.0007 atm. Attack of the CoCrAlY was limited to the depth shown in Figure 13, obviously much less than that of the higher SO_3 pressures but very significant in consideration of the negligible degradation produced by low temperature exposure of sulfate-coated CoCrAlY in atmospheres free of gaseous sulfur oxides. Degradation of the PWA 28 Co-base aluminide was also very slight, and the uncoated alloys were only moderately attacked (Figure 14).

CoCrAlY specimens tested at the three values of p_{SO_3} were examined by scanning microscopy; typical features of the corrosion front and element distribution in the corrosion products are illustrated in Figures 15 - 18. At the maximum rate of attack, produced by $p_{\text{SO}_3} = 0.004$ atm, there is an extremely well defined ghost image of the coating microstructure at the base of developing protrusions and the complete absence of a β -depleted zone in most areas of the attack front (Figure 15). The volume of the protrusion is Cr- and Al-rich oxides, and sulfur enrichment at the attack front is readily observable in X-ray area scans. At $p_{\text{SO}_3} = 0.0007$ atm, the attack is of similar nodular morphology, although SEM examination shows a thin but unequivocally recognizable β -depletion zone at the attack front (Figures 16, 17). The composition of oxides in the developing protrusion is again Cr- and Al-rich. Comparison of the X-ray maps in Figure 15 versus Figure 17 implies a difference in sulfur distribution, but the effect is possibly attributable to wet versus dry polishing as discussed below. At $p_{\text{SO}_3} = 0.0001$ atm, a well defined β -denuded zone at the scale/metal interface is typically of the thickness shown in Figure 17. A nodular morphology is not yet evident in all areas although X-ray maps again show the Cr- and Al-containing oxides and a characteristic presence of sulfur in the scale.

In considering the significance of sulfur in the corrosion products, it is important to note that the specimens of Figure 15 and 18 were prepared for metallographic examination by conventional wet polishing, which

would remove water-soluble salts from the scale. Hence the concentration of sulfur at the attack front must be due to an insoluble compound - perhaps an aluminum-chromium oxysulfide, or a type of complex sulfate or sulfite* - and not simply an accumulation of unreacted residual sulfate salt. Conversely, the sample of Figures 16 and 17 was dry polished and shows a more-or-less uniform distribution of both Na and S in the bulk of developing protrusions. This suggests that the corrosion products in the protrusion were soaked with sulfate salt during the test, and advance of the attack front involved reaction of this salt under the conditions of low oxygen activity which exist at the scale/metal interface.**

Similar microstructure and element distribution over a range of SO_3 pressures - excepting only a narrow β -depleted zone whose presence can be rationalized by slower attack at low SO_3 pressure - implies that the hot corrosion mechanism is essentially the same at the three values of SO_3 pressure used in these experiments. If such is the case, the rate of attack, measured in suitable units, should exhibit a systematic dependence on p_{SO_3} . Since the characteristic microstructure and failure mode of CoCrAlY coatings in marine service is generally a form of localized nodular attack, the rate of hot corrosion was expressed by estimating the time to penetrate the 125 μm (5 mil) coatings on the samples from these tests, assuming a linear increase in the depth of attack with increasing exposure time. The results, plotted in Figure 19, suggest an approximately linear dependence of log failure time on p_{SO_3} such that coating life can be expressed by an equation of the form

$$\log (\text{time to penetration}) = n \cdot \log p_{\text{SO}_3} + \log C$$

*X-ray profiles for Al, Cr, O, and S peak simultaneously at attack front, suggesting the corrosion product is a phase containing all four elements.

**Wet polished specimens have sometimes shown a generally broad distribution of sulfur (but not sodium) rather than the concentration of sulfur at the attack front as illustrated in Figure 15. Conversely it has been observed that dry polished specimens sometimes show a well defined sulfur-rich band at the attack front rather than the uniform distribution of sulfur shown in Figures 16 and 17. Easily detectable sulfur is invariably present, however, and the sulfur-containing scale is a characteristic feature with important implications regarding the mechanism of SO_3 -induced attack, even though the sulfur distribution (i.e. uniformly in the volume of the protrusion or concentrated at the attack front) may be variable and not well understood.

$$\text{or time to penetration} = C \cdot p_{\text{SO}_3}^n$$

Although the graph of Figure 19 must be interpreted with caution because of the limited testing and crude approximation of failure times, it is clear that severity of attack, under otherwise constant environmental conditions, is a strong function of SO_3 pressure.

c. SO_3 - Induced Attack at 899°C (1650°F)

As discussed in the introduction and the description of experimental procedure at the start of this section, it was known that a test temperature near 700°C with SO_3 in the gaseous environment would produce hot corrosion with microstructural features similar to those of low power marine hot corrosion. However, to insure a wise selection of test conditions for the rest of this program - both from the point of view of experimental convenience and relevance to the problem of marine hot corrosion - it was necessary to investigate the effect of metal temperature on the severity and microstructural features of SO_3 - induced hot corrosion.

Two approaches to specifying SO_3 pressures for comparing low temperature versus high temperature hot corrosion in tube furnace testing could be advocated:

- 1) Maintain constant SO_3 pressure at the two test temperatures by increasing the $\text{SO}_2:\text{O}_2$ ratio in the input gases to compensate for the temperature dependence of the $\text{SO}_2/\text{SO}_3/\text{O}_2$ equilibrium.
- 2) Maintain the same $\text{SO}_2:\text{O}_2$ ratio in the input gases, thus fixing the total sulfur content of the gaseous environment but allowing the SO_3 pressure to reach the lower equilibrium value characteristic of the higher temperature.

Since the results of the previous experiments had shown that SO_3 pressure is a critical variable in the hot corrosion process, it was decided that the former of these approaches would provide the more useful information with respect to the program objectives. Hence, as listed in Table I on page 6, the input gas compositions to the tube furnace were adjusted to provide two values of SO_3 pressure (0.0007 and 0.0001 atm) equal to those

used at 704°C. Results of the two high temperature tests were compared via surface condition, weight changes, and metallography to determine the influence of p_{SO_3} on severity of hot corrosion attack at 899°C. Also the 899°C data were compared with 704°C results to determine the effect of metal temperature on rate of attack and microstructural features at fixed values of p_{SO_3} .

In the initial high temperature test at $p_{\text{SO}_3} = 0.0007$ atm, the FWA 68 CoCrAlY was significantly attacked (Figure 20a), although half of one surface was still adherent alumina (Figure 20b) and a very small weight change (about 1 mg/cm² in 100 hours) suggested much less attack than that produced by the same SO_3 pressure at 704°C. At 0.0001 atm, attack of the CoCrAlY was limited to the very small spots of blue spinel shown in Figure 20c; post-test metallography showed no discernable microstructural degradation.

Microstructural features of the 0.0007 atm CoCrAlY specimen are shown in Figures 21 and 22. Optical photomicrographs of randomly selected areas (Figure 21) illustrate the varying severity of attack inferred from the surface condition. SEM examination of a more severely degraded area (Figure 22 and corresponding X-ray maps in Figure 23) shows a highly irregular scale/metal interface and a very prominent β -denuded zone. There is strong concentration of sulfur in the scale as well as sulfur-containing particles in the two-phase $\alpha + \beta$ structure in advance of the β -denuded zone. Line profiles along the path marked in Figure 22 show a slight gradient in Al and Cr content.

For the uncoated and aluminized alloys tested concurrently with the FWA 68 CoCrAlY, the most striking result was the severe attack of the Ni-base FWA 273 diffusion aluminide. Penetration of the coating at several sites was observed after the initial 20-hour exposure at both SO_3 pressures (Figure 24). Attack of both specimens was highly localized, however, and unaffected microstructure still exhibited the characteristic purple color of as-processed β -NiAl. Copious sulfide precipitation associated with the localized attack may reflect cut-edge degradation, although results presented in the following paragraph show that the uncoated alloy is susceptible to gross sulfidation under these environmental conditions.

Microstructural features developed by 100-hour exposure of uncoated and aluminized Mar-M509 and uncoated IN 792 are illustrated in Figures 25 - 27; Figure 25 also shows the degradation produced by 80-hour exposure of a duplicate specimen of aluminized IN 792 which replaced the initial coupon sectioned for metallography after 20 hours. At $p_{\text{SO}_3} = 0.0007$ (Figure 25), the uncoated Mar-M509 showed a relatively uniform external scale, preferential oxidation of interdendritic eutectic, and a few shallow protrusions typically of the depth in Figure 25a. The aluminide coating on Mar-M509 was substantially degraded but still protective; substrate attack was limited to the slight preferential carbide oxidation shown in Figure 25b. Consumption of the coating apparently involved β -depletion and sulfide precipitation.

In contrast to the moderate attack of the Co-base systems, Figures 25c and 25d show the almost catastrophic hot corrosion of IN 792 under the same test conditions. The uncoated alloy (Figure 25c) was severely sulfidized and the aluminide coating was completely consumed in approximately 80 hours or less. Figure 25d includes a remnant of the destroyed coating; the oxidized coating was spalled off in most locations, and depth of sulfide penetration was essentially the same as that of the uncoated alloy.

At $p_{\text{SO}_3} = 0.0001$ atm, uncoated and aluminized Mar-M509 were less attacked, although the variation in severity of hot corrosion with SO_3 pressure was not as pronounced as that observed for these alloys at 704°C . Nevertheless the scale thickness and depth of preferential oxidation were clearly less at 0.0001 atm (Figure 26a vs. Figure 25a), and examination of several areas of the aluminide-coated specimen showed there was generally more β -CoAl, less sulfide precipitation, and less material consumption (Figure 26b vs. Figure 25b).

The effect of p_{SO_3} on 899°C hot corrosion of uncoated IN 792 was very pronounced, as shown by weight change data and metallography (Figure 27). Characteristic features of the degradation microstructure appeared essentially the same, however, except for the difference in severity of attack. The external corrosion product was a mixture of metal and scale, and there was substantial alloy depletion and sulfide precipitation.

d. Temperature Effect at Constant SO_3 Pressure

The following discussion, supported by Figures 28 through 30, summarizes results of the 704 and 899°C hot corrosion experiments in terms of relative performance versus temperature and SO_3 pressure.

1) FWA 68 CoCrAlY Coating

It is clear that SO_3 -induced hot corrosion of CoCrAlY is less severe at 899 than at 704°C. Although 100-hour exposure at 899°C and $p_{\text{SO}_3} = 0.0007$ atm produced substantial microstructural degradation in some areas (e.g. Figure 22), examination of the test coupons after 20 hours showed extensive corrosion at 704°C versus negligible attack at 899°C, and weight changes were much less at the higher temperature (Figure 28). At 0.0001 atm, the negligible 899°C attack indicated by surface condition (Figure 20c) and post-test metallography contrasts with the significant extent of corrosion shown in Figures 13 and 18.

2) Mar-M509

Weight change data for uncoated Mar-M509 at $p_{\text{SO}_3} = 0.0007$ atm are also dramatically greater at 704°C (Figure 29a), although corresponding metallography (Figure 25a) showed greater attack at 899°C than implied by the relatively small weight changes. At $p_{\text{SO}_3} = 0.0001$ atm, small weight changes and moderate surface degradation at both test temperatures were not significantly different.

Somewhat surprisingly in view of the performance of CoCrAlY and the uncoated Co-base Mar-M509, the aluminide coating on Mar-M509 was more severely attacked at 899 than at 704°C. Figure 29b shows a relatively large 899°C weight loss at 0.0007 atm; at the lower SO_3 pressure, Figure 26b versus Figure 14b again indicates greater microstructural degradation at 899°C, perhaps resulting from coating-substrate interdiffusion.

3) IN 792

At $p_{\text{SO}_3} = 0.0007$ atm, uncoated IN 792 suffered large weight changes at both 704 and 899°C (Figure 30a). Although the weight loss at 704°C may have been anomalously large (Figure 6), it is clear from corresponding

metallography that high temperature promoted gross sulfidation (Figure 25c) in contrast to negligible internal attack at 704°C (Figure 12b). At 0.0001 atm, a small but clearly measurable weight gain at 899°C (Figure 30b) again suggests more substantial ingress of sulfur into the alloy due to the higher test temperature.

The aluminide coating on IN 792 was resistant to SO_3 effects at 704°C; although significant weight losses and surface degradation were observed, the coating was not penetrated even by 100 hours at 0.004 and 0.0007 atm (Figure 10, 12). Conversely, exposure to SO_3 at 899°C caused rapid sulfidation and penetration of the coating after only 20 hours (Figure 24).

e. Summary and Discussion of SO_3 Effects

Of obvious relevance to the problem of marine hot corrosion are the following results of service experience and laboratory testing:

- Substantial hot corrosion has been observed in shipboard engines operating at low shaft horsepower - hence low metal temperatures
- The typical degradation microstructure in these engines was apparently produced by in-situ corrosion of the CoCrAlY coating; i.e. there was minimal alteration of coating chemistry by long range diffusion and minimal internal attack in advance of the scale/metal interface
- Microstructural features of low power marine hot corrosion can be reproduced in a low temperature (approximately 650 to 750°C) laboratory furnace test using only Na_2SO_4 salt and SO_3 in the gaseous environment
- Coatings resistant to Na_2SO_4 deposits heated in sulfur-free air are substantially degraded when the atmosphere contains SO_3 . The degradation rate is proportional to the partial pressure of SO_3
 - The SO_3 effect is observed at temperatures as high as 899°C, although microstructural features produced in testing at this temperature show important dissimilarities (primarily the pronounced β -denuded zone) from those developed in low power marine service

- At fixed SO_3 pressure, CoCrAlY is more severely degraded at 704 than at 899°C

Probably the most critical item in establishing the relevance of laboratory test results to service experience is comparison of degradation microstructures. Unfortunately the comparison is not always straightforward, and inferences from a one-time destructive metallographic examination of service hardware must be drawn with extreme caution (e.g. did the observed corrosion occur at a more-or-less uniform rate during typical operating conditions, or rapidly during brief excursions from the normal operating profile of the engine?). Hence it must be understood that similarity of degradation microstructures in engine hardware and laboratory test specimens is not conclusive proof that test conditions have reproduced the causes and mechanism of the hot corrosion which occurred in service. On the other hand, the microstructures observed in hardware from many marine engines does unequivocally restrict their time-at-temperature history to conditions which caused no alteration of the coating microstructure by long-range diffusion and likewise eliminates any combination of metal temperature and corrosive agents which results in substantial alloy depletion or internal oxidation in advance of the attack front.

Based on this reasoning and the information summarized in the bullet items just listed, it is strongly believed that hot corrosion of the type illustrated in Figure 31 is due to low temperature (i.e. about 750°C or below) exposure to condensed Na_2SO_4 salt and SO_3 in the combustion gases.

2. CHLORIDE EFFECTS AND CHLORIDE - SO_3 INTERACTIONS

a. Objective and Approach

The objective of the work in this section is to determine if the sulfate- SO_3 type of hot corrosion attack believed to be the primary mechanism of degradation of shipboard engines is significantly affected by NaCl. The experimental approach was to compare weight change data and microstructural degradation from three types of tests:

- 1) Sulfate - SO_3 hot corrosion in the absence of NaCl
(i.e. the work in Section 1)
- 2) Condensed and vaporous chloride effects in the absence of SO_3 gas
- 3) Sulfate - SO_3 - NaCl hot corrosion testing at concentrations of SO_3 and NaCl selected from results of the preceeding experiments.

As described in the preceeding section, the sulfate- SO_3 experiments were run at 704 and 899°C to compare severity of attack and degradation microstructure at two temperatures. The chloride experiments were done at 899°C with high concentrations of condensed and/or vaporous NaCl to accelerate testing; low temperature experiments were considered unnecessary because earlier work (Ref. 6) had shown similar degradation microstructures and comparable behavior at 649 and 899°C except for more rapid attack at the higher temperature. The SO_3 - NaCl interaction experiments were again run at both 704 and 899°C, since the relative severity of NaCl- and SO_3 -induced degradation would be expected to vary significantly with temperature.

b. Condensed and Vaporous Chloride Effects

The five test materials (IN 792/PWA 68 CoCrAlY, uncoated and aluminized Mar-M509, uncoated and aluminized IN 792) were concurrently exposed at 899°C to the following combinations of condensed and gaseous oxidants:

<u>Salt Deposit</u>	<u>Furnace Gas</u>
None	Air
None	Air with 300 ppm NaCl
1 mg/cm ² Na_2SO_4	Air
1 mg/cm ² Na_2SO_4	Air with 300 ppm NaCl
1 mg/cm ² Na_2SO_4 - 50 wt% NaCl	Air
1 mg/cm ² Na_2SO_4 - 50 wt% NaCl	Air with 300 ppm NaCl

The air experiments were performed in a vertical tube furnace; those involving NaCl vapor were run in the horizontal furnace of Figure 2 by inserting a salt-filled boat upstream of the specimens. Material behavior

was evaluated by visual inspection and weighing at 20-hour intervals and by post-test metallography. The salted specimens were washed and recoated with fresh salt at the 20-hour inspections.

Results are summarized in Table II. Metallography and weight change data of selected specimens are presented as considered necessary in the following discussion:

1) Effect of Chloride Vapor on Simple Oxidation (compare Column 2 vs. Column 1)

The term simple oxidation indicates the lack of condensed corrosive on the material surface.

In the 200-hour testing time of these experiments, the effect of the chloride vapor was not dramatic. On visual inspection, only the uncoated Mar-M509 was considered unequivocally more degraded as a result of the chloride vapor, although subsequent metallography suggested slightly greater preferential oxidation of carbide phases in the Co-base aluminide coating as well. There was no discernable difference in the nature or extent of attack of the CoCrAlY or the Ni-base materials in chloride-containing versus chloride-free air.

2) Sulfate-Induced Hot Corrosion in Clean Air (Column 3 vs. Column 1)

The term clean air indicates the lack of significant concentrations of gaseous reactants other than oxygen.

Hot corrosion is generally defined as increased oxidation due to the presence of condensed salt deposits on the material surface, and, as expected, all of the specimens were more degraded in hot corrosion than in simple oxidation. However the extent of attack could at most be described as moderate; none of the coatings failed, and microstructural degradation of CoCrAlY was negligible.

3) Effect of Chloride Vapor on Sulfate-Induced Corrosion (Column 4 vs. Column 3)

Significant differences in hot corrosion behavior were observed under identical test conditions except for the presence of 300 ppm NaCl vapor.

Alloy/ Coating	Oxidation In Air (1)	Oxidation In Air with 300ppm NaCl Vapor (2)	Sulfate Hot Corrosion In Air (3)	Sulfate Hot Cor- rosion In Air + 300ppm NaCl (4)	Sulfate-Chloride Hot Corrosion In Air (5)	Sulfate-Chloride Hot Corrosion In Air + 300ppm NaCl (6)
Mar-M509	Surface scale; preferential oxidation of carbides and grain boundaries	Thicker scale with more CoO; carbide and grain boundary oxidation	About the same as oxidation without salt deposit; slightly thicker scale	Substantially increased attack due to the NaCl vapor	Very severe attack; large weight loss and extensive microstructural degradation	Very severe attack
IN 792	Cr ₂ O ₃ scale, Al ₂ O ₃ sub-scale	About the same as in air	Increased attack because of salt deposit	Less attack than hot corrosion in air	Much more severe than sulfate induced corrosion	Slightly more severe than sulfate-chloride in air
Mar-M509/ PWA 28	Little attack; slight preferential oxidation of carbide and/or refractory metal phase	Slightly increased preferential oxidation	Moderate attack; increased scale thickness and deeper preferential attack	Severe preferential attack of carbide and/or refractory metal phase	Very severe degradation; coating failure and substrate attack	Very severe degradation
IN 792/ PWA 273	Very little attack; slight preferential oxidation of α -phase	Same as oxidation in air	Slightly thicker scale and more pronounced preferential attack	Same as hot corrosion in air; i.e. relatively little attack	About the same as sulfate induced corrosion	Severely attacked; substantial dealloying, internal oxidation, and sulfide precipitation
IN 792/ PWA 68	Very little attack	Thin β -depleted zone	Thin, adherent scale; very little attack	Thin β -depleted zone with slight internal oxidation in some areas	Severe attack; extensive dealloying, internal oxidation, and sulfide precipitation	Very severe attack; coating completely destroyed in most areas

TABLE II. Summary of oxidation and hot corrosion tests using chloride vapor (300 ppm) in the gaseous environment and chloride-containing (50 wt%) salt deposits.

Uncoated Mar-M509 was substantially more degraded in the experiment with NaCl vapor (Figure 32). The effect is believed to be real, although the relatively slight degradation of the specimen tested in air is of questionable reproducibility and the chloride effect might not be as pronounced as the results of these two experiments suggest. For the Co-base coatings, observation of a number of randomly selected areas on the entire cross section would support the conclusion that degradation was slightly greater due to the NaCl vapor, especially for the aluminized Mar-M509. The CoCrAlY coatings were only lightly attacked in both tests and the difference might have been within experimental scatter.

The concurrently exposed Ni-base alloys were less corroded in the chloride-containing atmosphere, as shown in Figure 33 by surface condition and metallography of uncoated IN 792. Visual inspection of the aluminized sample indicated minimal attack except for a massive edge failure which is not attributed to the chloride vapor; post-test metallography confirmed minimal microstructural degradation except for cut-edge attack.

4) Sulfate-Condensed Chloride Hot Corrosion in Clean Air (Column 5 vs. Column 4)

As expected, the addition of 50% NaCl to the condensed salt deposit caused severe hot corrosion of all the specimens except the aluminized IN 792. Both Co-base coatings failed, and degradation microstructures showed the extensive dealloying, pore formation, and internal oxidation characteristic of chloride-induced attack.

5) Effect of Chloride Vapor on Sulfate-Condensed Chloride Corrosion (Column 6 vs. Column 5)

Again as expected from trends of the previous experiments, the combination of condensed chloride in the salt deposit and 300 ppm NaCl vapor in the furnace atmosphere produced very severe degradation, including attack of the Ni-base aluminide which was resistant to sulfate-chloride deposits heated in air. The PWA 68 CoCrAlY was also substantially more degraded than in the equivalent test with sulfate-chloride salt in clean air.

c. Chloride - SO_3 Interactions

It is evident from the trends shown in Table II - as well as from the work of other investigators* - that NaCl tends to promote cracking and spallation of protective scales, thereby accelerating the onset of the propagation stage of oxidation or hot corrosion attack. Such an effect could significantly aggravate hot corrosion, even in the case where condensed or vaporous chloride is a minor species and the mechanism of attack is that characteristic of another corrodent (i.e. Na_2SO_4 - SO_3). Hence the following work was carried out to compare the rate of attack observed in the experiments of Section 1 with that produced by the same salt deposit and SO_3 pressure plus a small concentration of vaporous sodium chloride.

The horizontal tube furnace described in Section 1 was modified as shown in the sketch of Figure 34 to permit exposure of the test specimens to both SO_3 and NaCl vapor. Gas flow rates and $\text{SO}_2:\text{O}_2$ input ratios were the same as those of the preceding experiments with SO_3 gas, but it was necessary to introduce the SO_2 down stream of the NaCl boat to prevent consumption of the SO_2 via reaction with the solid NaCl. Tests were run at an SO_3 pressure of 0.0007 atm, since degradation produced by this concentration was known to be substantial but not sufficiently catastrophic to overwhelm a possible effect of the chloride. A chloride vapor concentration of 30 ppm - maintained by heating the NaCl to 677°C (1250°F) - was arbitrarily selected.

1) NaCl - SO_3 Effects at 704°C

The five test materials were concurrently exposed as described previously. The test was terminated after 60 hours, when it was felt that visual inspection and weight changes had indicated a similarity or difference in the extent of attack versus the equivalent test in Section 1 with the same salt deposit and SO_3 pressure but no chloride vapor.

*Fourteen papers on Combustion Processes and Kinetics and the Influence of Halides in Hot Corrosion are included in the Proceedings of the Symposium on High Temperature Metal Halide Chemistry, D. L. Hildenbrand and D. D. Cubicciotti, Eds., Proceedings Volume 78-1, The Electrochemical Society, Princeton, N.J. 08540.

Visual inspection after the initial 20-hour exposure cycle suggested increased attack of all of the specimens except the uncoated Mar-M509, although the effect was not dramatic. After 60 hours, consistently larger weight losses of Mar-M509 and aluminized IN 792 (Figure 35) apparently reflect increased scale spallation due to the chloride. Weight changes of the other test materials were not significantly different in chloride-containing versus chloride-free atmospheres.

Post-test metallography showed an unusual superposition of microstructural features characteristic of low temperature SO_3 -induced attack and chloride-induced dealloying. The mixed microstructure was especially prevalent in the CoCrAlY coating, where adjacent areas showed a sharp transition between the complete absence of internal oxidation typical of SO_3 effects and the substantial dealloying and pore formation typical of chloride corrosion (Figure 36). Areas with the SO_3 -type morphology were also characterized by sulfur in the scale (Figure 37a, 37b); other areas showed variations in the composition and ghost microstructure of the scale which suggested that attack may have oscillated between SO_3 - and chloride-type (Figure 37c).

In spite of the simultaneous operation of two types of corrosion mechanisms indicated by these microstructures, there does not seem to have been a synergistic effect between SO_3 and NaCl. Depth of attack was not greater than that attributable to the same SO_3 pressure acting alone.

In the case of the other test materials, microstructural effects of the chloride vapor were not evident in Mar-M509 (Figure 38a), although the concurrently tested IN 792 (Figure 38b) exhibited many areas of internal oxidation (arrow) which were not observed in degradation microstructures produced by SO_3 only. Both aluminide coatings showed a more or less uniform microstructure of the attack front with chloride-type dealloying and internal oxidation proceeding the nodular attack typical of SO_3 (Figures 38c, 38d). As in the case of the CoCrAlY, depth of penetration was not significantly greater than that expected from SO_3 alone.

2) NaCl - SO₃ Effects at 899°C

All specimens were exposed for 100 hours. The most apparent effect on visual inspection was generally greater surface degradation of CoCrAlY, including slight but clearly noticeable attack after 20 hours versus the negligible degradation observed after the same exposure time in the equivalent test without NaCl vapor. In the opposite direction, uncoated Mar-M509 and aluminized IN 792 appeared to be less severely attacked with NaCl vapor. Uncoated IN 792 and aluminized Mar-M509 experienced much smaller weight changes with the NaCl vapor, although visual inspection suggested considerable attack.

In spite of the greater surface attack and a slightly larger weight loss, post test metallography showed that depth of penetration of the CoCrAlY coating was no greater than observed without NaCl vapor. Microstructural features (Figure 39) included an aluminum-rich sulfur-containing corrosion product at the scale/metal interface and metallic sulfide in the two phase zone, apparently the same phases observed in the previous 100 hour test at this SO₃ pressure (compare Figure 39 with Figures 21 and 22). In contrast to the 704°C experiment at the same SO₃ and NaCl vapor concentrations, there were no microstructural effects clearly attributable to the presence of the chloride vapor.

Microstructures of the uncoated and aluminized alloys exposed to NaCl and SO₃ at 899°C are presented in Figure 40; comparison with the structures developed at the same temperature with SO₃ alone (Figure 25) shows substantially less attack in the experiment with NaCl vapor. The Co-base system (uncoated and aluminized Mar-M509) shows no features attributable to NaCl, while the concurrently tested Ni-base system apparently exhibits the type of internal oxidation characteristic of chlorides.

d. Summary and Discussion of Chloride Effects and NaCl - SO₃ Interactions

It appears conclusively established that chloride-induced dealloying, such as that produced by condensed deposits of Na₂SO₄ - 50% NaCl in the experiments described in one of the preceeding subsections, is not the mechan-

ism of marine hot corrosion. It is felt that microstructural dissimilarity alone is sufficient to justify this conclusion, even though arguments can be advanced that small concentrations or a transient presence of chloride can affect hot corrosion.

Unfortunately this question of whether or not small concentrations of chloride significantly aggravate a mechanism of attack determined by another corrosive species is far more difficult than the rather unequivocal interpretation of laboratory tests with high concentrations of chloride and comparison of these results with service microstructures. In principle, the approach used in this program - namely to compare the severity of attack produced by a given temperature, salt deposit, and SO_3 pressure with that of the same conditions except for the addition of a small concentration of NaCl - should demonstrate a negligible effect or the aggravation of attack. However the scatter normally encountered in hot corrosion experiments may render interpretation difficult, unless, of course, a marked synergistic effect is clearly observed.

Such an effect, if present, would almost surely have caused a substantially increased degradation rate of the samples in Figures 35 to 40, where a relatively high SO_3 pressure and a relatively high concentration of NaCl vapor left microstructural features characteristic of both processes. Indeed, as mentioned in presenting the results, the degradation of several of the specimens did appear greater than in the corresponding test at the same SO_3 pressure but without chloride vapor. However the difference was probably within experimental scatter, or at most could be considered an additive effect of increased scale spallation and SO_3 -induced attack. The depth of attack in no case was significantly greater than that attributable to the SO_3 pressure alone.

In the 899°C experiment with SO_3 and NaCl, visual inspection suggested increased attack of CoCrAlY in the form of general surface degradation, and post-test metallography showed features of both SO_3 -induced nodular attack and chloride-type internal oxidation of the Ni-base alloys. However the depth of attack of all of the specimens was less than that observed at the same temperature and SO_3 pressure in the absence of NaCl vapor.

In evaluating the results of the SO_3 - NaCl interaction experiments, it is critical to bear in mind the distinction between the initiation stage (where a protective reaction product barrier reduces the rate of attack) and the propagation stage (where a less protective reaction product allows more rapid material consumption) of the hot corrosion process. A potentially important effect of chloride vapor - even at the relatively low concentrations expected in the gas turbine environment - is to shorten the initiation stage by promoting scale spallation. Such an effect was clearly observed on some of the specimens in the experiments just described. However an increase in the rate of hot corrosion propagation due to a synergistic interaction between SO_3 and NaCl vapor was not encountered, even though the test conditions appear to have been extremely favorable for inducing such an interaction. Hence it is felt that the chloride effect observed in these experiments involved a role of NaCl vapor in hastening the onset of SO_3 - induced propagation rather than an SO_3 - NaCl synergism which increased the rate of attack in the propagation stage of hot corrosion.

e. Choice of Conditions for Mixed Sulfate Experiments

The results at this point seemed to support emphasis on testing at 704 rather than 899°C, since SO_3 effects - at least in the case of the CoCrAlY coating whose corrosion behavior is of most direct relevance to degradation of shipboard engines - were more pronounced at this temperature and microstructural features better reproduced the narrow β -denuded zone usually observed in service hardware. Of the SO_3 pressures used in the preceeding experiments, the intermediate value - namely 0.0007 atm - still appeared to induce the severe but less than catastrophic corrosion which offered the optimum compromise between accelerated testing and minimum danger of overwhelming other potentially significant factors.

In spite of the belief that the 30 ppm NaCl vapor used in the immediately preceeding tests was not of major significance, there appeared to be no compelling reason for removing it from the system prior to initiating the mixed sulfate experiments, especially since small amounts of NaCl vapor would be present during service operation of shipboard gas turbine engines.

3. MIXED SULFATE EFFECTS AT 704°C

a. Introductory Remarks and Experimental Procedure

There are several reasons to suspect that a mixture of Na_2SO_4 and metallic sulfates may be a significant factor in low temperature marine hot corrosion.

Most evident is that contamination could readily occur from such sources as impurities in the fuel, the metallic content of ingested sea salt, rust or paint in the ductwork leading to the engine, as well as formation of cobalt sulfate during corrosion. These impurities would lower the melting point of the salt deposit, thus tending to promote corrosion which might otherwise be negligible because the salt deposit was not molten.

Slightly more sophisticated thermomechanical considerations show that mixed sulfates formed or deposited at low temperatures may influence the hot corrosion process by supplying SO_3 on decomposing at higher metal temperatures. Indeed the nodular morphology and characteristic element distribution of low power marine hot corrosion was first reproduced in the laboratory by heating in air of specimens with very thick deposits of $\text{Na}_2\text{SO}_4 - \text{CoSO}_4$ which supplied SO_3 by decomposition of the CoSO_4 at 760°C.

To determine if mechanisms other than lowering of the melting point and thermal decomposition are involved in mixed sulfate hot corrosion, samples of FWA 68 CoCrAlY were coated with a 1 mg/cm^2 deposit of $\text{Na}_2\text{SO}_4 - 50\text{m}\% \text{CoSO}_4$ and $\text{Na}_2\text{SO}_4 - 50\text{m}\% \text{ZnSO}_4$ and exposed under the same environmental conditions ($t = 704^\circ\text{C}$, $p_{\text{SO}_3} = 0.0007 \text{ atm}$, 30 ppm NaCl vapor) as in a preceding experiment where the applied deposit was 100% Na_2SO_4 . Included in the same test was a mixture of $\text{Na}_2\text{SO}_4 - \text{CoO}$ on CoCrAlY and $\text{Na}_2\text{SO}_4 - \text{CoSO}_4$ on an aluminized nickel-base alloy. The former was to investigate the possibility of accelerated formation of CoSO_4 via reaction of the CoO and SO_3 ; the latter, to determine the effect of applied CoSO_4 versus that which could form during corrosion of a Co-base material.

Isolated tests were also run to look at other potentially important factors:

- 1) a thick deposit (5 mg/cm^2) on CoCrAlY

- 2) a vapor honed surface on CoCrAlY
- 3) a thin deposit of Na_2SO_4 on a tablet of $\alpha\text{-Al}_2\text{O}_3$
- 4) a thin deposit of $\text{Na}_2\text{SO}_4 - \text{CoSO}_4$ on a tablet of $\alpha\text{-Al}_2\text{O}_3$

b. Test Results

- 1) Effect of CoSO_4 and ZnSO_4 on CoCrAlY

In comparison to the equivalent test with 100% Na_2SO_4 , the mixed sulfate samples experienced more surface degradation (i.e. more of the surface was black CoO after comparable exposure time) but smaller weight losses. Depth of nodular attack as determined by post-test metallography was characteristic of the SO_3 pressure and apparently not increased due to the mixed salt deposit. The structure of the attack front showed evidence of both SO_3 - and NaCl-induced corrosion. To optical metallography, the Co- and ZnSO_4 specimens were indistinguishable from each other, and there was no apparent effect of the mixed sulfates versus 100% Na_2SO_4 (Figure 41).

- 2) Salt - Cobalt Oxide Mixture

A deposit of approximately 2 mg/cm^2 - intended to be equal parts by weight of salt and oxide - was applied by spraying with a water-base slurry. The specimen was tested concurrently with those which experienced the relatively deep nodular attack shown in Figure 41. However both visual inspection and small weight changes during test suggested only superficial surface oxidation, and post-test metallography confirmed that microstructural degradation was limited to the narrow β -denuded zone and fine sulfide precipitation shown in Figure 42. Presumably the lack of significant hot corrosion is because the CoO was effectively gettering the SO_3 ; if the deposits had been left until all the CoO was converted to CoSO_4 , normal SO_3 -induced corrosion would have been observed.

- 3) $\text{Na}_2\text{SO}_4 - \text{CoSO}_4$ on Ni-Base Aluminide

Visual inspection and weight changes during test indicated an extent of attack comparable to that previously observed with Na_2SO_4 deposits exposed in the same gaseous environment. Metallographic examination also showed the

substantially corroded but still intact coating observed previously (Figure 43). Somewhat surprisingly, there was no indication of the chloride-type attack observed in concurrently tested specimens and in the sample of aluminized IN 792 exposed to 30 ppm NaCl vapor in a previous test.

4) Thick Deposit and Vapor Honing Effects

Testing of a CoCrAlY specimen coated with a 5 mg/cm^2 salt deposit was terminated after 20 hours because visual inspection indicated substantial corrosion; surface condition before and after water washing and depth of attack revealed by sectioning the specimen are shown in Figure 44. Note the chloride-type attack, in spite of the very thick salt deposit.

The specimen was replaced with one prepared by masking half of the surface with tape and vapor honing the other half; Figure 45 shows the pre-test surface condition and the dramatic difference in extent of attack after 20 hours exposure. Sectioning of the specimen showed material consumption to a depth of about $100 \mu\text{m}$ on the vapor honed half versus a maximum depth of about $50 \mu\text{m}$ on the masked surface.

5) Na_2SO_4 and Mixed Sulfate Deposits on Alumina

Deposits of 1 mg/cm^2 of Na_2SO_4 and $\text{Na}_2\text{SO}_4 - 50\% \text{ CoSO}_4$ were applied to single crystal tablets of high purity alumina. On visual inspection after a 20-hour exposure, the Na_2SO_4 deposit was of uniform thickness except for small areas where flakes of salt had spalled off; there was no clear evidence that the deposit had melted (Figure 46a). In striking contrast, the mixed sulfate deposit was small globules of solidified liquid (Figure 46b).

After water washing to remove the residual salt, the surfaces of both tablets appeared to be lightly etched. However there was no measurable weight loss and no aluminum was detected in the wash solution.

c. Summary and Discussion of Mixed Sulfate Experiments

No effect of mixed sulfates, other than depression of the melting point of a salt deposit, was observed in these tests.

Depression of the melting point may be extremely important, however, and intimately connected with SO_3 effects. The experiment with salt deposits

on high purity alumina has important implications in this respect. The deposit of 100% Na_2SO_4 barely (if at all) melted,* while that of mixed Na_2SO_4 - CoSO_4 was highly fluid. Yet in previous experiments there is apparently no question that deposits of 100% Na_2SO_4 applied to metallic specimens were definitely molten at the 704°C test temperature, even at 0.0001 atm SO_3 pressure. The correlation of all of these observations suggests that a deposit of Na_2SO_4 at 704°C must react with a metallic impurity before it melts. The only reasonable source of such an impurity in these experiments is transient oxidation products, such that cobalt (or nickel) sulfate is formed via $\text{CoO} + \text{SO}_3 \rightarrow \text{CoSO}_4$, which serves to lower the melting point of the deposit.

More rapid melting of an applied deposit which already contained sufficient metallic sulfate to depress its melting point would explain the observation that the CoSO_4 and ZnSO_4 specimens showed significantly greater surface degradation (versus previous tests with Na_2SO_4) in the initial 20-hour exposure cycle. However both the weight changes and post-test metallography showed no increase in the rate of the propagation stage of hot corrosion due to the mixed sulfates.

4. PRELIMINARY BURNER RIG TESTING

Controlled atmosphere tube furnace testing of the type so far described in this report has the advantage of low cost, experimental convenience, and generally good control over test conditions. Obviously, however, burner rig testing better simulates the conditions experienced by turbine hardware - i.e. condensation of salt from a combustion flame and hot corrosion induced by the condensed salt and gas chemistry. Hence, one of the purposes of the furnace testing so far described was to select conditions for burner rig experiments in which the only test variable would be the amount of salt ingested into the combustor. Although a linear correlation between ingestion rate and deposition rate would not necessarily be expected, the deposition

*An experiment performed on another program with Na_2SO_4 salt on platinum foil showed that the SO_3 pressure alone (0.0007 at 704°C) was not sufficient to melt pure Na_2SO_4 .

rate, in principle at least, is easily measured with an inert probe in the gas stream, and severity of attack, determined by visual inspection, weight changes, and metallography as in the tube furnace experiments, can be evaluated as a function of deposition rate.

It was decided to perform all burner rig tests at 704°C, since both experimental results and service experience show that hot corrosion near this temperature can be severe. The most suitable salt appeared to be ASTM standard sea salt, having been widely used by other investigators and the results of the tube furnace experiments presenting no compelling reason for choosing anything else.

A high velocity ducted burner rig (Figure 47) previously used for oxidation and hot corrosion testing at relatively high temperatures (870 to 1000°C) was equipped with provision for mixing SO₂ with the primary air supply. To achieve the lower test temperature desired for this program, the burner rig operating parameters (primary air pressure, secondary air pressure, and fuel pressure) were adjusted empirically until a suitable temperature distribution on dummy specimens was measured with a calibrated infrared pyrometer. Testing was initiated using a salt ingestion rate of approximately 0.9 grams/hour, based on experience from a previous program. An SO₂ flow rate of 30 liters/hour was arbitrarily chosen to compromise between a desire for high SO₃ pressure to accelerate testing and environmental considerations which dictated minimizing the SO₃/SO₂ effluent to the atmosphere.

The initial experiment was terminated after 26 hours because a large mass of carbon was building up inside the burner rig and small amounts appeared to be depositing on the specimens as well. However a cross section of the CoCrAlY coating showed nodular attack of morphology resembling that of the 704°C tube furnace tests (Figure 48), in spite of the low SO₃ pressure (calculated as 5.3×10^{-7} atm, assuming 0.1 wt% sulfur in the fuel and equilibrium at the specimen temperature) and operating conditions in which carbon was being deposited on the burner liner and probably on the test specimens.

Fortunately a new fuel nozzle and minor changes in air pressures eliminated the coking problem, and testing was resumed using a salt solution of MgSO_4 - Na_2SO_4 and a higher flow rate of SO_2 (60 liters/hour). The sulfate salt was used to avoid any possibility of reducing the SO_3 pressure by sulfidation of the chloride content of the sea salt. These conditions resulted in relatively little surface degradation but substantial and apparently deep pitting attack as shown in Figure 49. Although the type and severity of this attack seemed appropriate, it was discovered during the test that the electronic Hastings gage being used to monitor the SO_2 flow rate was apparently being affected by the burner rig vibration. Testing was therefore interrupted to install a ball flowmeter in the SO_2 line to confirm the Hastings gage reading.

Metallographic examination of the CoCrAlY specimen tested with the $\text{Mg-Na}_2\text{SO}_4$ salt mixture confirmed deep pitting after only 10 hours exposure time (Figure 50). Since the SO_3 pressure at the 60 liter flow rate was apparently high enough (calculated as 5×10^{-5} atm) to promote substantial attack, it was decided to resume testing with the ASTM sea salt for the compatibility with other programs which was originally the reason for choosing it.

5. HOT CORROSION - SALT DEPOSITION DEPENDENCE TESTS

a. Ducted Burner Rig

Four ducted burner rig tests were run under nominally identical conditions except for the salt ingestion rate. The initial rate was that used in a previous program and in the preliminary experiments to set up the rig for this work; the other three were chosen based on results of the preceding test.

Ingestion rates, calculated salt fluxes, and measured deposition rates are listed in Table III. Considerable scatter in deposition rate measurements was encountered, especially at the high deposition rate where salt tended to spall off and at the low rate where weight changes of the platinum probe were small. Further, the deposit was not of uniform thickness and the area covered by salt was not restricted to the exposed gage section be-

Concentration of Salt Solution grams/liter	Flow Rate liters/hr	Ingestion Rate grams/hr	Salt Flux mg/cm ² /hr	Deposition Rate mg/cm ² /hr
3.78	0.227	0.585	42.33	0.3
18.90	"	4.290	211.64	5.0
0.74	"	0.168	8.29	0.1
0.36	"	0.082	4.04	Not Measurable

Table III. Conditions for hot corrosion - deposition rate dependence tests in ducted burner rig. Ingestion rate = concentration x flow rate and was varied by adjusting the concentration of the salt solution. Salt flux = ingestion rate ÷ area of burner rig nozzle. Deposition rate was measured by weighing an inert platinum probe exposed concurrently with the specimens.

cause of leakage around the oversize holes for insertion of the specimens into the transition duct. It is clear, however, that only a small fraction (of the order of 1%) of the total salt flux deposited on the leading edges of the specimens, and there was no visually discernable salt on the trailing edge.

Weight change data for the three tests in which $\Delta M/A$ was measurable are plotted on the same scale in Figure 51 to show parallel behavior of the CoCrAlY and X-40 which indicates that the data are internally consistent. Maximum attack was encountered at the intermediate deposition rate. At the lower rate, general surface degradation was much less extensive, but small pits were observable after the first hour of testing.

Depth and morphology of hot corrosion attack of the CoCrAlY specimens was determined by conventional metallography of cross sections through the exposed portion of the cylinder. The X-40 was not examined, since performance of the uncoated alloy was of limited practical concern.

Photomicrographs showing the nature and severity of attack of the CoCrAlY specimen at the 0.3 mg/cm²/hr deposition rate are presented in Figure 52. As expected, the cross section through the cylinder showed a marked angular dependence of severity of attack, with the portions of the leading edge exposed to high angle impingement of the salt-containing gas stream being more deeply corroded than the sections which experienced low angle gas impingement. The trailing edge showed no discernable micro-

structural degradation, apparently indicating that the temperature and gas chemistry of the test were innocuous in the absence of a condensed salt deposit.

In the second test, at a higher deposition rate, the general surface degradation and localized pitting attack shown in Figure 53a were observed after 28 hours, and a deposit of the thickness shown in Figure 53b built up during the final overnight run prior to termination of the test. Detailed examination of the surface condition after 47 hours showed that many of the small pits observed at 28 hours apparently had not grown on further exposure; also the final weight loss was not as large as expected from the projection of the curve established by previous weighings. Such behavior - i.e. the failure to sustain a rate of hot corrosion propagation apparently established in previous exposure periods - is not uncommon in burner rig testing but is rarely observed under the more precisely controllable conditions of tube furnace experiments. An obvious possibility is a decrease in the severity of the reactive environment due to random fluctuations in burner rig operating conditions, with a ducted rig being perhaps especially susceptible to random variations in SO_3 pressures. Also, especially in the case of this test, the large ingestion rate may have built up a deposit of such thickness that the innermost salt/metal interface was protected from the effects of the reactive gaseous environment. Neither of these rationalizations, however, is supported by the large weight loss of the concurrently tested X-40 (see Figure 51).

Post-test metallography on three sections through the CoCrAlY specimen showed maximum attack of about 50 μm and evidence of substantial chloride-induced dealloying in some areas (Figure 54). Of course it was initially suspected that the large amount of salt was not completely sulfated, but simple calculation showed that the moles of SO_2 added to the burner rig air supply was almost two orders of magnitude greater than the moles of chloride in the ingested sea salt and chemical analysis of the deposit washed from the sample indicated no detectable chloride.

At the 0.168 g/hr ingestion rate, surface degradation of both CoCrAlY and X-40 were detectable after 1 hour of testing, and small but clearly measurable weight losses of the X-40 indicated continuing corrosion during a 61-hour exposure. Post-test metallography of the CoCrAlY showed less attack than anticipated from the surface condition; microstructural degradation in most areas was negligible and the deepest pit observed on several planes of polish was about 20 μm (Figure 55).

Based on the result just presented, it was decided to run the burner rig at the lowest reasonable salt ingestion rate and determine if detectable corrosion could be observed in exposure times comparable to those of the previous tests. The last value in Table III corresponds to only 22 grams of sea salt in the 16 gallon (60.5 liter) tank being used to feed the solution into the burner.

Visual observation of the CoCrAlY specimen after 2 hours of testing and careful water washing to remove rig spatter showed small green areas where the oxidation product was not the uniformly protective alumina characteristic of the trailing edge. Testing was continued, and the surface condition documented after a total exposure time of 6 hours (Figure 56). Continued exposure for a total of 21 hours resulted in slightly increased darkening of the leading edge surface, and careful examination with binocular and metallurgical microscope showed small pits of depth and frequency greater than attributable to oxidation in the absence of a condensed salt deposit.

No apparent differences in the general surface condition of the leading and trailing edges were evident on post-test scanning microscopy. Also the dull green areas observed on visual inspection were not discernable on the SEM, even though the transition between a greenish-colored area and the surrounding gray alumina had been marked with a microhardness indenter. However the line of fine dots marked in Figure 56 was found to be a series of small pits, typically of the size, depth, and morphology shown in Figure 57. Examination of randomly selected areas suggested that the entire leading edge was characterized by numerous pits of this type (of the order of 100 per cm^2), and no features of this nature were observed on the trailing edge.

The specimen was cut for metallography approximately in the center of the test zone. Metal consumption up to 5 μm was observed in several areas (e.g. Figure 58a), and the corrosion products were rich in sulfur (Figure 58b).

The surface features in Figures 56 - 57 and the sulfur enrichment in the shallow pit of Figure 58 are considered unequivocal indication of hot corrosion attack induced by salt condensed from the burner rig flame. Such attack occurred even though the salt deposition rate was barely discernable by visual inspection. Moreover the fact that degradation of this extent was observable after a relatively short testing time is believed to represent an unacceptable rate of hot corrosion.

b. Tube Furnace Test with Various Deposit Thicknesses

To supplement the results of the burner rig experiments on severity of hot corrosion versus salt deposition rate, the effect of deposit thickness on furnace hot corrosion was studied by applying deposits of 1/8, 1/4, 1/2, and 1 mg/cm^2 of Na_2SO_4 on CoCrAlY and exposing the samples at 704°C and $P_{\text{SO}_3} = 0.0007$ atm, a total exposure time of 100 hours was accumulated in five 20-hour cycles with washing and reapplication of fresh salt after each cycle. A fifth specimen with 1 mg/cm^2 of salt was exposed continuously without washing and application of fresh salt (although it was removed from the furnace with the others every 20 hours).

Visual inspection after 20 hours showed an obvious dependence of severity of attack on amounts of applied salt (Figure 59). The difference in surface condition became less apparent as all of the specimens continued to degrade on further exposure, although weight change data remained remarkably consistent up to 100 hours (Figure 59). Post-test metallography showed that even the specimen with the thinnest deposit had suffered consumption of up to half of the coating thickness.

A previous test of this type with salt deposits of 1/4, 1/2, 1, 2, and 5 mg/cm^2 was suspect because of furnace contamination with condensed SO_3 . Nevertheless, the samples had been concurrently exposed to the same temper-

ature and atmosphere, so the comparison of their relative performance as a function of deposit thickness should be valid. At $1/4$, $1/2$, and 1 mg/cm^2 , severity of attack clearly increased with increasing deposit thickness, but the specimens with 2 and 5 mg/cm^2 of salt experienced smaller weight losses and less penetration than with the thinner deposits.

Finally, the case in which a specimen was continuously exposed without reapplication of fresh salt has interesting implications. A single weighing after 100 hours showed a loss of 22 mg/cm^2 (versus a total weight loss of 77 mg/cm^2 for the specimen where a fresh deposit of the same thickness had been reapplied every 20 hours), and post-test metallography also showed less attack. Experiments on another program, however, are suggesting that an initially applied salt deposit will be an effective corrodent for a substantial period, as long as SO_3 is continuously supplied by the gaseous environment. Hence the primary effect of applying fresh salt may be the scale spallation due to washing and mechanical handling rather than a necessity of supplying fresh salt to maintain continuing corrosion. Such a hypothesis suggests that any salt deposit, no matter how small or thin, is capable of causing significant corrosion.

c. Summary and Discussion of Hot Corrosion-Salt Deposition Dependence

Both the burner rig tests with varying deposition rate and the tube furnace experiments with varying thickness of applied deposit show a strong dependence on severity of attack on the amount of salt. Under conditions where the rate of attack is influenced by a partial pressure of gaseous sulfur trioxide maintained by an external source (rather than decomposition of a salt deposit on thermal cycling), it appears that maximum corrosion will occur at intermediate deposit thicknesses of the order of 0.1 to 1 mg/cm^2 . Within this range, severity of attack will consistently and reproducibly increase with increasing deposit thickness. Amounts greater than 1 mg/cm^2 , however, will not significantly increase the severity of attack.

In the direction of thinner deposits and low deposition rates, an amount of salt at which hot corrosion can be regarded as negligible will be

very difficult - if not impossible - to define. It is unlikely, for example, that a very small amount of salt will be uniformly distributed over a large area. More likely, a small area will be covered with a deposit of sufficient thickness to affect oxidation behavior, and any adverse effect of any detectable salt deposition cannot safely be neglected.

SECTION III

SUMMARY AND CONCLUSIONS

1. DEPENDENCE OF HOT CORROSION ATTACK ON SO_3 PRESSURE

Specimens of uncoated and aluminized Mar-M509 (Co-base), uncoated and aluminized IN 792 (Ni-base), and CoCrAlY-coated IN 792 were exposed in a controlled atmosphere tube furnace at 704 and 899°C (1300 and 1650°F) and SO_3 pressures from 3.5×10^{-3} to 1.4×10^{-4} atm. All specimens were coated with a salt deposit of 1 mg/cm² of 100% Na_2SO_4 . Testing times up to 100 hours consisted of 20-hour cycles with washing and reapplication of fresh salt after each cycle.

A strong dependence of severity of attack on SO_3 pressure was observed on all materials. At a fixed SO_3 pressure, the Co-base systems were more severely degraded at 704 than at 899°C, excepting only the case of aluminized Mar-M509, where degradation of the relatively thin coating may have been influenced by dissolution of the β -CoAl layer by inward diffusion. Conversely, the Ni-base alloy, especially with an aluminide coating, was more resistant to SO_3 effects at 704°C but suffered almost catastrophic sulfidation at 899°C and high SO_3 pressure.

The degradation microstructures of the CoCrAlY coatings tested at 704°C were apparently indistinguishable from the features characteristic of low power marine hot corrosion (i.e. a tendency for nodular attack, a ghost microstructure in the scale, negligible or at most minimal β -depletion at the attack front). At 899°C, the corrosion products at the scale/metal interface appeared to be the same as at the lower temperatures, but there was a wide (about 25 μm) β -depleted zone and sulfide precipitation which are not typical of service-induced degradation.

2. CHLORIDE EFFECTS AND CHLORIDE- SO_3 INTERACTIONS

As expected, a high concentration of chloride in the condensed salt deposit (Na_2SO_4 - 50% NaCl) produced severe corrosion, but microstructural features were markedly dissimilar from those typical of service degradation

of shipboard engines. Also as expected, chloride vapor was observed to produce increased attack by shortening the initiation period for the onset of hot corrosion propagation. However, the rate of attack in the propagation stage was not increased by an SO_3 -NaCl synergism, even though a relatively high concentration of chloride vapor (30 ppm) resulted in microstructural features characteristic of both corrodents.

3. MIXED SULFATE EFFECTS AT 704°C

A conceptual difficulty in considering mixed sulfate effects is that a deposit of pure Na_2SO_4 becomes contaminated with metallic ions as soon as SO_3 -induced hot corrosion starts to occur. The practical question thus reduces to whether metallic sulfates deposited from an external source (e.g. metallic impurities in the fuel, metallic chlorides in sea salt, etc.) cause more severe hot corrosion than would result if the initially applied or deposited salt was essentially pure Na_2SO_4 .

A key point in this report is that mixtures of sodium and metallic sulfates will have a lower melting point than pure Na_2SO_4 . Hence the service or test conditions could be such that a deposit of externally mixed sulfates would melt immediately, while a deposit of higher purity Na_2SO_4 would remain solid or highly viscous until it reacted with transient oxidation products. Longer exposure to a more fluid deposit would tend to cause increased attack, and it is felt that such an effect was observed in this program in the case where mixed sulfate deposits with 50m% Co- and ZnSO_4 produced more surface degradation in the initial 20-hour test cycle than in the equivalent test with a deposit of 100% Na_2SO_4 . Once the deposit was effectively molten, however, there was no indication of a change in rate or mechanism of attack due to the high concentration of metallic sulfate in the applied deposit.

The conclusion that mixed sulfates have no effect other than depression of the melting point applies only to the case of relatively thin deposits where the SO_3 pressure is maintained by the gaseous environment rather than thermal decomposition of the metallic sulfate (as may occur upon thermal cycling).

4. DUCTED BURNER RIG EXPERIMENTS

Degradation microstructures apparently the same as those generated in the 704°C tube furnace experiments were produced at the same metal temperature in a high velocity ducted burner rig. Gaseous sulfur oxides were provided by mixing SO_2 with the primary air, and trial experiments were run with ASTM sea salt (approximately 58% NaCl , 26% MgCl_2 , 10% Na_2SO_4) and a eutectic mixture of MgSO_4 - Na_2SO_4 . There was no apparent difference in the microstructures produced by the sea salt and the magnesium-sodium sulfate, suggesting that the chloride in the sea salt did not play a significant role in the hot corrosion mechanism.

5. DEPENDENCE OF HOT CORROSION ON AMOUNT OF SALT

Ducted burner rig tests were run over an order of magnitude range of salt deposition rates, and severity of attack versus amount of applied salt was determined in tube furnace experiments with varying deposit thicknesses.

The flux of sea salt in the four burner rig experiments was 212, 42, 8, and 4 $\text{mg}/\text{cm}^2/\text{hr}$; accumulations of salt observed on the specimens and on an inert platinum probe showed that approximately 1% of the salt flux condensed, even at the very low ingestion rates. Maximum hot corrosion was observed in the test with 42 $\text{mg}/\text{cm}^2/\text{hr}$ flux (0.3 $\text{mg}/\text{cm}^2/\text{hr}$ deposition rate); a substantially thicker salt deposit did not increase the severity of attack. Surface degradation and depth of nodular attack were much less at the lower values of salt flux. However, the extent of hot corrosion attack, even at the ingestion rate where salt deposition was barely discernable, cannot reasonably be considered negligible.

Tube furnace tests with SO_3 in the gaseous environment also demonstrated substantial hot corrosion with the thinnest deposit considered experimentally feasible (approximately 0.1 mg/cm^2).

Limitations of time and scope of this program precluded a detailed examination of hot corrosion behavior at low deposition rates which might well be the subject of further studies. The results so far obtained support

the suspicion that any salt deposit will cause unacceptable hot corrosion, providing, of course, that the component temperature and SO_3 pressure in the gaseous environment are within the regime where hot corrosion can be induced by liquid sulfate salts. Hence a safe ingestion rate at which hot corrosion is negligible is that which does not produce any condensed deposit on the turbine components.

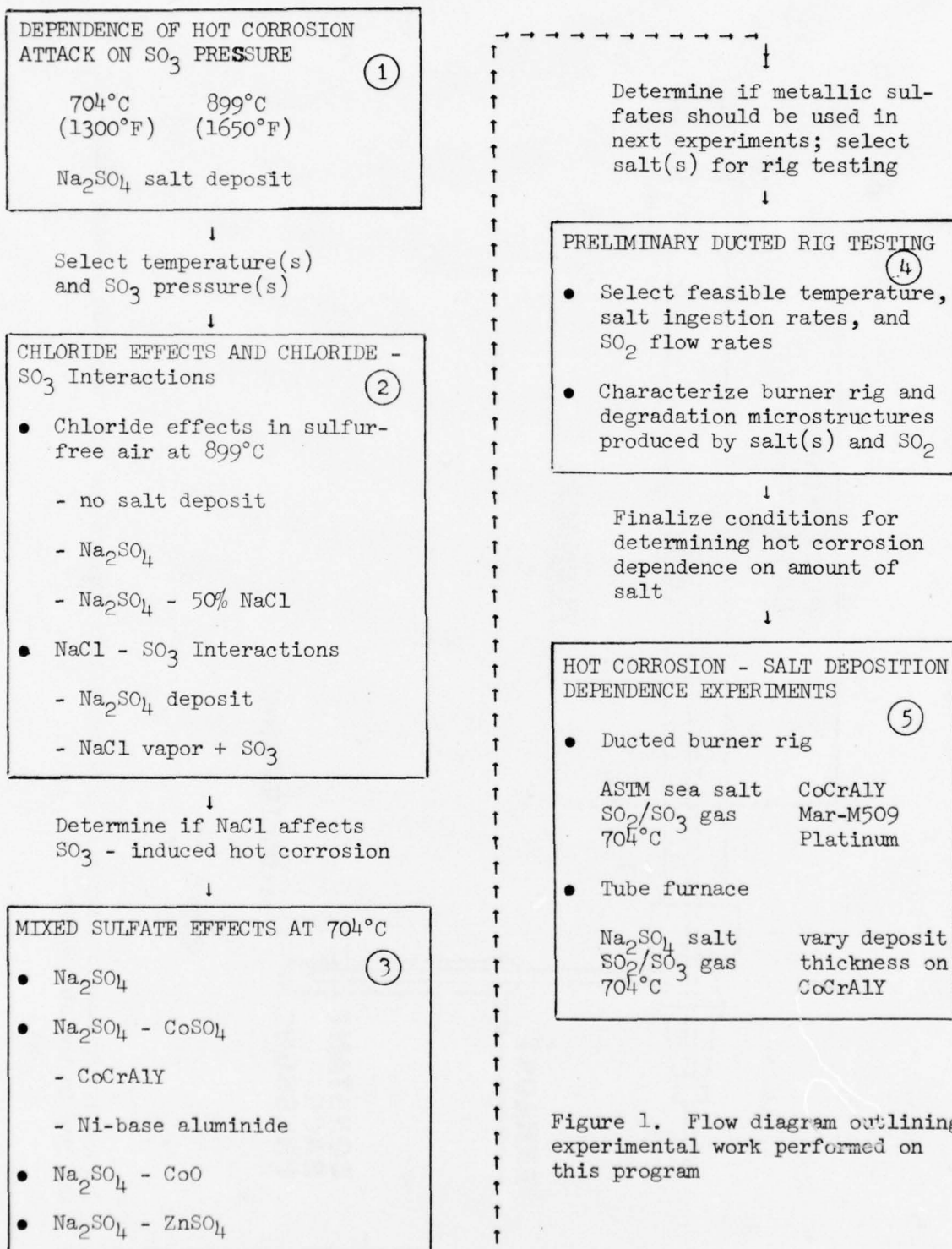


Figure 1. Flow diagram outlining experimental work performed on this program

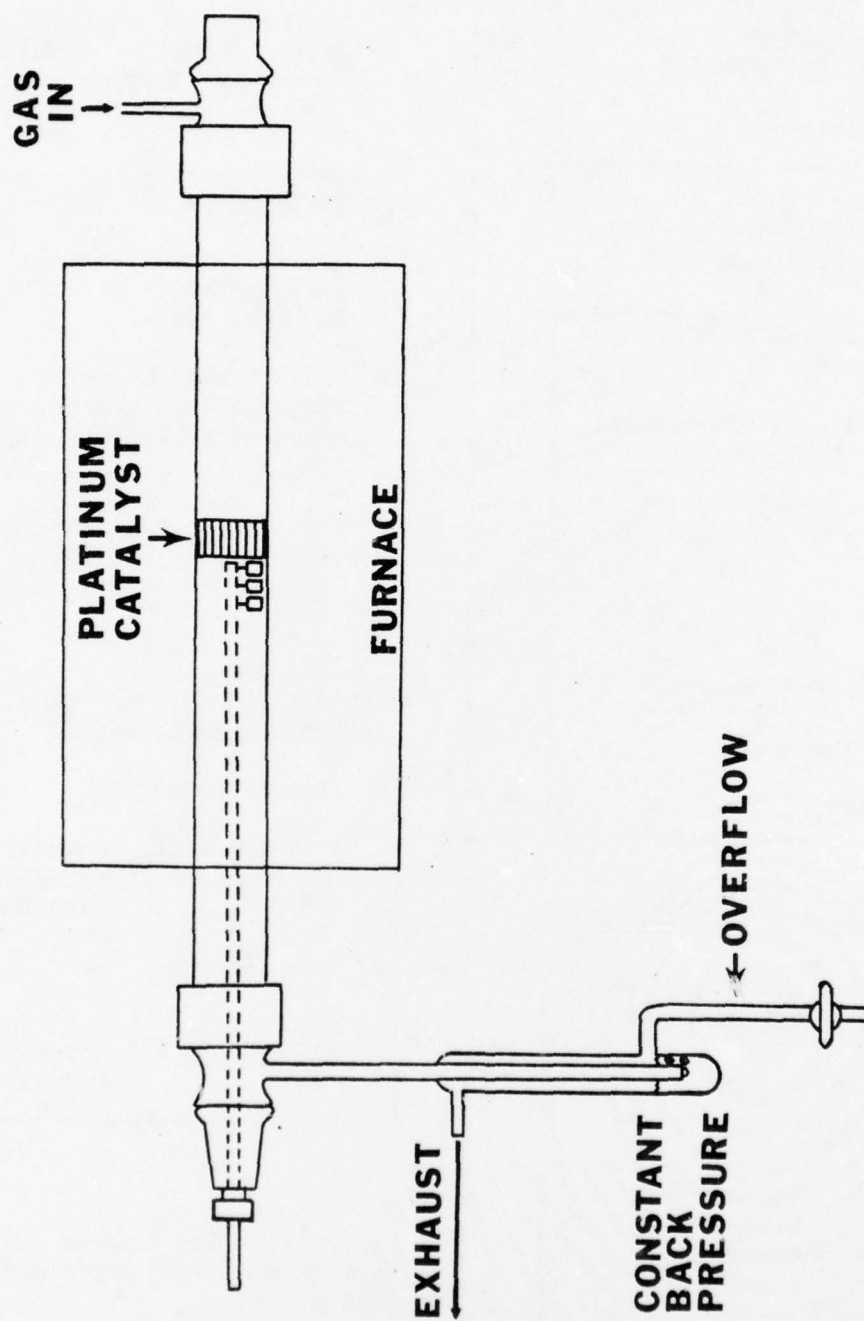
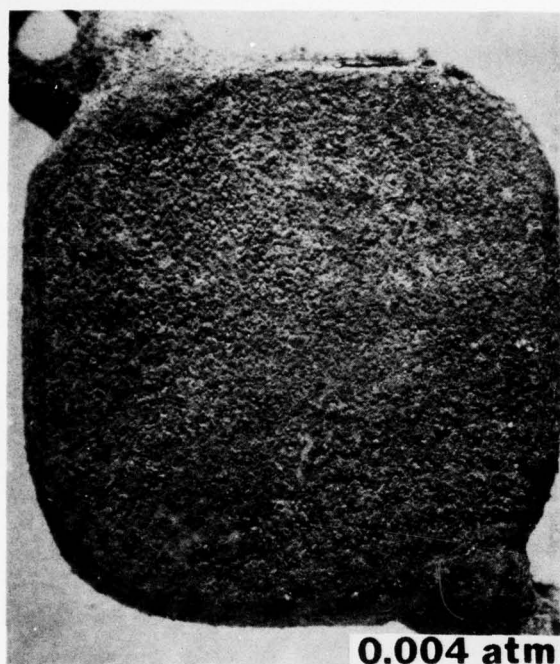


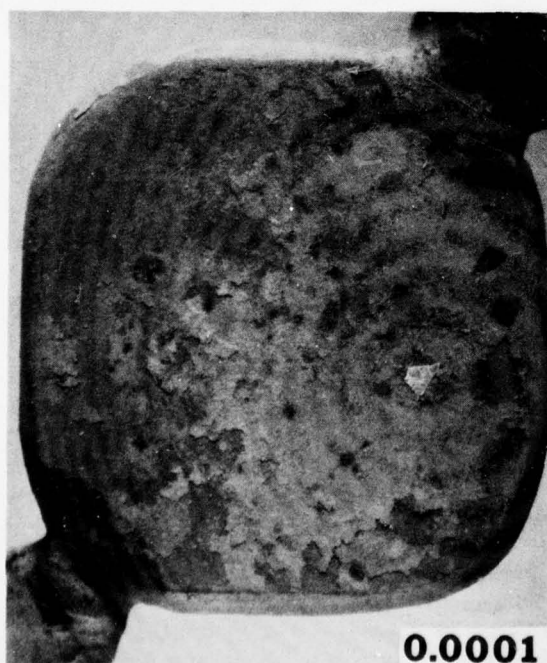
Figure 2. Schematic diagram of horizontal tube furnace for hot corrosion testing with SO_3 gas in the atmosphere.



0.004 atm



0.0007



0.0001

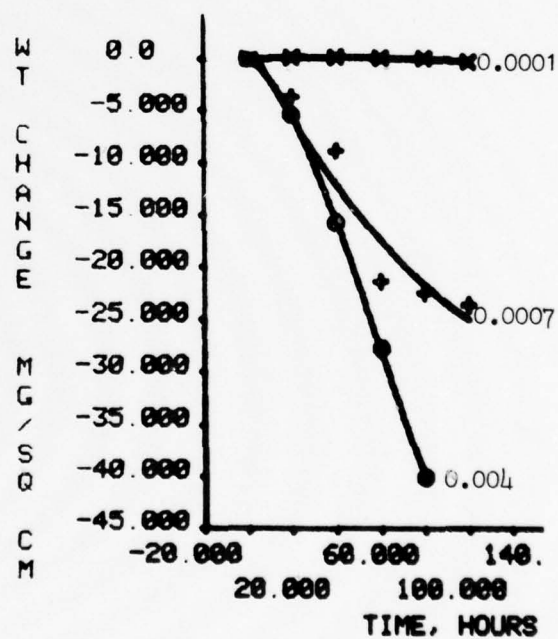
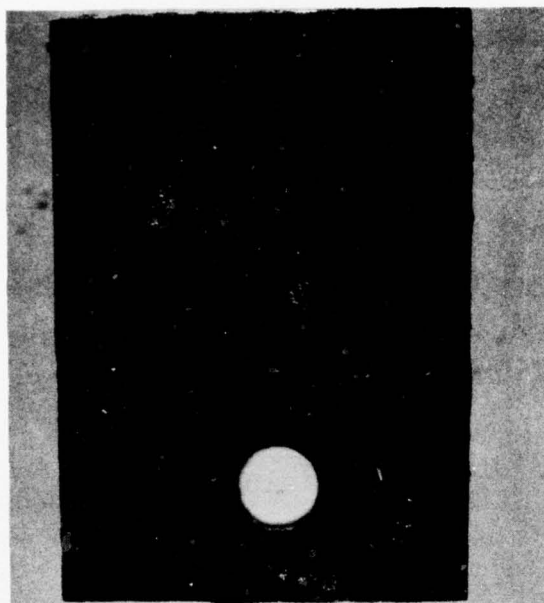


Figure 3. Effect of SO₃ pressure on 704C sulfate-induced hot corrosion of CoCrAlY-coated (PWA 68; Co - 15 to 24 Cr - 11.5 to 13.5 Al - 0.2 to 0.7 Y) IN 792, as shown by surface condition after 20 hours and weight change data for 100-hour cyclic exposure.



0.004 atm



0.0007

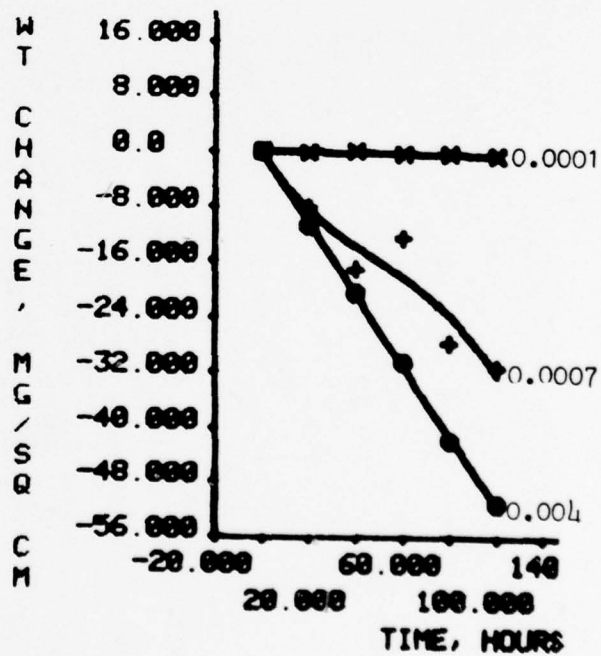


Figure 4. Effect of SO_2 pressure on 704C sulfate-induced hot corrosion of uncoated Mar-M509 (Co-23.4Cr-10.0Ni-0.2Ti-7.0W-3.5Ta-0.5Zr-0.6C), as shown by surface condition after 20 hours and weight change data for 100-hour cyclic exposure.

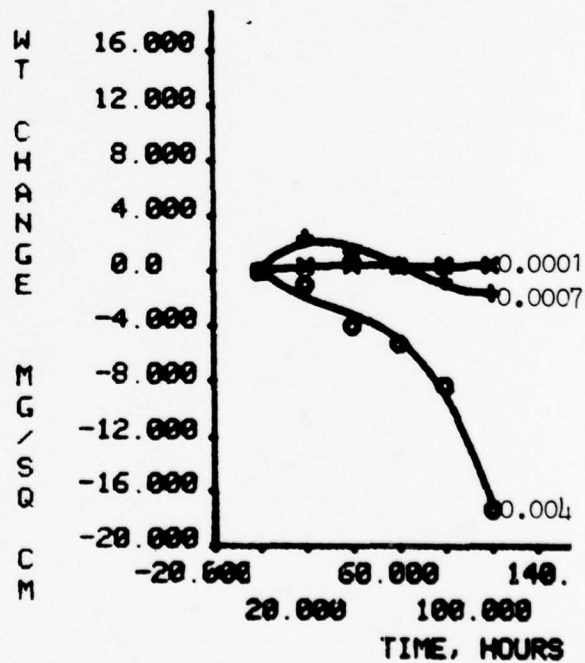
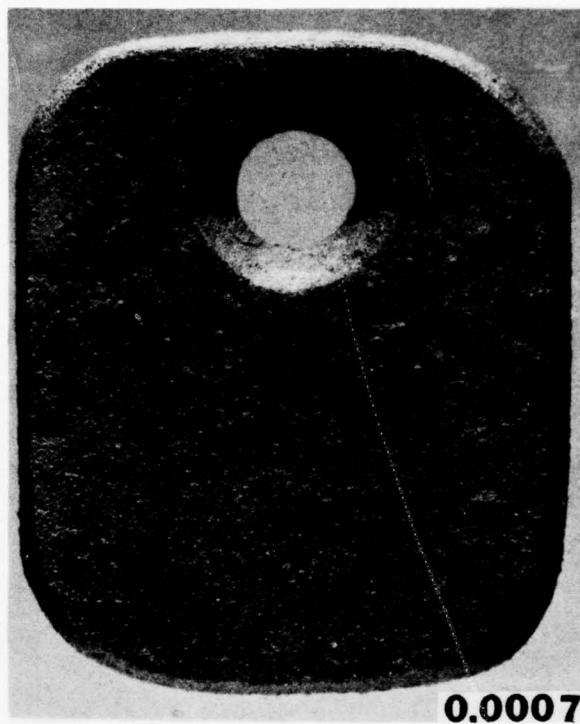
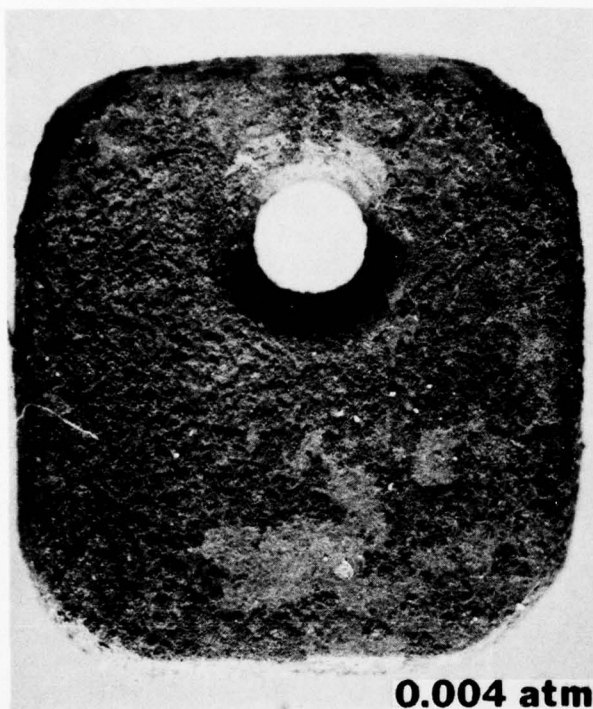
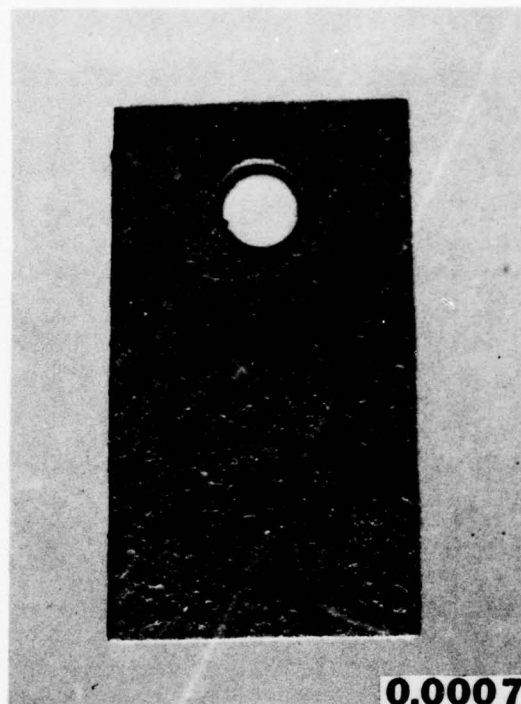


Figure 5. Effect of SO_2 pressure on 704C sulfate-induced hot corrosion of aluminized (PWA 28) Mar-M509, as shown by surface condition after 20 hours and weight change data for 100-hour cyclic exposure.



0.004 atm



0.0007



0.0001

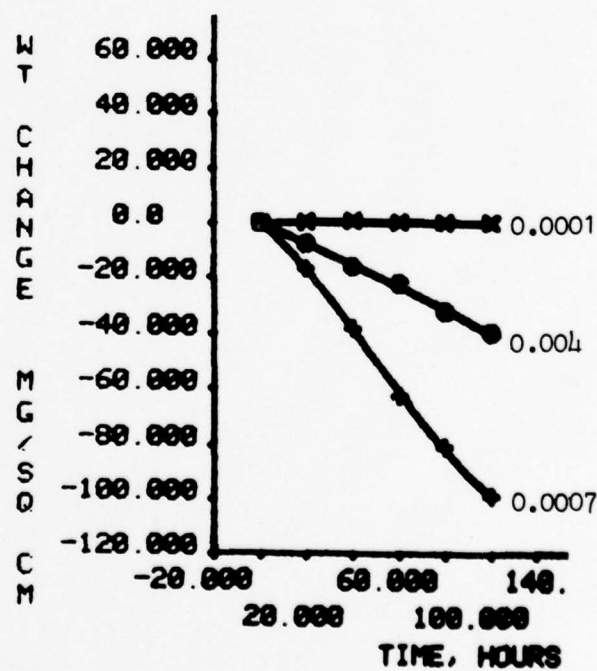


Figure 6. Effect of SO_2 pressure on 704C sulfate-induced hot corrosion of uncoated IN 792 (Ni-12.0Cr-9.0Co-4.5Ti-3.1Al-1.9Mo-3.8W-3.9Ta-0.12C-0.1Zr-0.02B), as shown by surface condition after 20 hours and weight change data for 100-hour cyclic exposure.

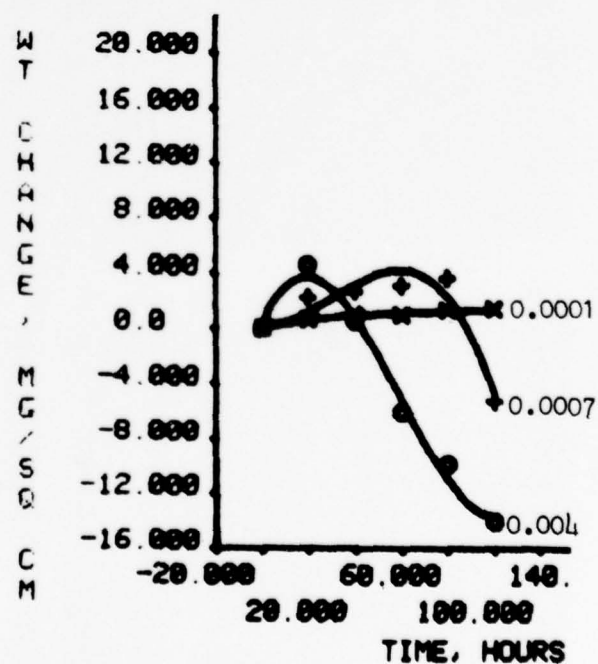
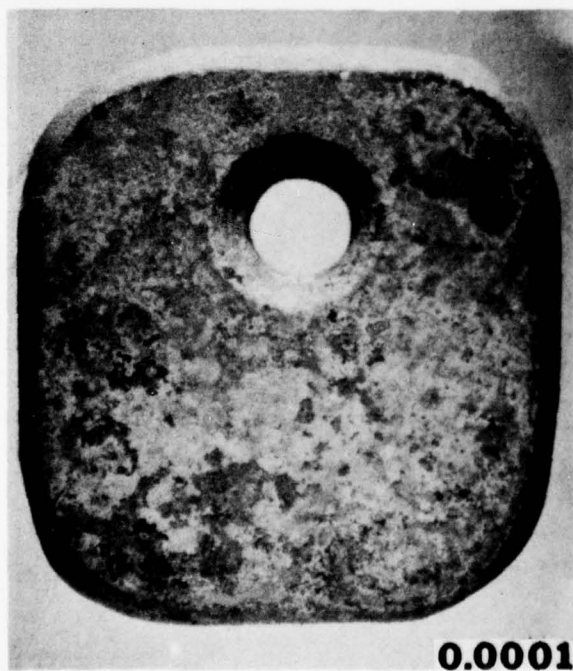
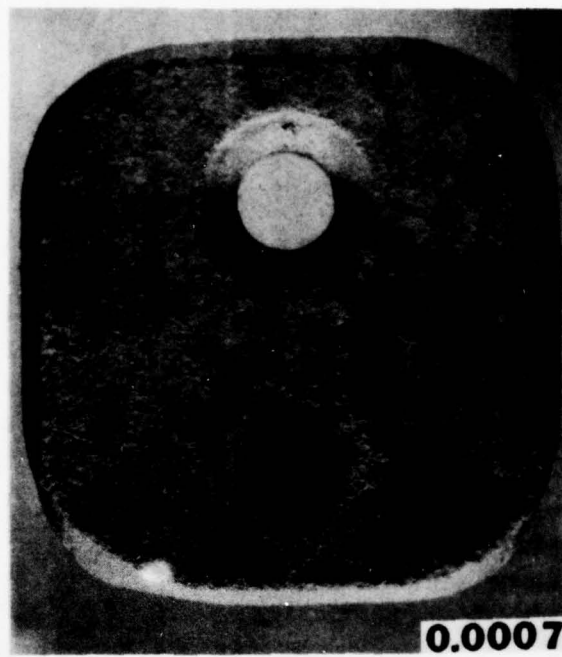
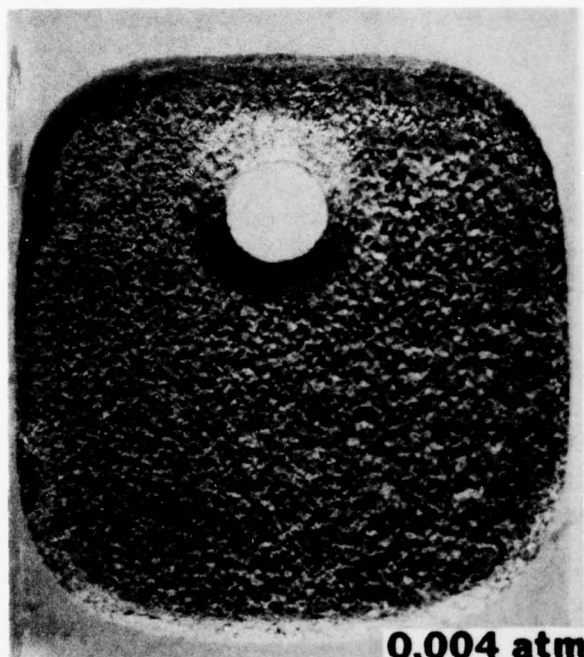
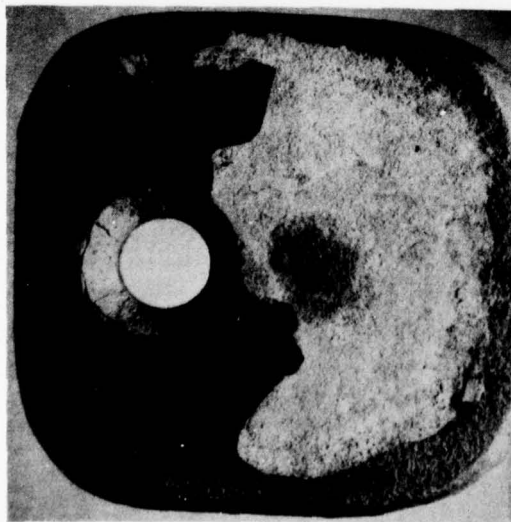
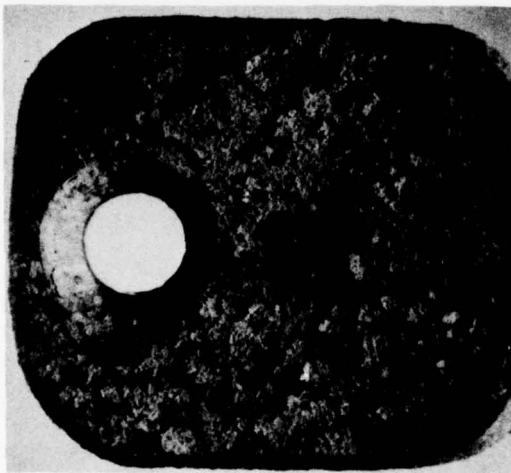


Figure 7. Effect of SO_3 pressure on 704C sulfate-induced hot corrosion of aluminized (PWA 273) IN 792, as shown by surface condition after 20 hours and weight change data for 100-hour cyclic exposure.



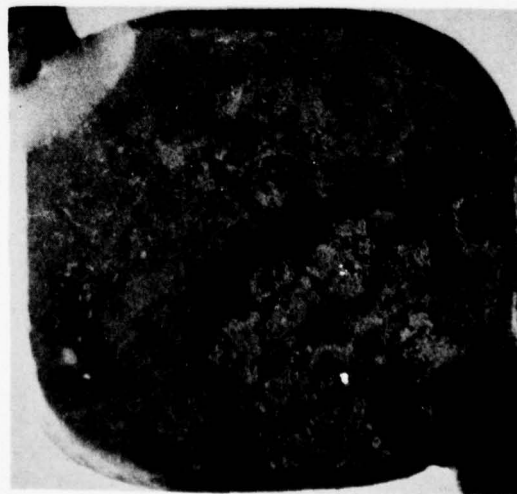
CoCrAlY, 0.0007 atm



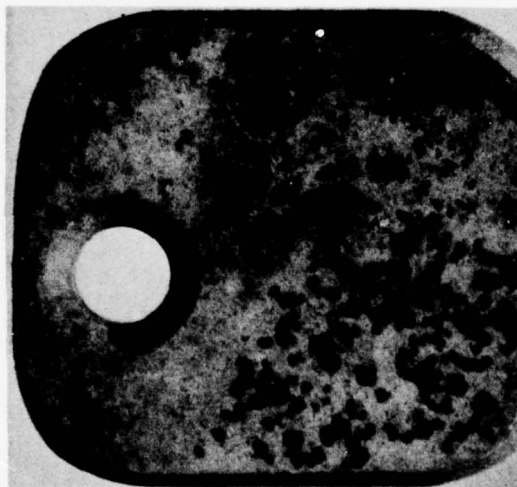
PWA 28, 0.0007 atm



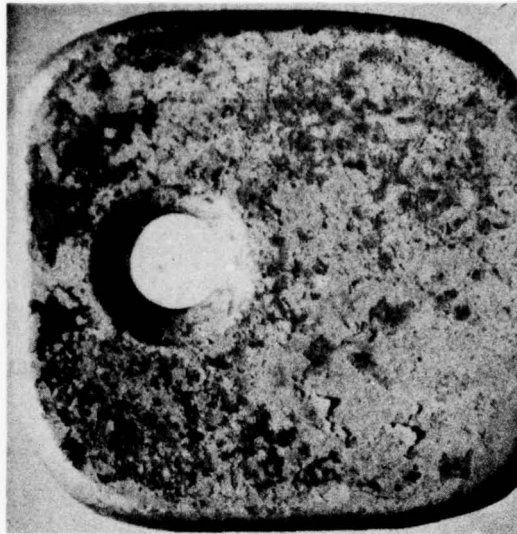
PWA 273, 0.0007 atm



CoCrAlY, 0.0001 atm



PWA 28, 0.0001 atm



PWA 273, 0.0001 atm

Figure 8. Effect of SO_2 pressure on 704C sulfate-induced hot corrosion of CoCrAlY and aluminide coatings (PWA 68 on IN 792, PWA 28 on Mar-M509, and PWA 273 on IN 792), as shown by surface condition after 100-hour cyclic exposure.

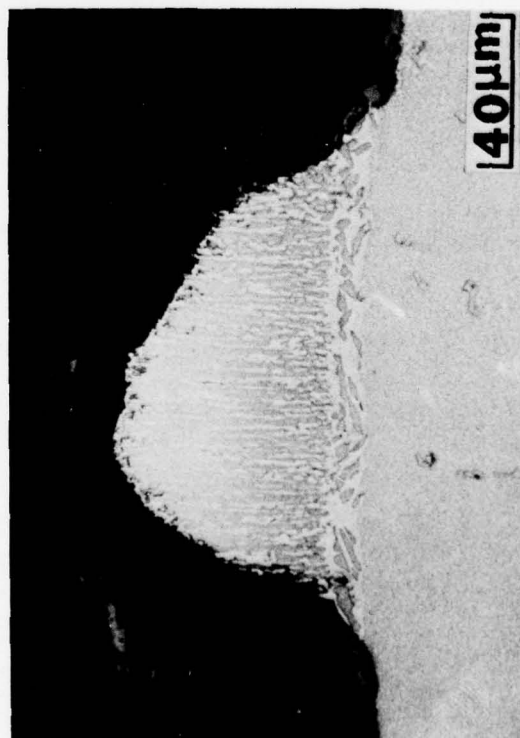
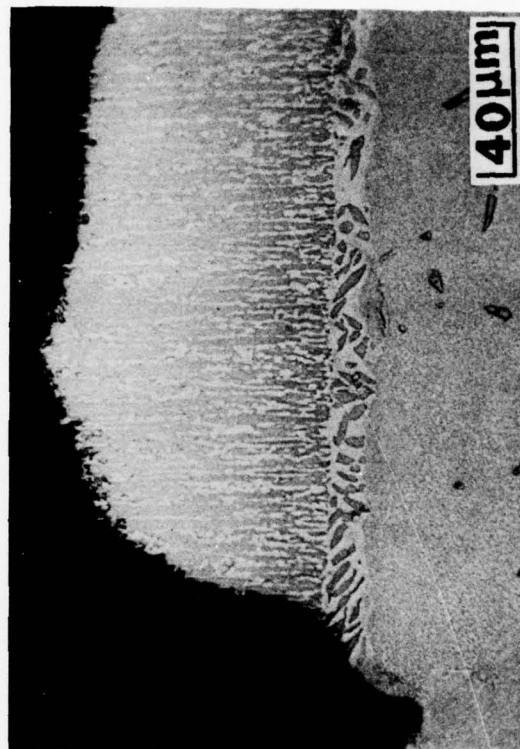
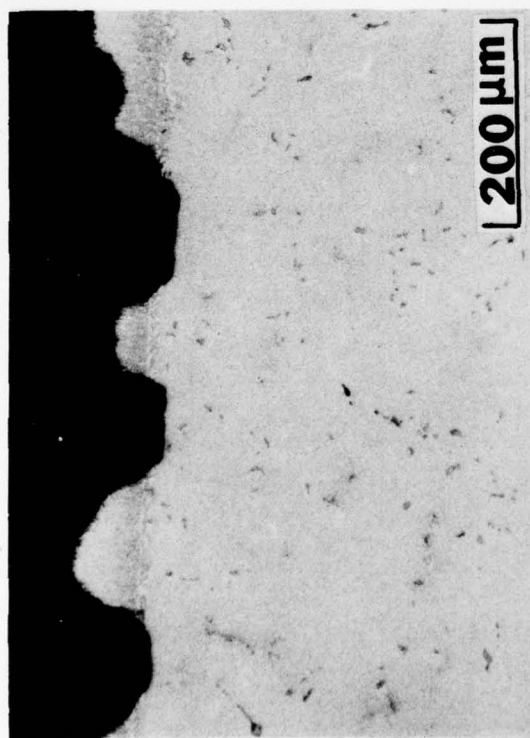
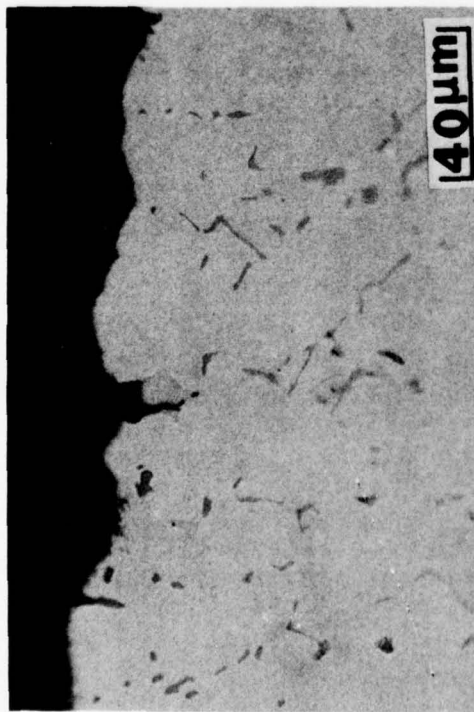
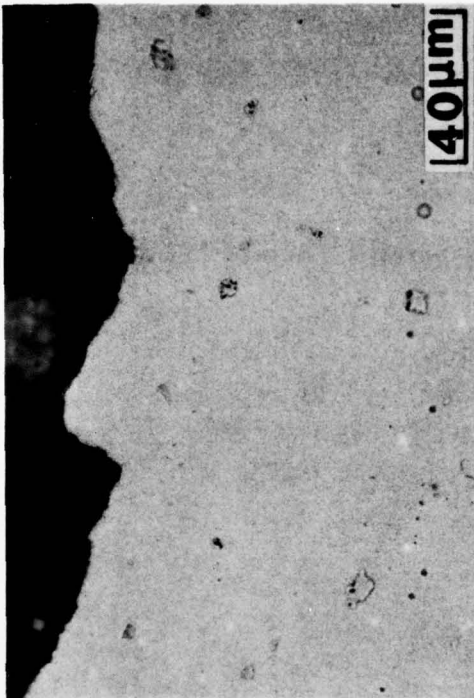


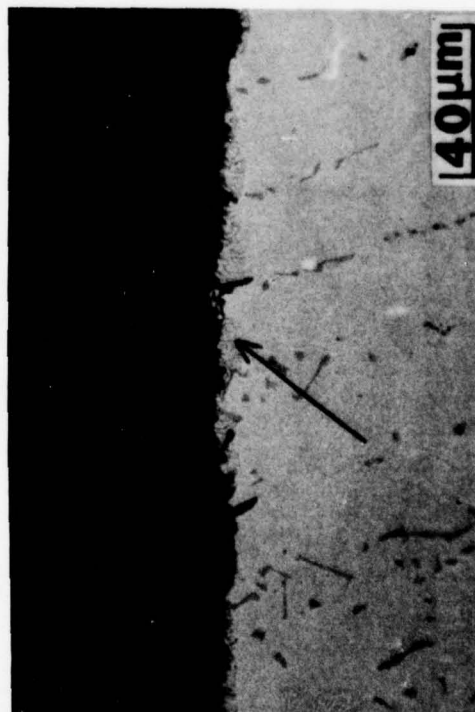
Figure 9. Typical depth of attack and nodular morphology of corrosion front produced by cyclic exposure of PWA 68 CoCrAlY for 100 hours at 704°C and $PSO_3 = 0.004$ atm. Specimen was lightly etched to emphasize coating thickness and microstructure.



10a. Uncoated Mar-M509



10b. Uncoated IN 792



10c. Mar-M509/PWA 28 aluminide



10d. IN 792/PWA 273 aluminide

Figure 10. Uncoated and aluminized alloys tested concurrently with the CoCrAlY coating of Fig. 9 (i.e. 100 hours at 704C, $PSO_3 = 0.004$ atm). Arrow in 10c shows innermost diffusion zone of the PWA 28 microstructure; the rest of the coating was completely oxidized and spalled off in most areas.

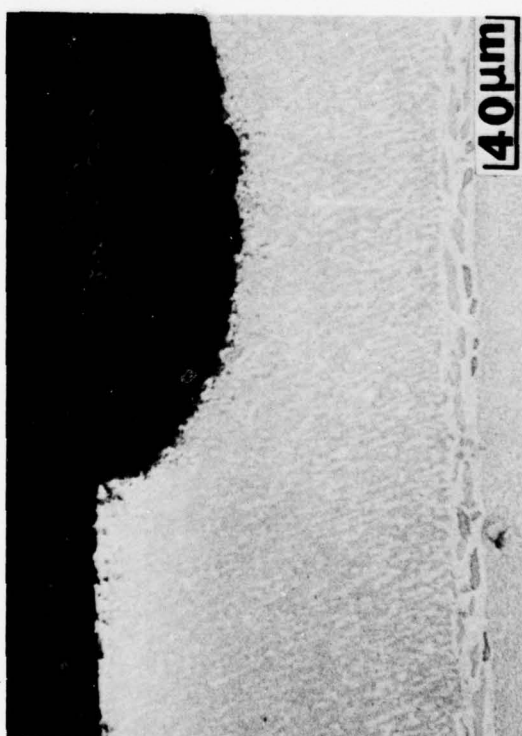
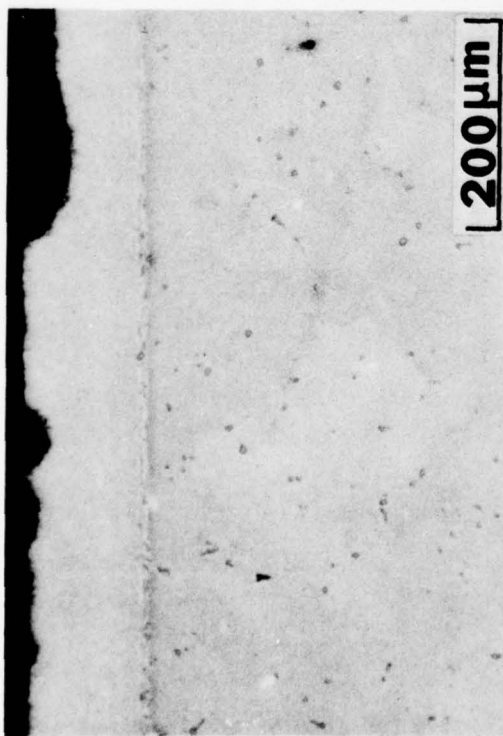
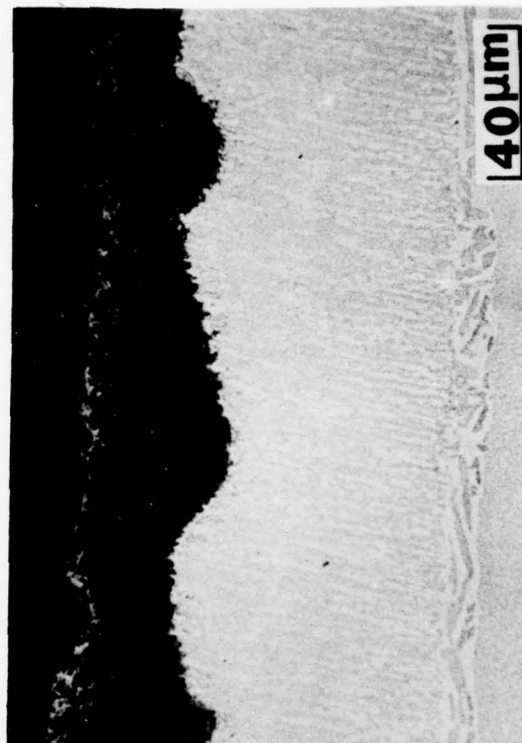
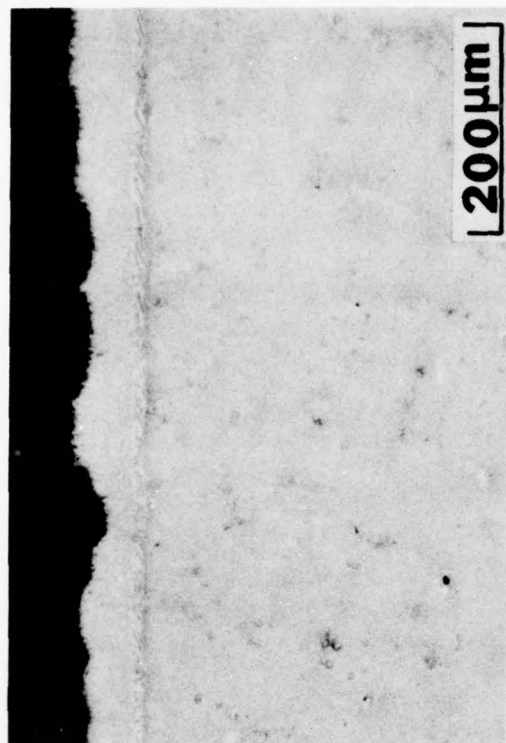
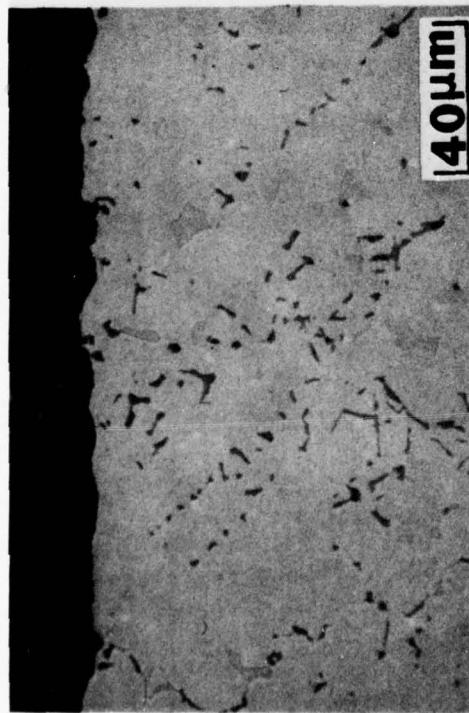
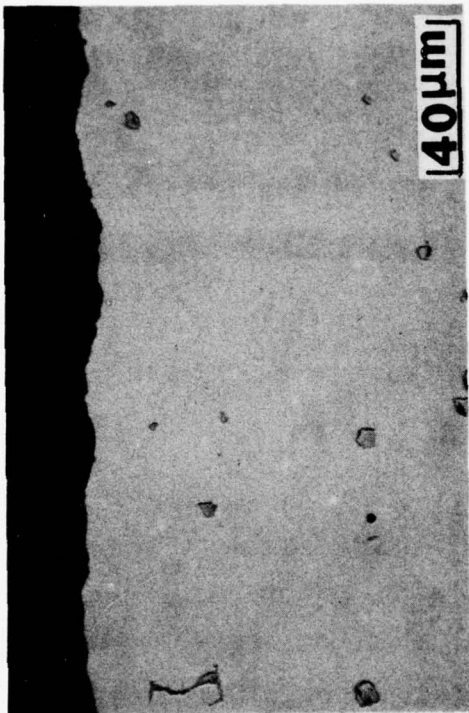


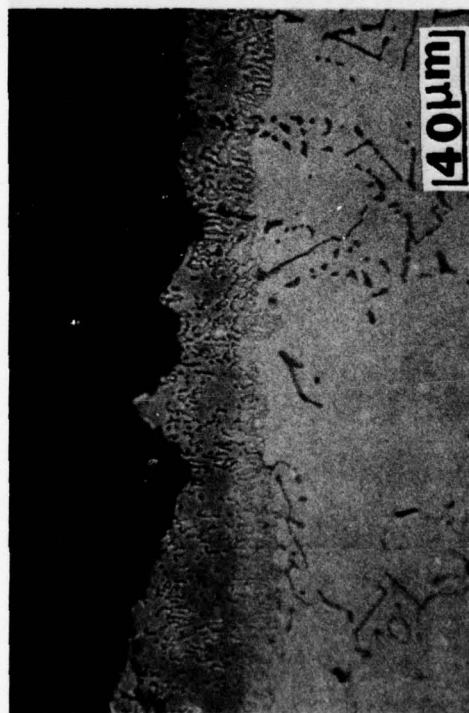
Figure 11. Typical depth of attack and nodular morphology of corrosion front produced by cyclic exposure of PWA 68 CoCrAlY for 100 hours at 704°C and $p_{SO_2} = 0.0007$ atm. Consumption of approximately half of the coating was observed in many areas, but the coating was apparently not penetrated.



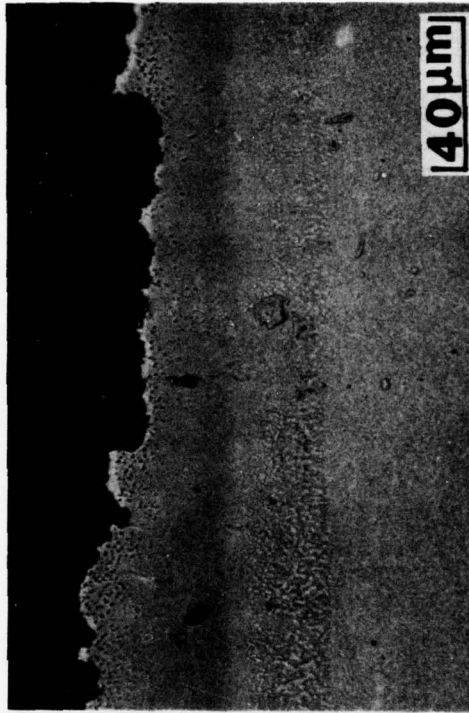
12a. Uncoated Mar-M509



12b. Uncoated IN 792



12c. Mar-M509/PWA 28 aluminide



12d. IN 792/PWA 273 aluminide

Figure 12. Uncoated and aluminized alloys tested concurrently with the CoCrAlY coating of Fig. 11 (i.e. 100 hours at 704C, $PSO_3 = 0.0007$ atm).

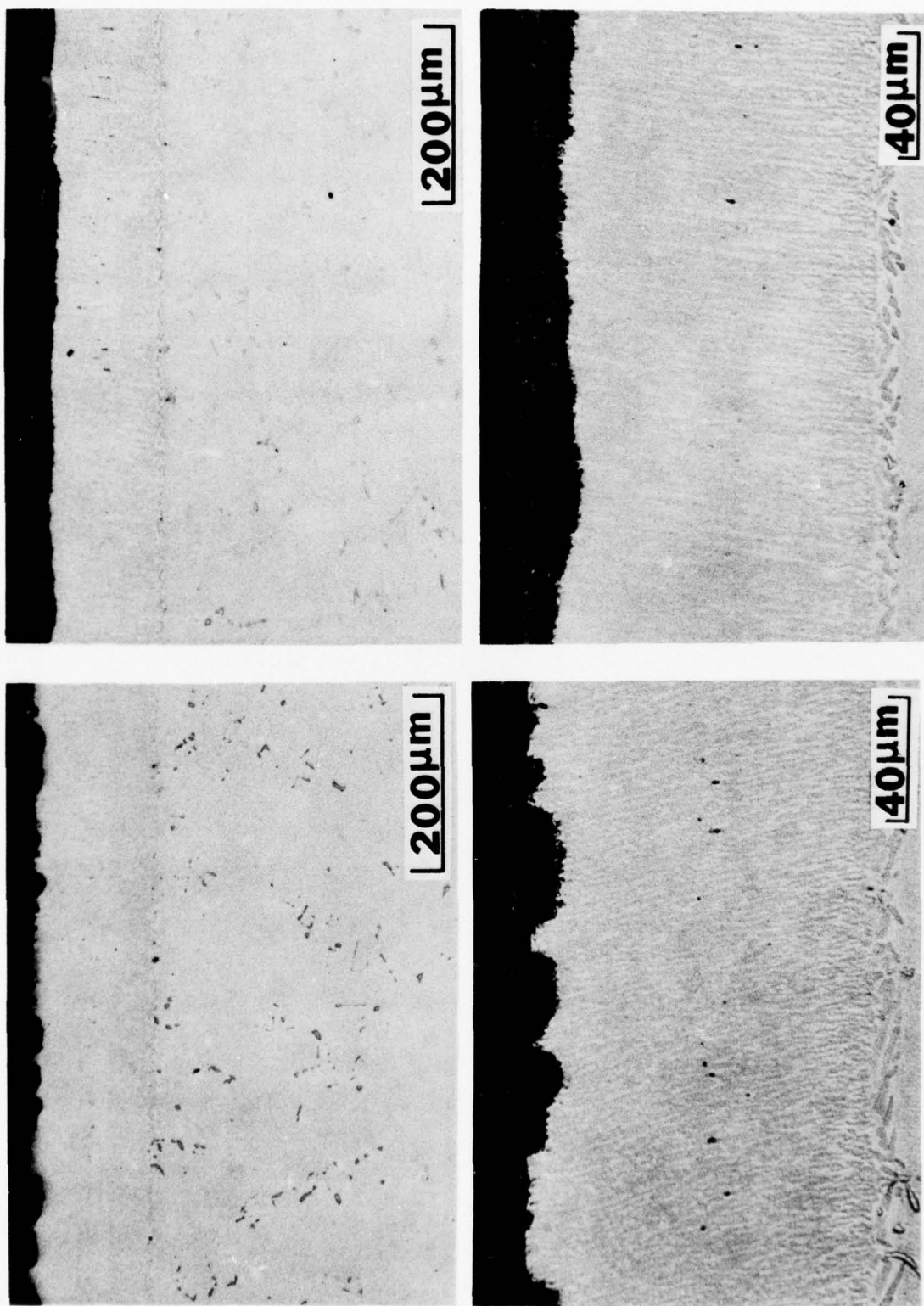
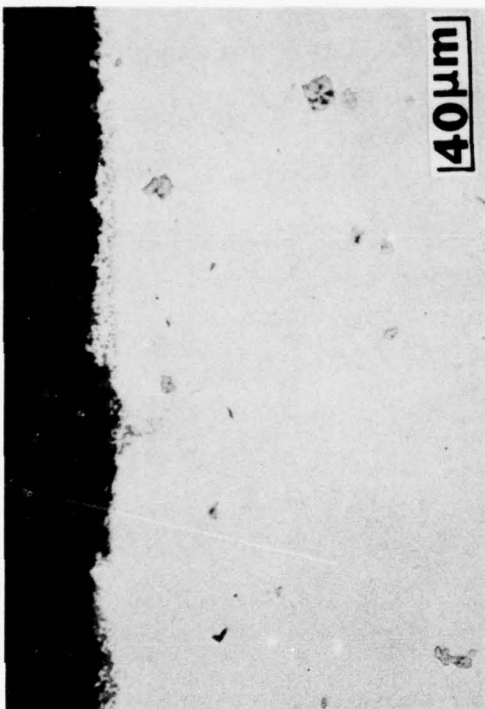


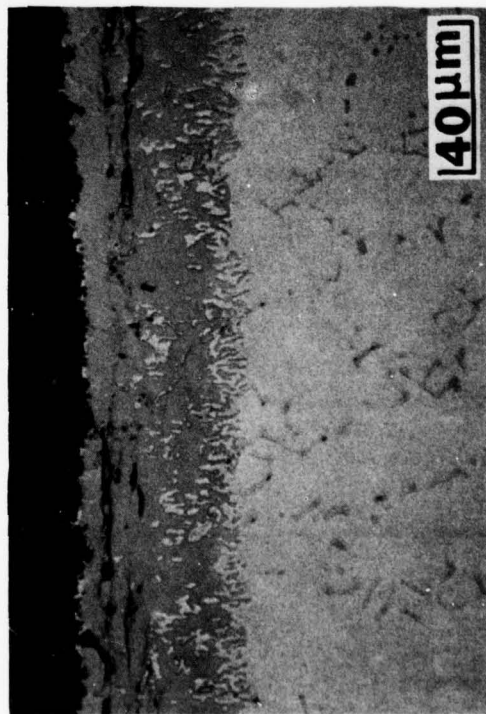
Figure 13. Typical microstructural degradation of PWA 68 CoCrAlY coating produced by cyclic hot corrosion testing for 100 hours at 704°C and $PSO_3 = 0.0001$ atm. Comparison with Figs. 9 and 11 shows effect of SO_3 pressure on depth of attack.



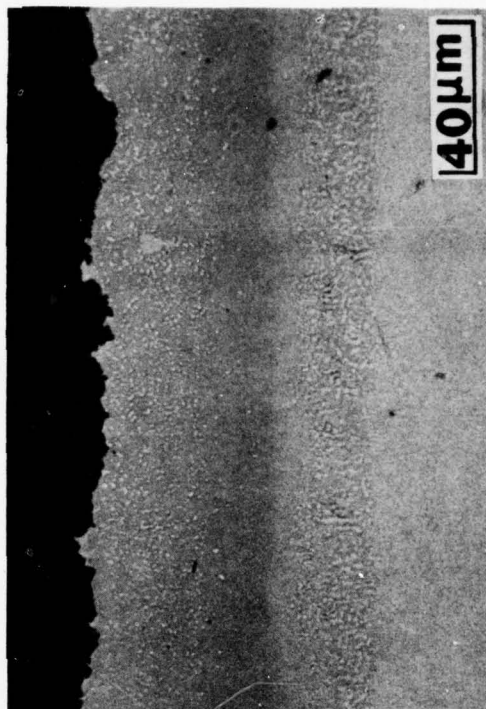
14a. Uncoated Mar-M509



14b. Uncoated IN 792

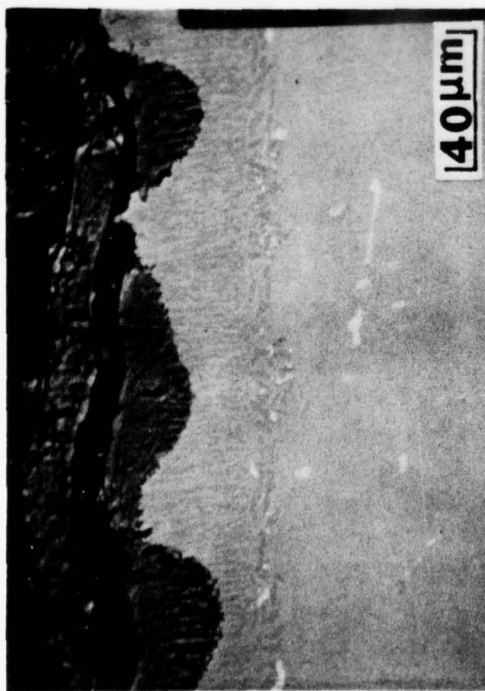


14c. Mar/M509/FWA 28 aluminide

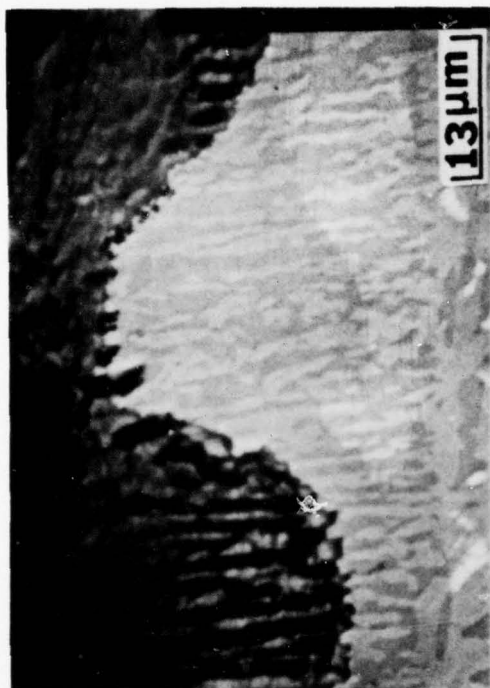


14d. IN 792/FWA 273 aluminide

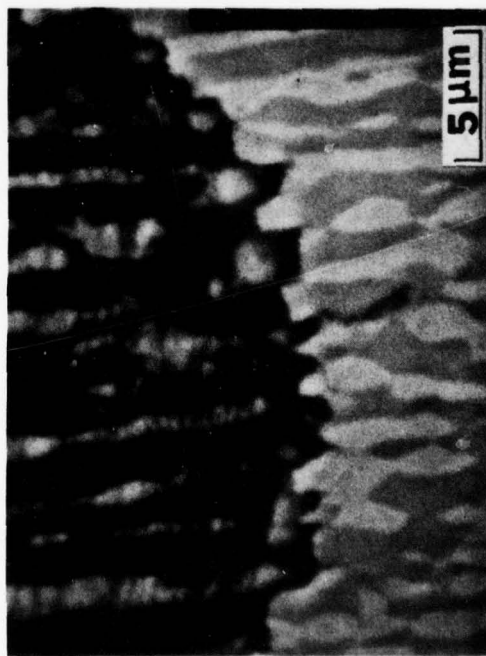
Figure 14. Uncoated and aluminized alloys tested concurrently with the CoCrAlY coating of Fig. 13 (i.e. 100 hours at 704C, $PSO_3 = 0.0001$ atm). Comparison with Figs. 10 and 12 shows effect of SO_3 pressure on microstructural degradation.



15a. Nodular attack and surface scale



15b. Ghost microstructure of oxidized coating



15c. Attack front at bottom of nodule

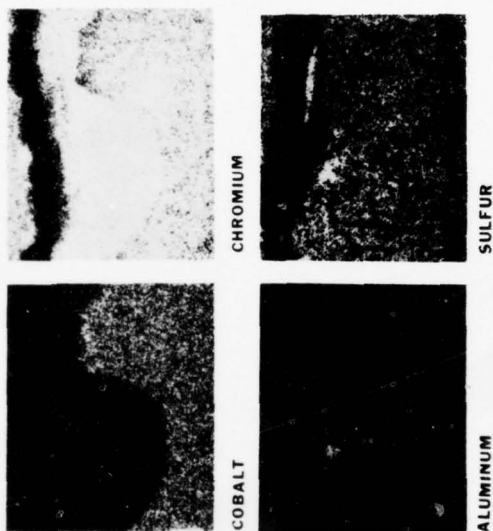
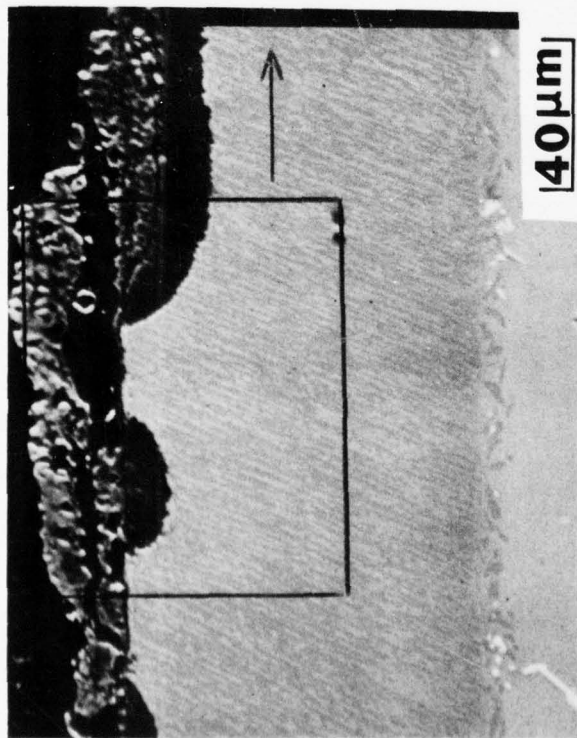


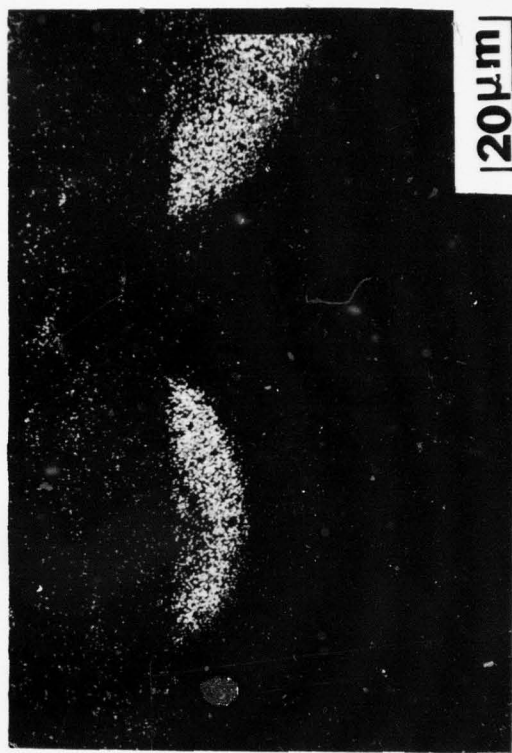
Figure 15. SEM photomicrographs (back scattered electrons) and X-ray maps (approximately the area of 15b) showing the structure and composition of the scale and scale/metal interface after 704C hot corrosion of PWA 68 CoCrAlY at $PSO_3 = 0.004$ atm. Figs. b and c show areas in 15a at higher magnification.



Typical scale thickness and depth of attack

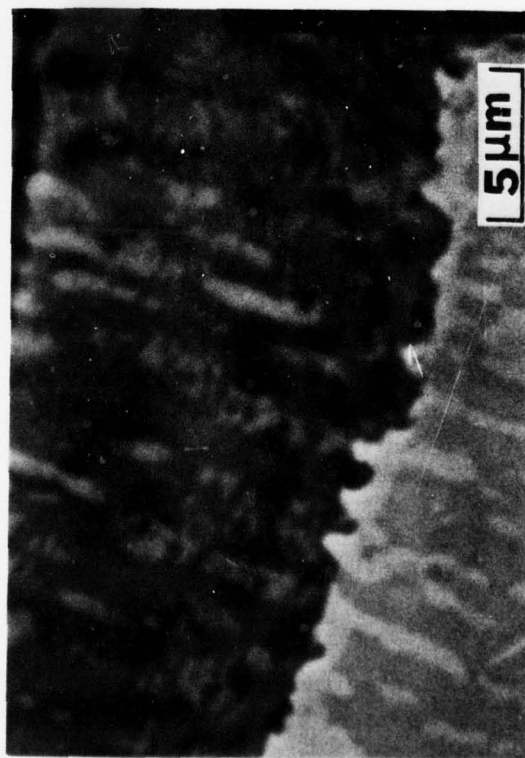
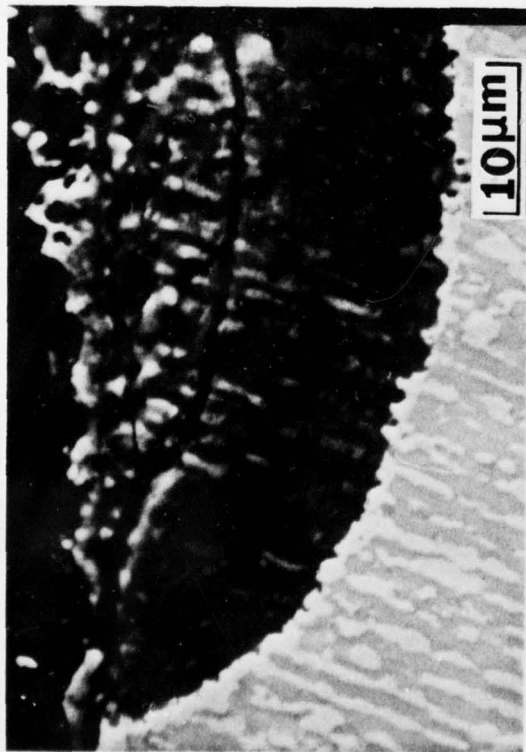


Sodium X-rays



Sulfur X-rays

Figure 16. Accumulation of Na_2SO_4 salt in developing protrusion, as shown by sodium and sulfur X-ray images of a dry polished specimen. Depth of attack illustrated was produced by exposure for 40 hours at 704C with $p\text{SO}_3 = 0.0007$ atm. Area at right of box is shown at higher magnification in Fig. 17



Back scattered electron photomicrographs

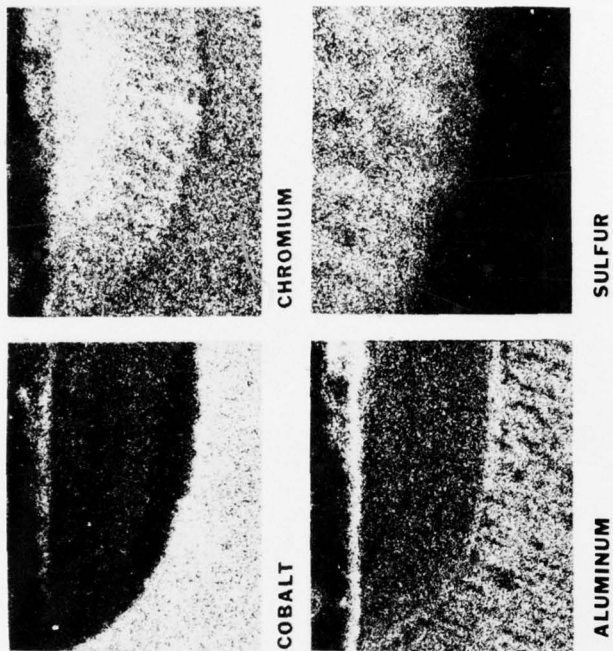
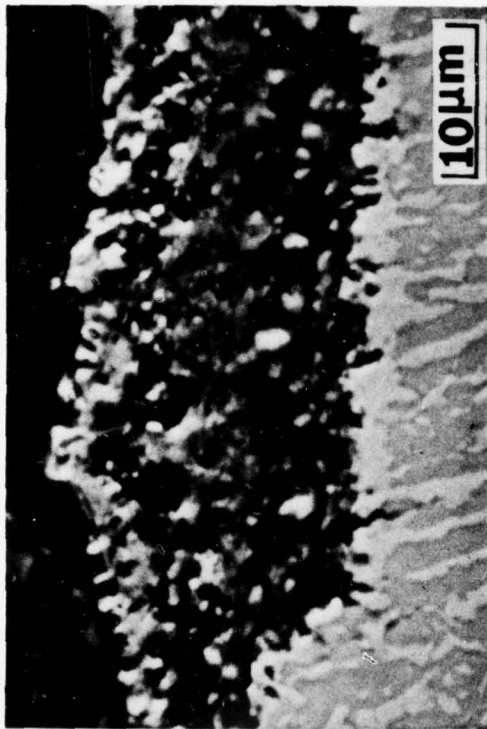


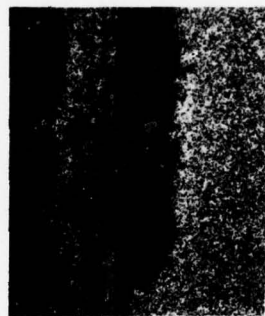
Figure 17. High magnification SEM photomicrographs of a portion of the developing protrusion illustrated in Fig. 16. Note the ghost image in the oxidized coating, including resolution of the columnar microstructure in the Cr X-ray map. Also evident are the fine striations parallel to the scale/metal interface and a very thin β -denuded zone at the corrosion front.



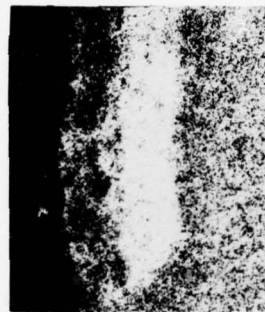
Typical depth of attack and scale thickness



Microstructure of attack front



COBALT



CHROMIUM



ALUMINUM



SULFUR

X-ray maps of above area

Figure 18. SEM photomicrographs (back scattered electrons) and X-ray maps showing the structure and composition of the scale and scale/metal interface after 100 hours at 704C and $p_{SO_2} = 0.0001$ atm. Note the characteristic Co depletion and Co-rich cap, the presence of Al and Cr in both the pit and the external scale, and the presence of sulfur in the scale at the corrosion front.

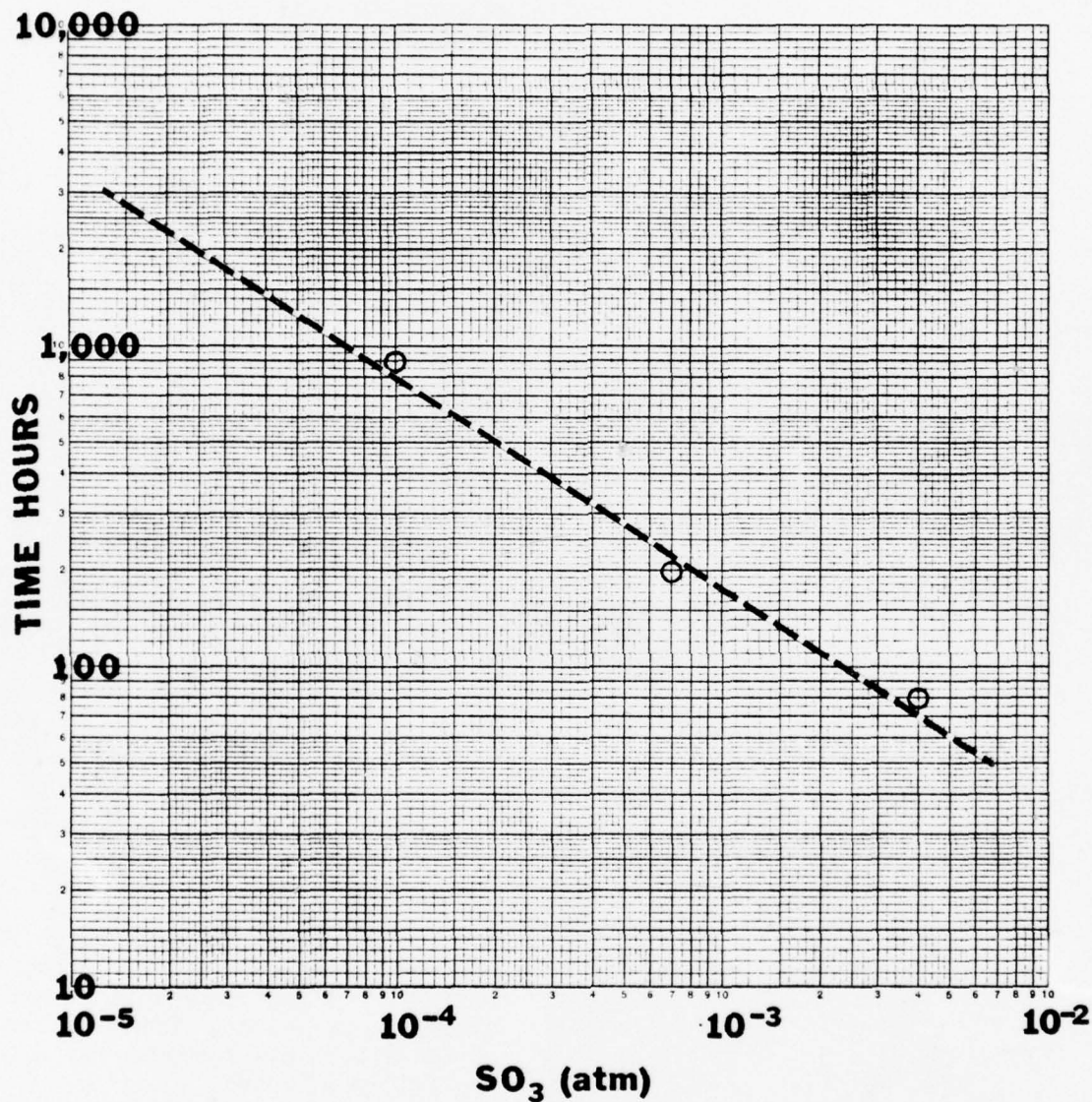


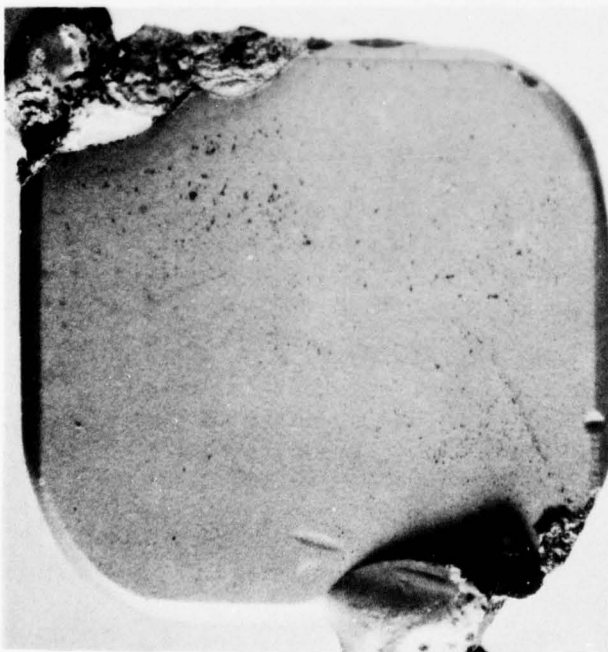
Figure 19. Time to penetration versus SO_3 pressure for PWA 68 CoCrAlY coating tested as described in text. Note that the graph is an approximation serving only to demonstrate a dependence of rate of attack on SO_3 pressure under otherwise constant test conditions. It is not a prediction of service lifetime versus SO_3 pressure in a gas turbine engine.



20a. $\text{PSO}_3 = 0.0007 \text{ atm}$



20b. 0.0007 atm , opposite side



20c. $\text{PSO}_3 = 0.0001 \text{ atm}$

Figure 20. Surface condition of PWA 68 CoCrAlY coatings after 100 hours in 899°C hot corrosion test at indicated SO_3 pressures. Opposite side of the 0.0001 atm specimen was also negligibly affected.

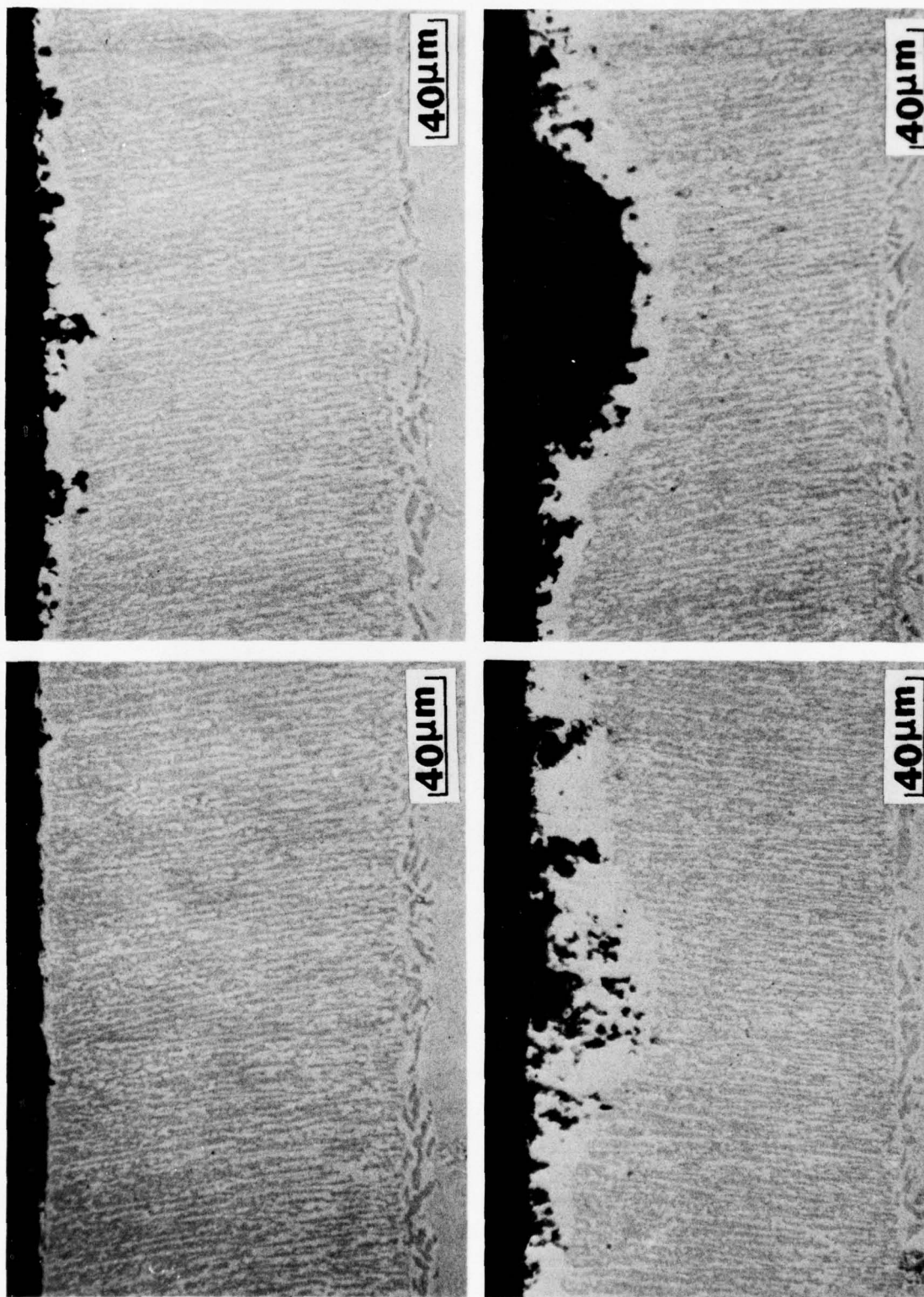


Figure 21. Microstructures of PWA 68 CoCrAlY exposed 100 hours at 899°C and $p_{SO_3} = 0.0007$ atm.

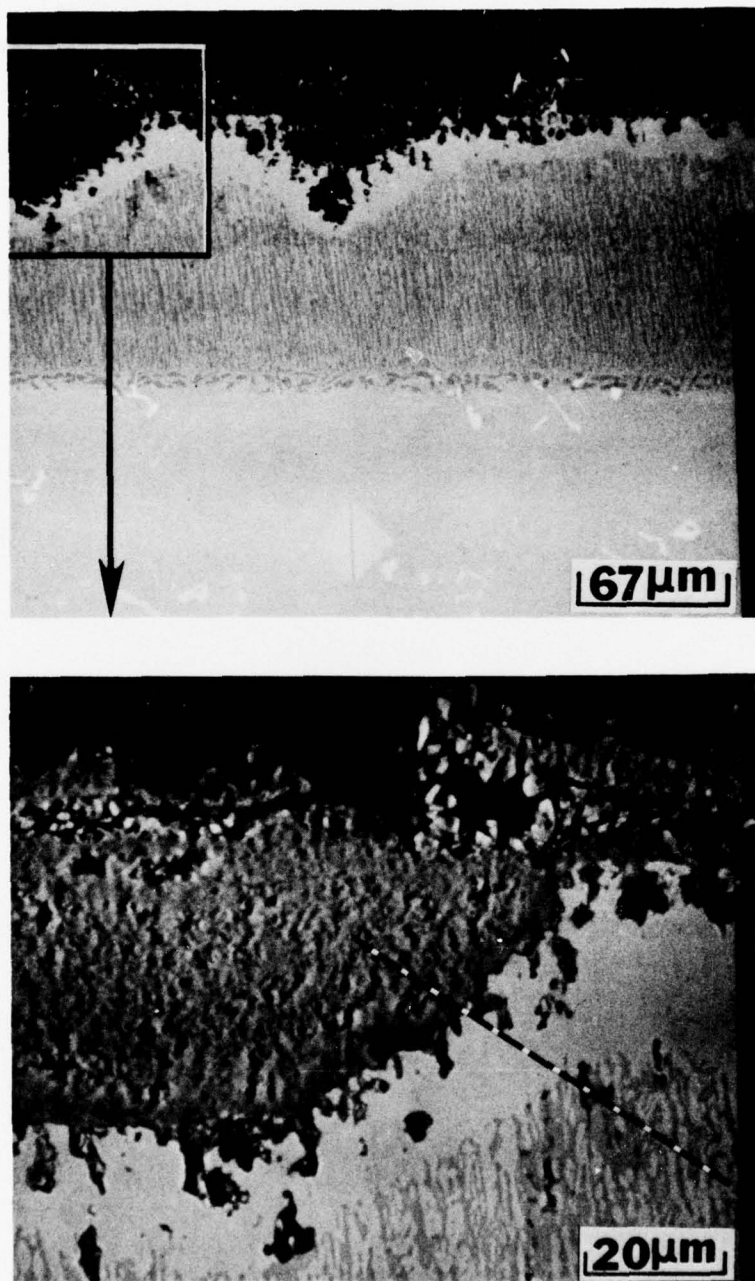
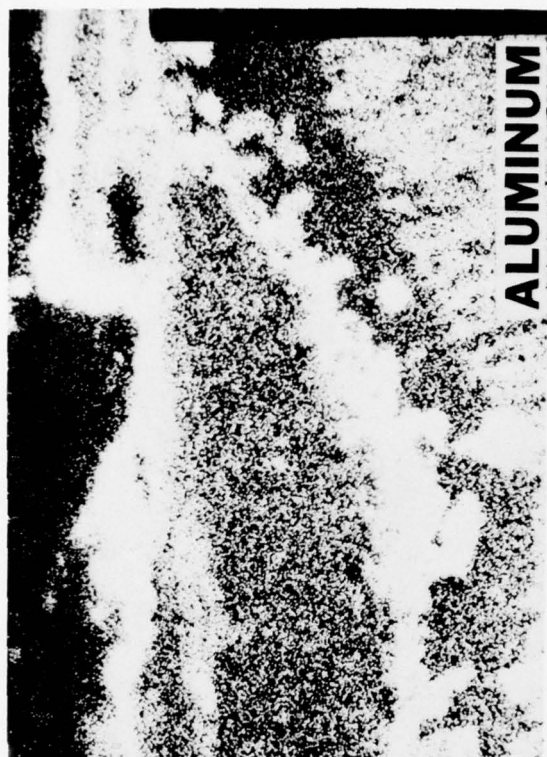
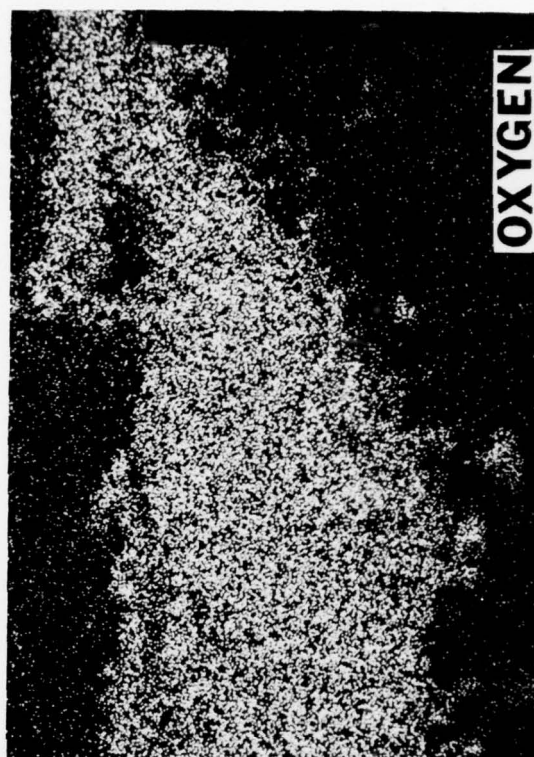


Figure 22. Back scattered electron photomicrographs of heavily corroded area in the CoCrAlY specimen of Fig. 21. X-ray maps in Fig. 23 are the area of the lower photo, but slightly distorted (compressed vertically) due to electronic problems. Dotted line is path of concentration profiles for Al, Cr, S, and O.



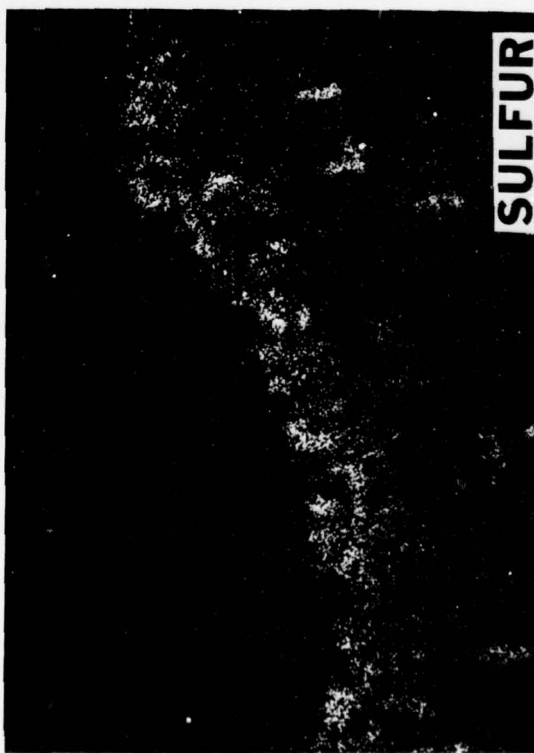
ALUMINUM



OXYGEN

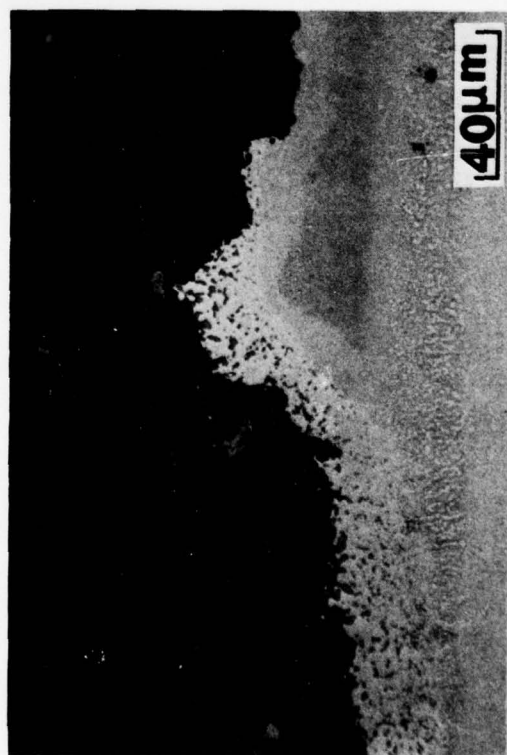
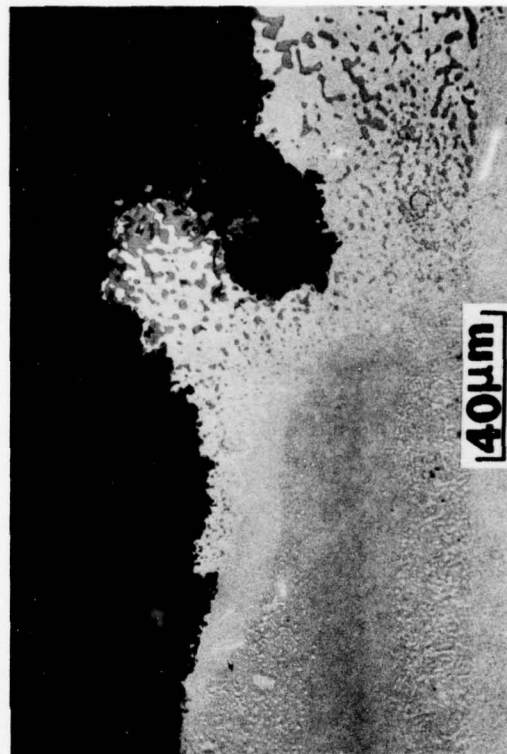
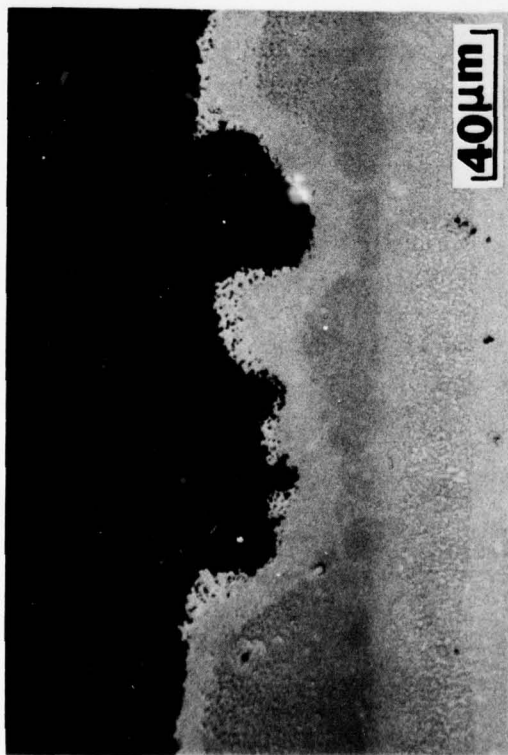
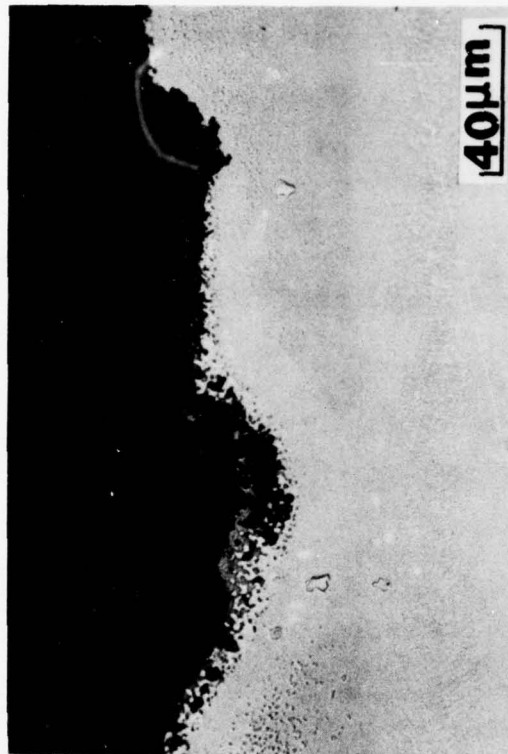


CHROMIUM



SULFUR

Figure 23. X-ray maps showing element distribution characteristic of SO_3 -induced hot corrosion of CoCrAlY coating at 899C.



a. 20 hours at $P_{SO_3} = 0.0007$ atm
 b. 20 hours at $P_{SO_3} = 0.0001$ atm
 Figure 24. Degradation and failure of PWA 273 aluminide coating by SO_3 -induced hot corrosion at 899C.

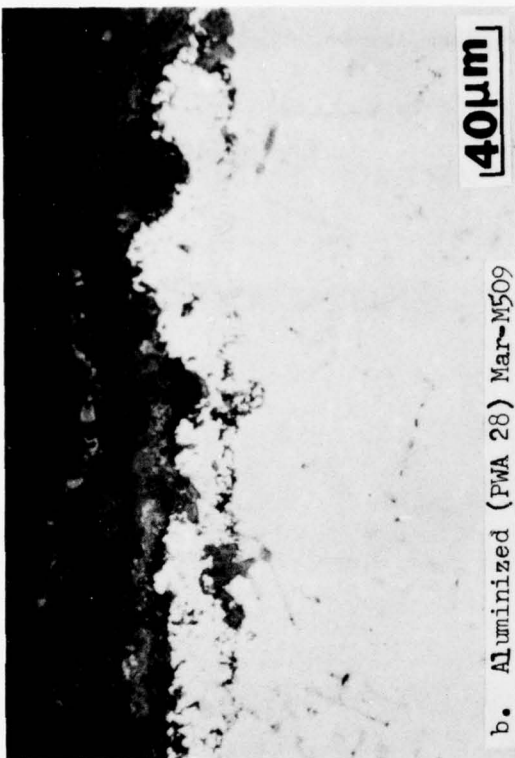
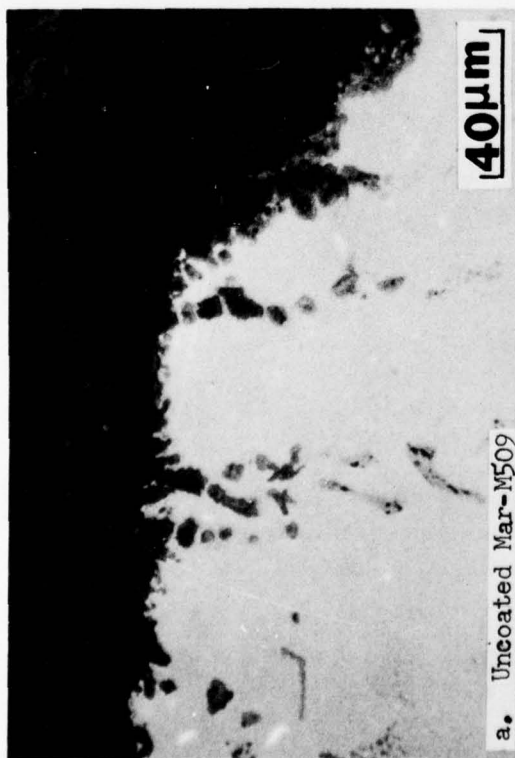
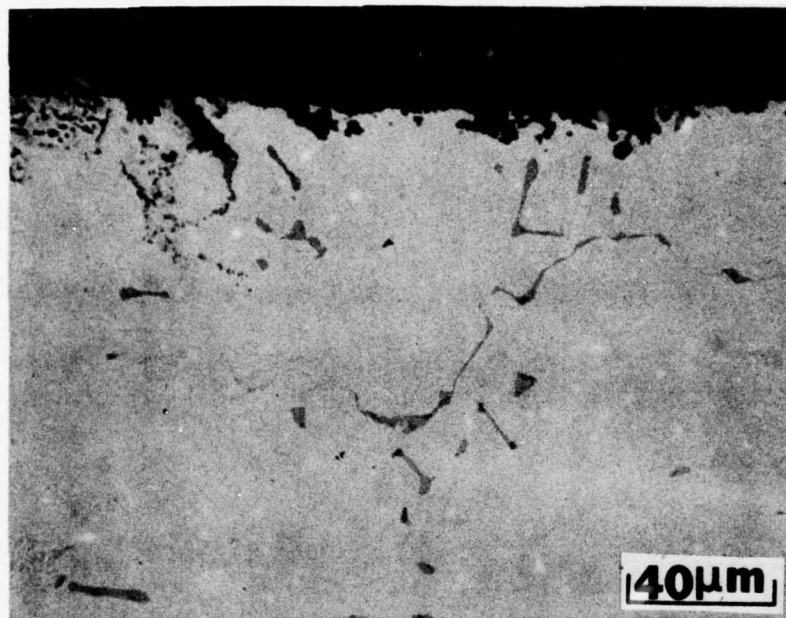
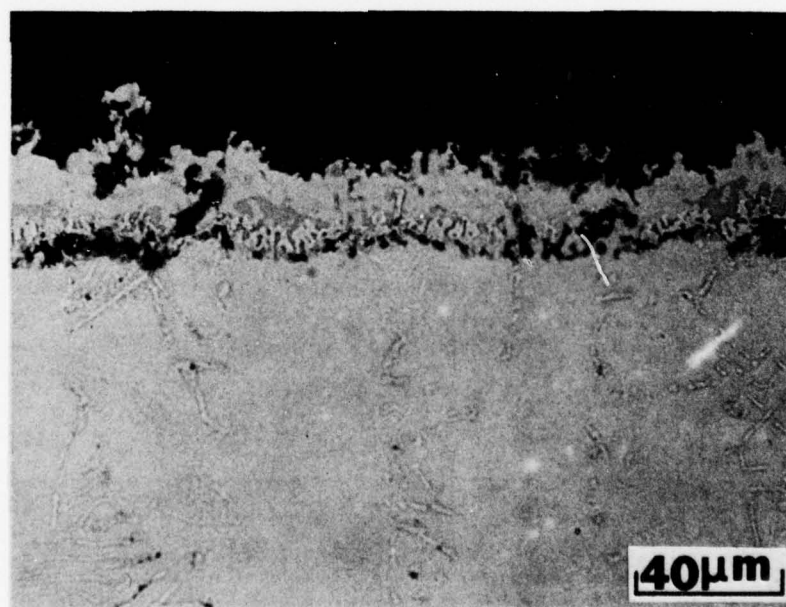


Figure 25. Uncoated and aluminized alloys exposed 100 hours (except 80 hours for aluminized IN 792) at 899C and $p_{SO_3} = 0.0007$ atm. Note different magnification of Co-base and Ni-base alloys.



a. Uncoated



b. Aluminized

Figure 26. Typical microstructures and depth of attack of uncoated and aluminized Mar-M509 exposed 100 hours at 899C and $p_{SO_3} = 0.0001$ atm.

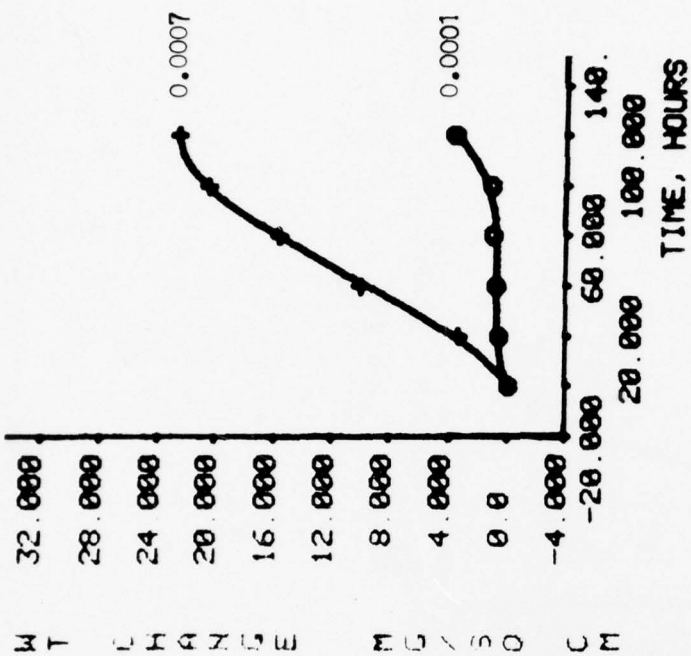
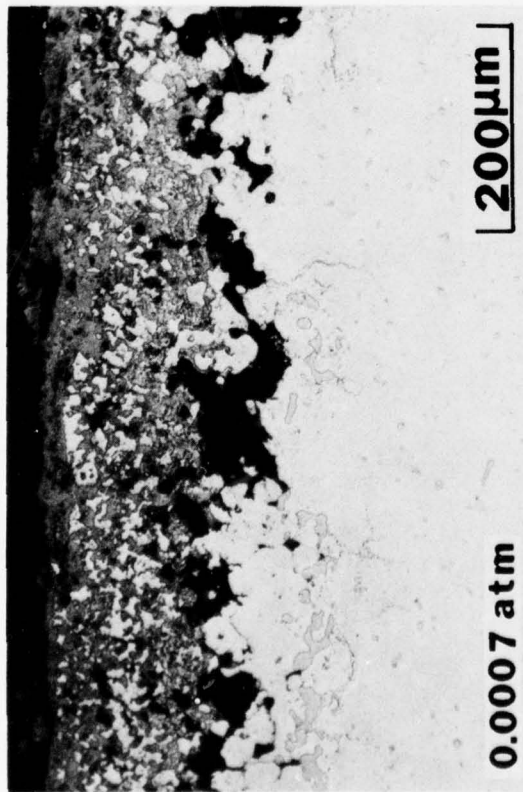


Figure 27. Effect of SO_2 pressure on 899C hot corrosion of uncoated IN 792, as shown by depth of attack and weight change data for 100-hour exposure at 0.0007 and 0.0001 atm. Note different magnification of the two photomicrographs.

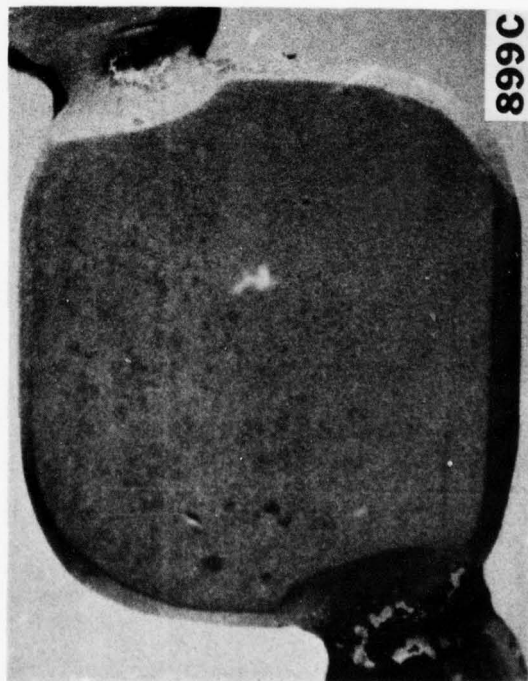
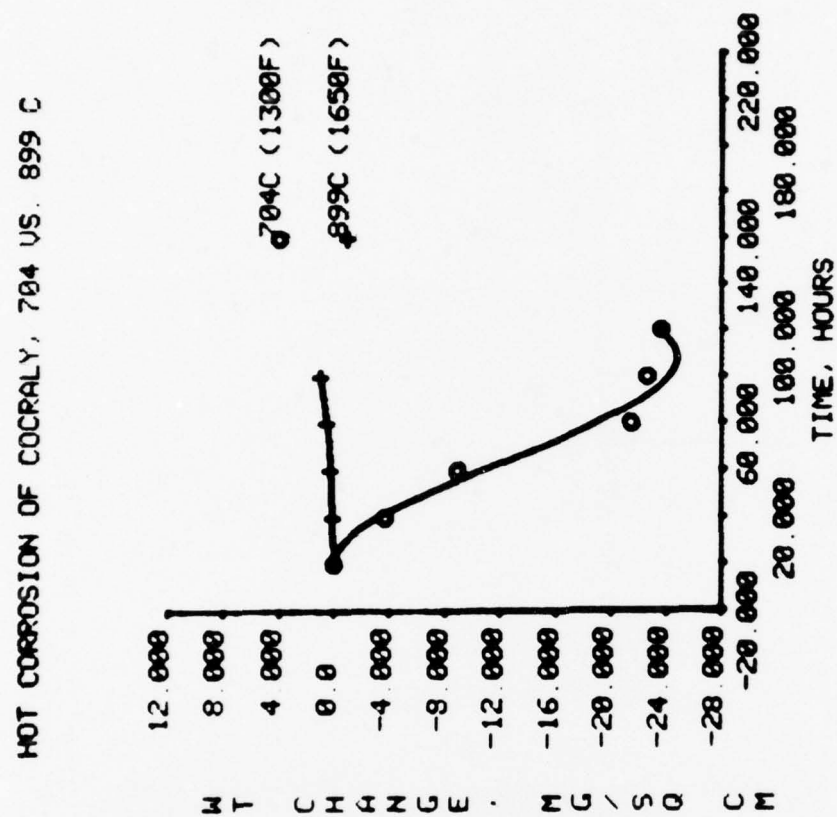
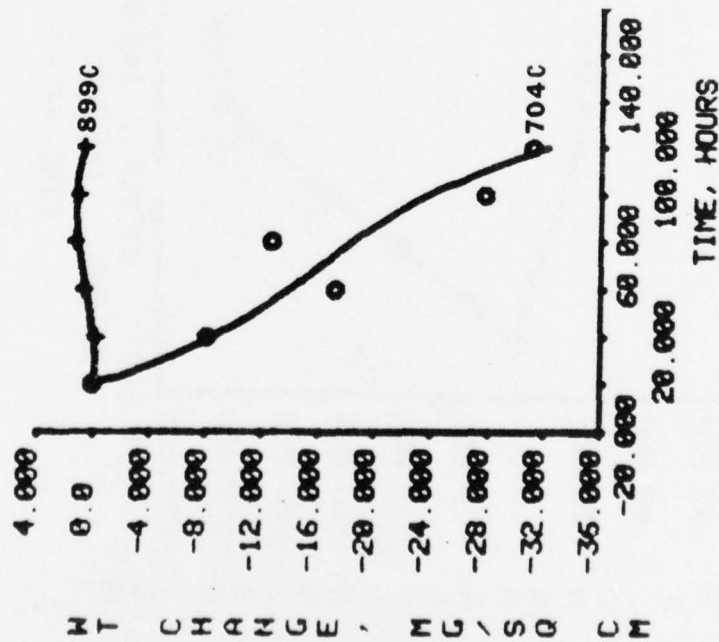
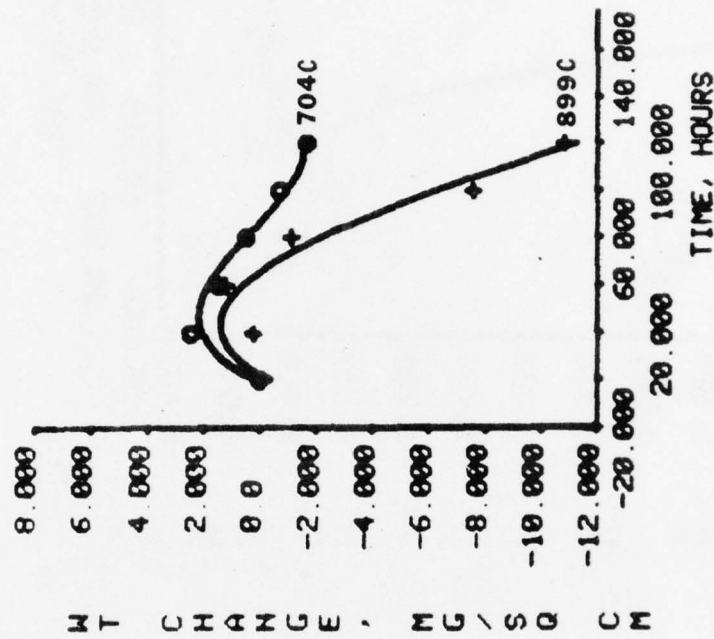


Figure 28. Effect of temperature on severity of attack of FWA 68 CoCrAlY coating at fixed SO_3 pressure of 0.0007 atm, as shown by surface condition after 20 hours and weight change data for 100-hour cyclic exposure.



a. uncoated



b. aluminized

Figure 29. Weight change data showing effect of temperature on severity of attack of uncoated and aluminized Mar-M509 at fixed SO_3 pressure of 0.0007 atm.

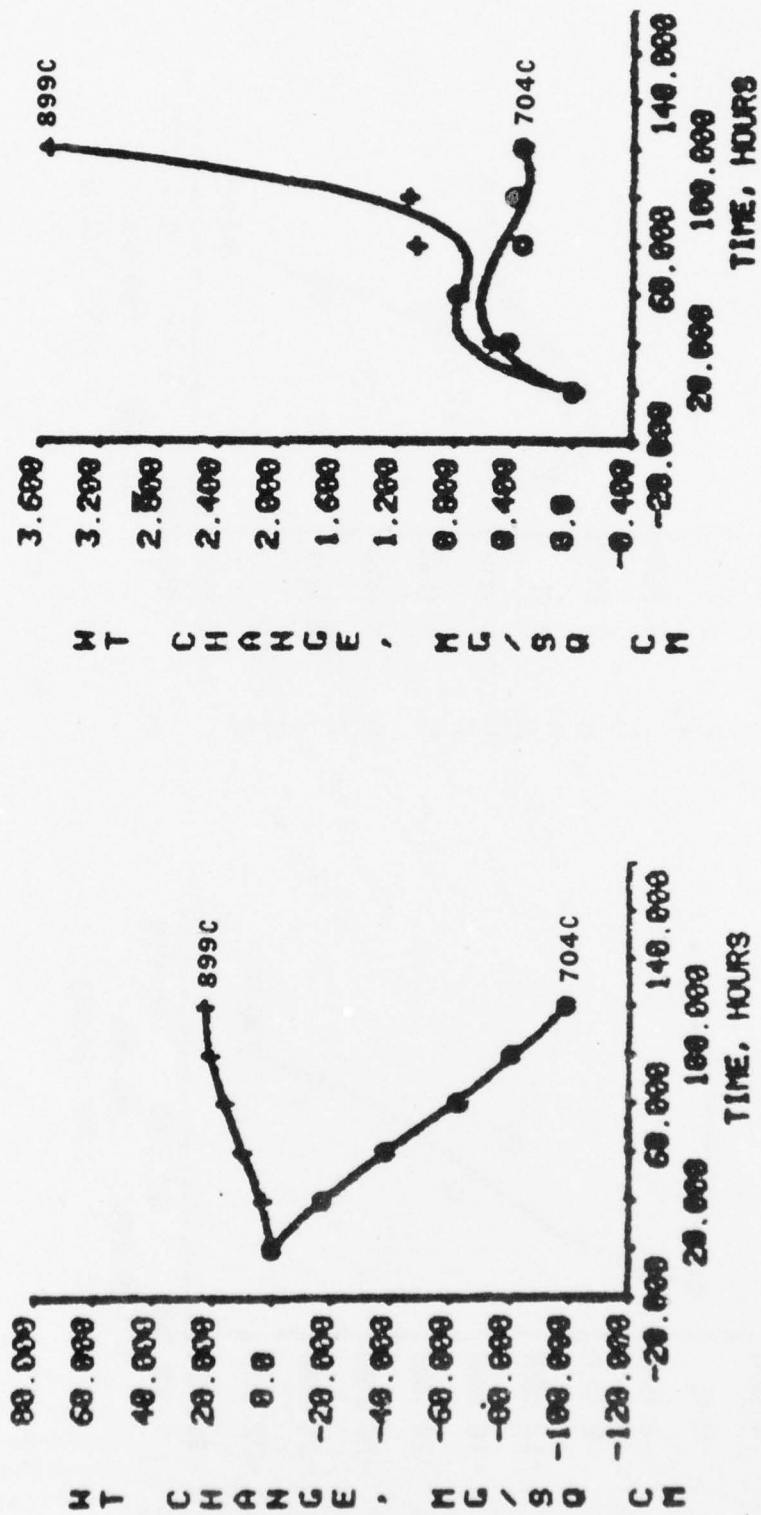


Figure 30. Effects of temperature and SO_3 pressure on severity of attack of uncoated IN 792, as shown by weight change data at fixed SO_3 pressure (30a and 30b respectively) and relative magnitude of $\Delta M/A$ values at 0.0007 versus 0.0001 atm.

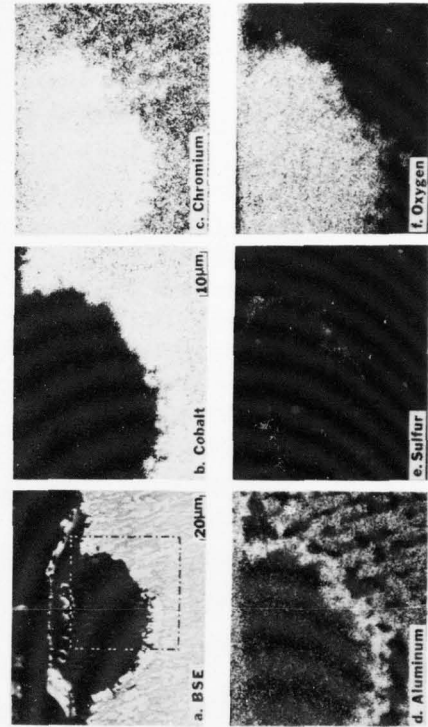
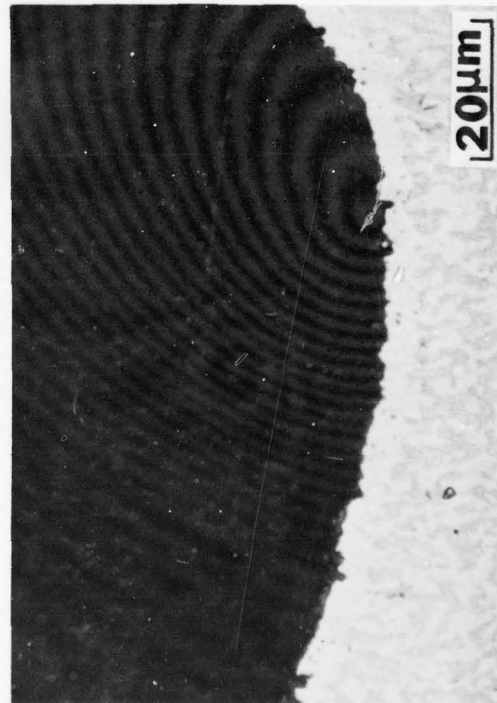
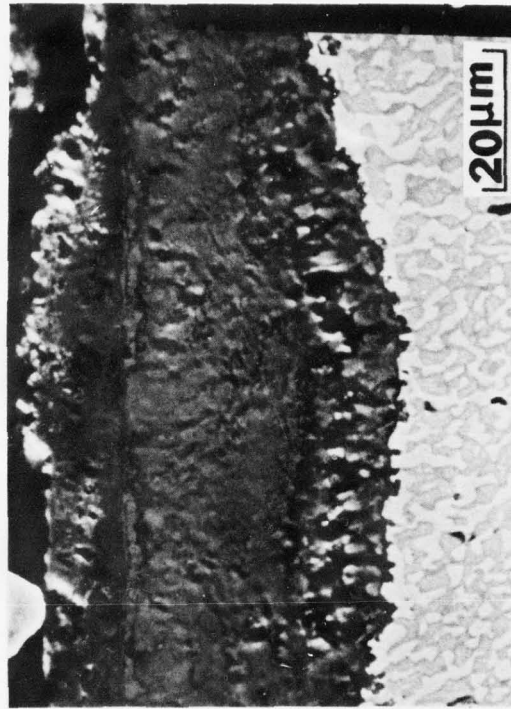
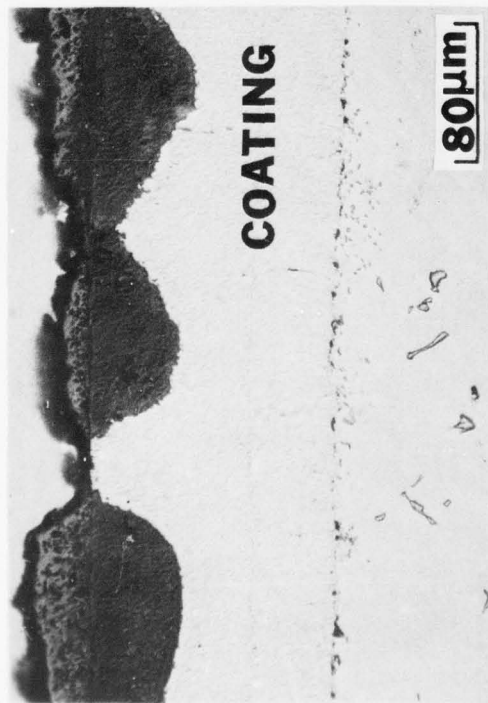
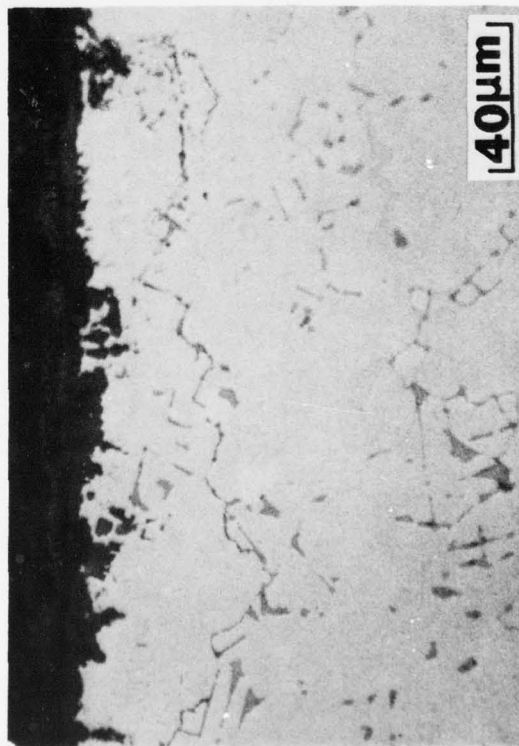
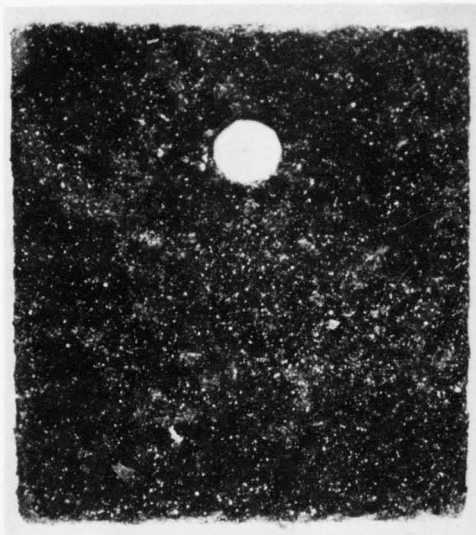
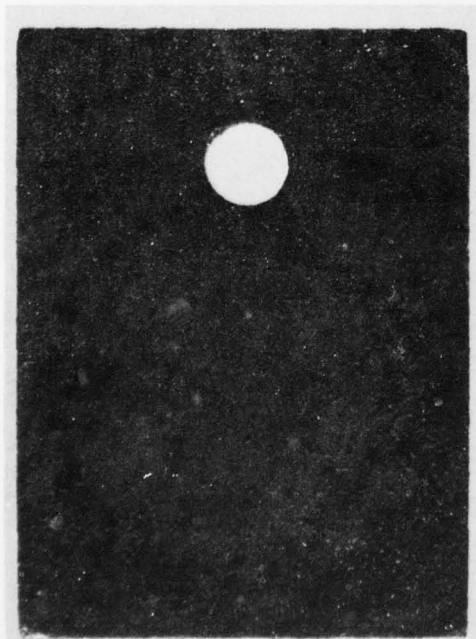


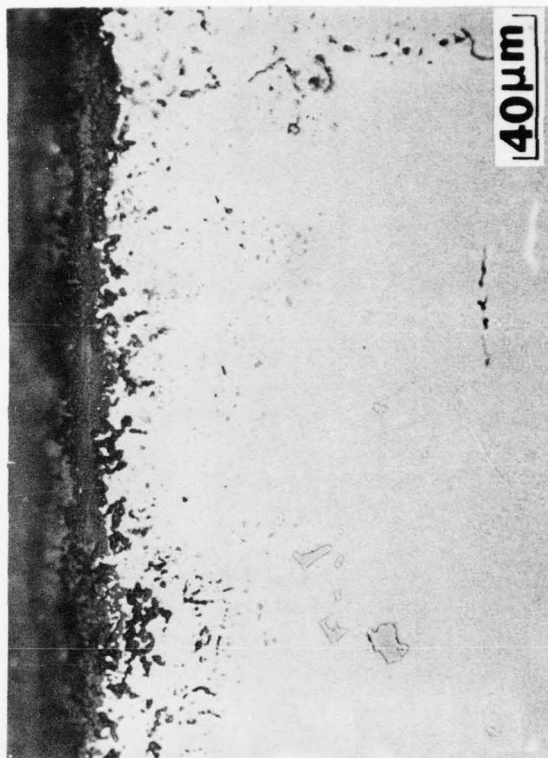
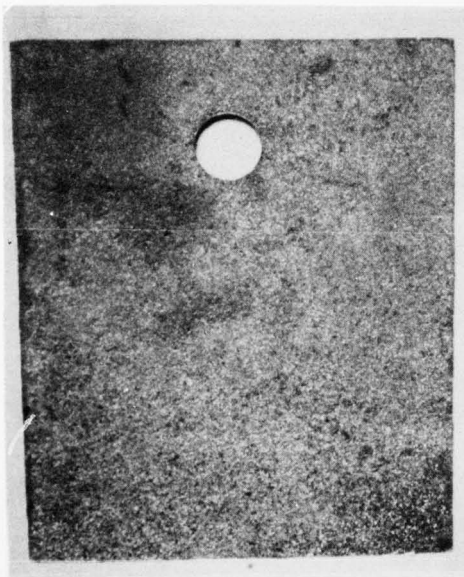
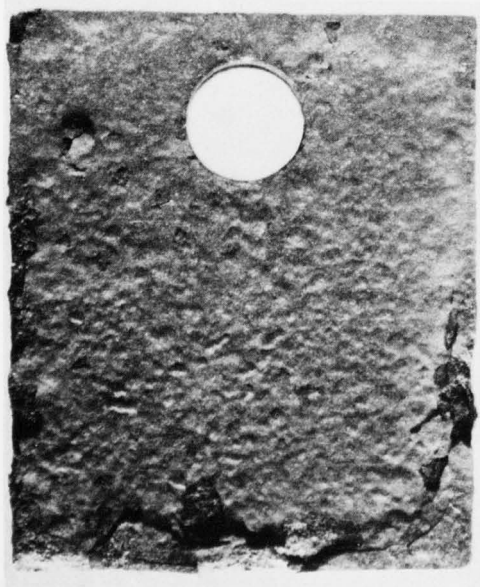
Figure 31. Typical degradation microstructures observed in CoCrAlY-coated turbine hardware from GTV Asiafreighter after approximately 4200 hours service.



a. Chloride-free air

b. Air with 300 ppm NaCl vapor

Figure 32. Effect of chloride vapor on sulfate-induced hot corrosion of uncoated Mar-M509. Specimens were exposed under identical conditions (200 hours at 899C, 1 mg/cm² Na₂SO₄ salt deposit) except for chloride-free air versus 300 ppm NaCl vapor in the furnace atmosphere.



a. Chloride-free air

b. Air with 300 ppm NaCl vapor

Figure 33. Effect of chloride vapor on sulfate-induced hot corrosion of uncoated IN 792. Specimens were concurrently tested with those of Fig. 32.

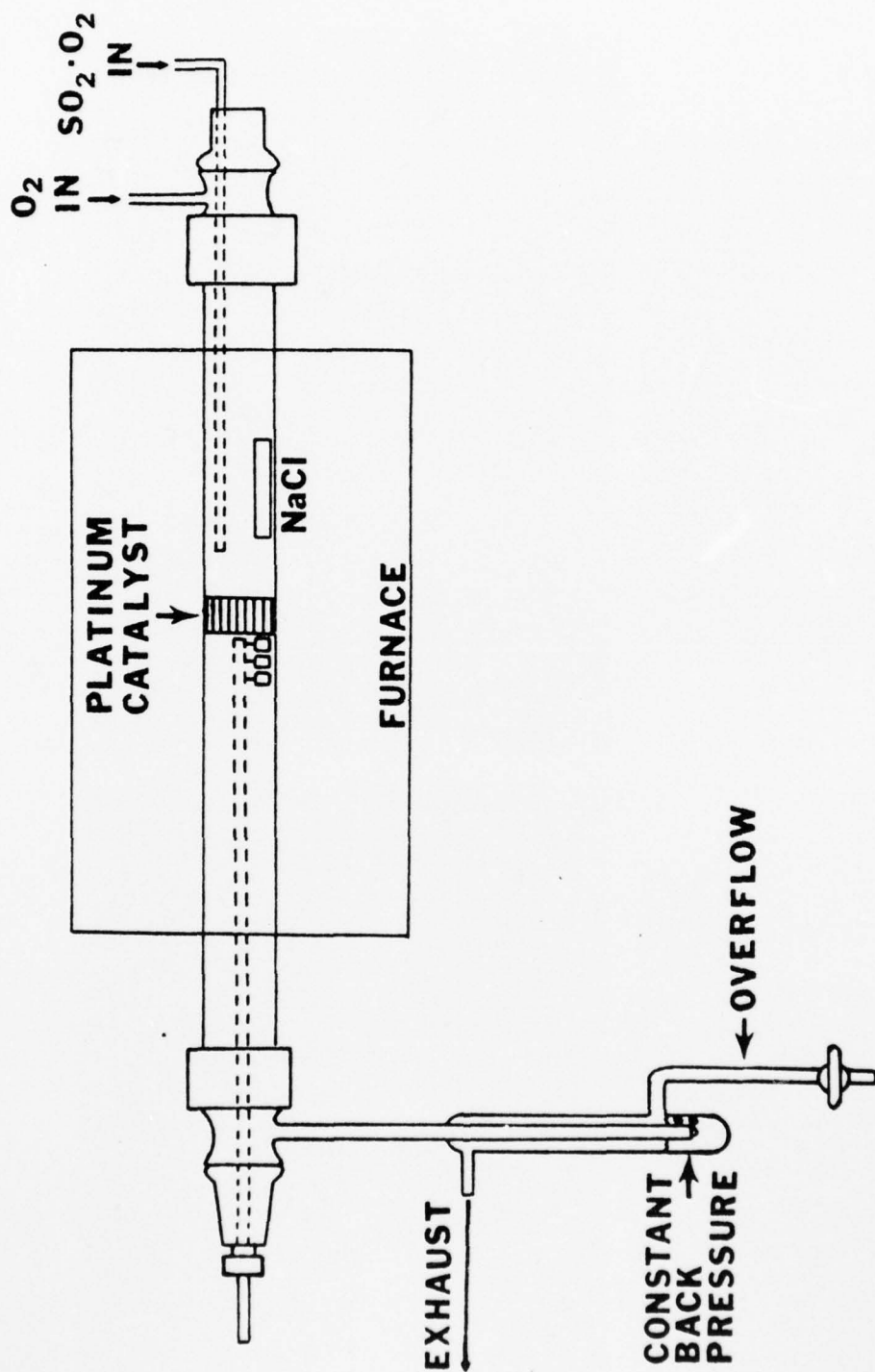
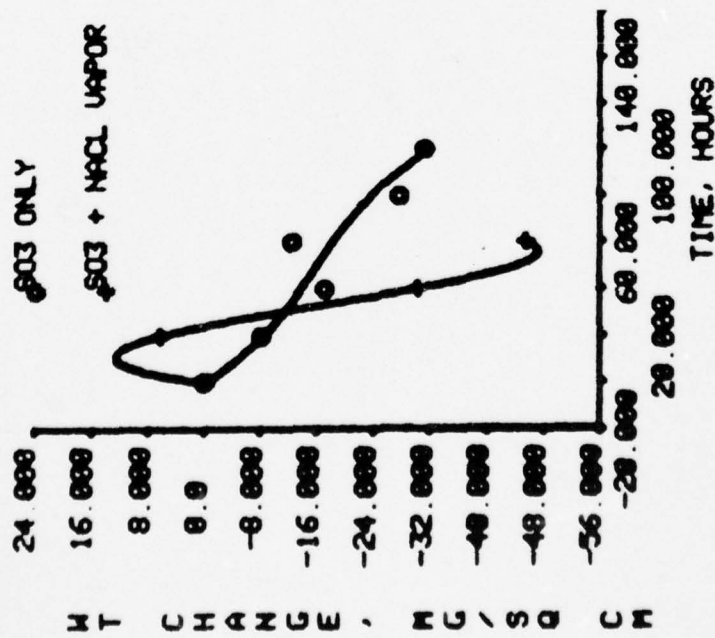
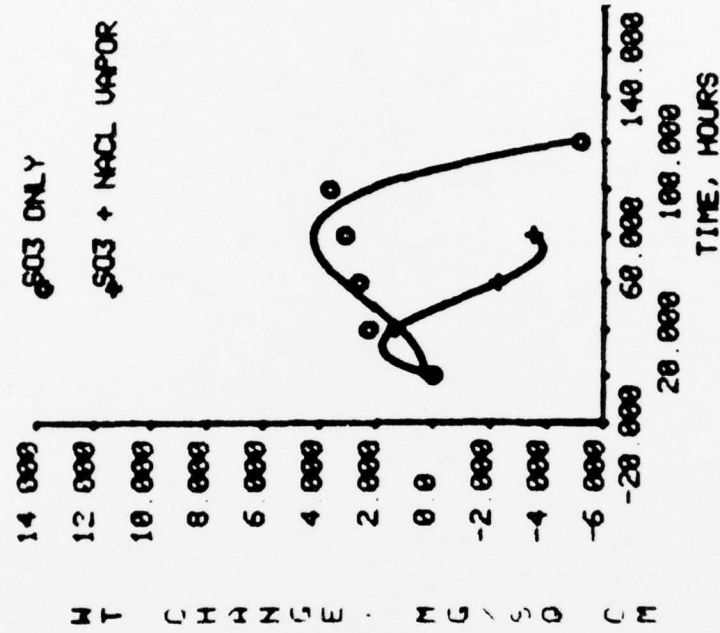


Figure 34. Schematic diagram of horizontal tube furnace for hot corrosion testing with both SO_3 gas and NaCl vapor in the atmosphere. Apparatus is the same as that in Figure 2 except for the separate input of oxygen and $SO_2 \cdot O_2$, which is necessary to avoid reaction of the SO_2 with solid NaCl prior to reaching the catalyst and the specimens.



a. Mar-M509



b. Aluminized IN 792

Figure 35. Weight change data for uncoated Mar-M509 and aluminized IN 792 in SO₃ and SO₃ + NaCl atmospheres (704C, P_{SO₃} = 0.0007 atm, NaCl vapor concentration = 30 ppm).

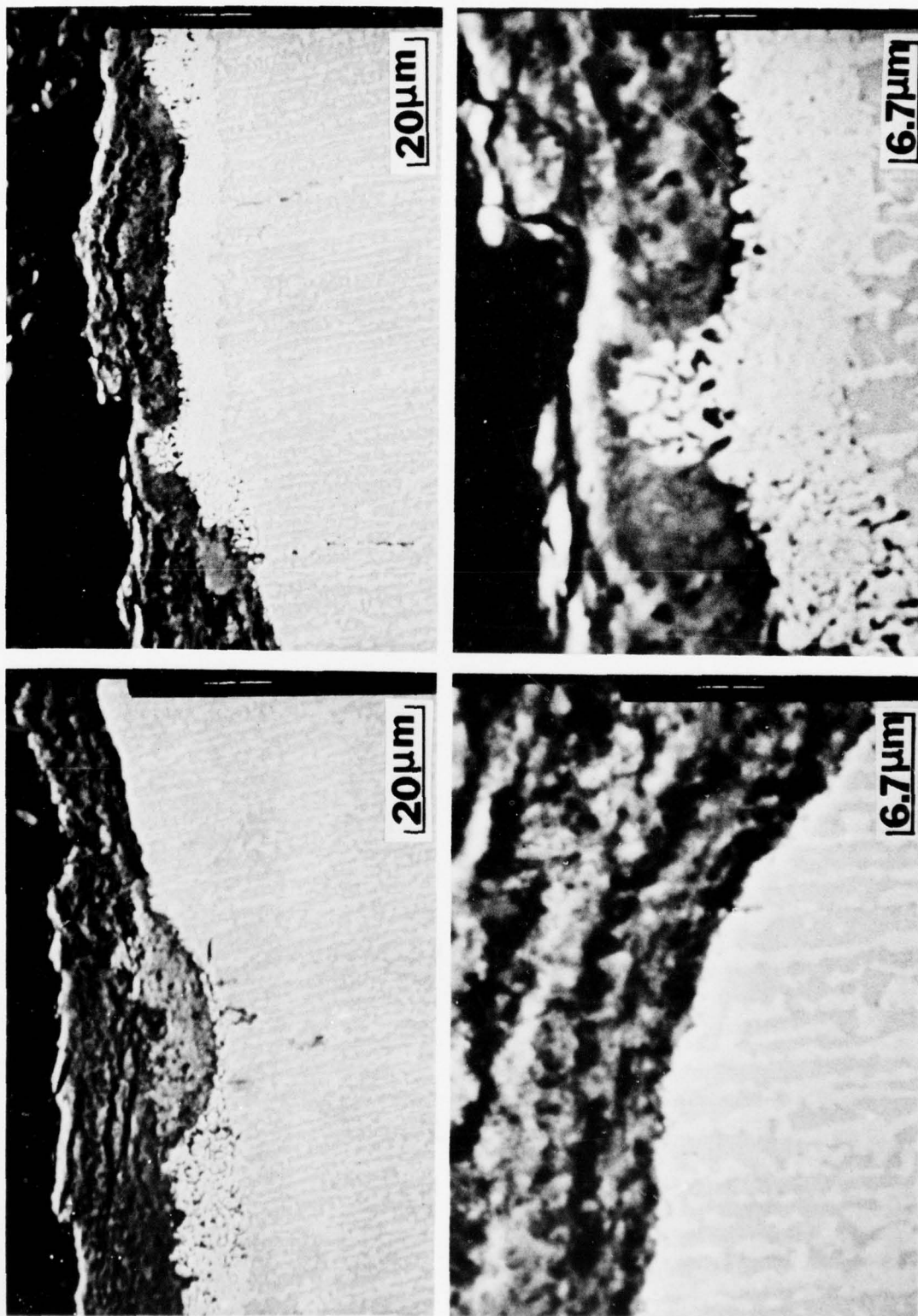
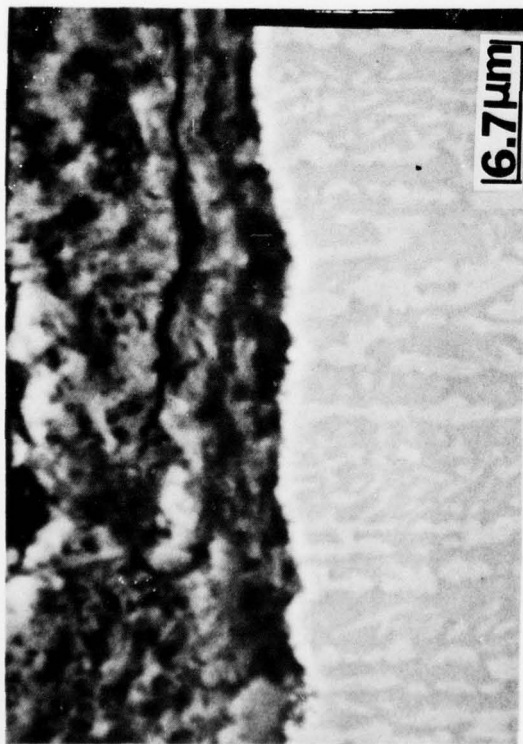
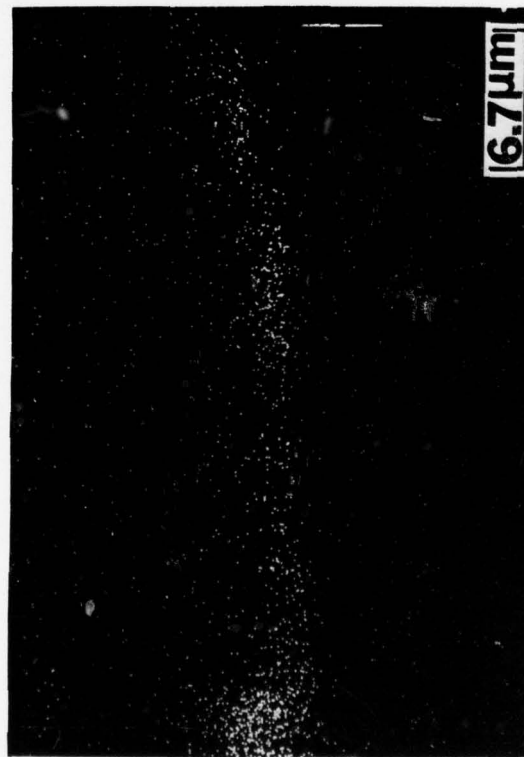


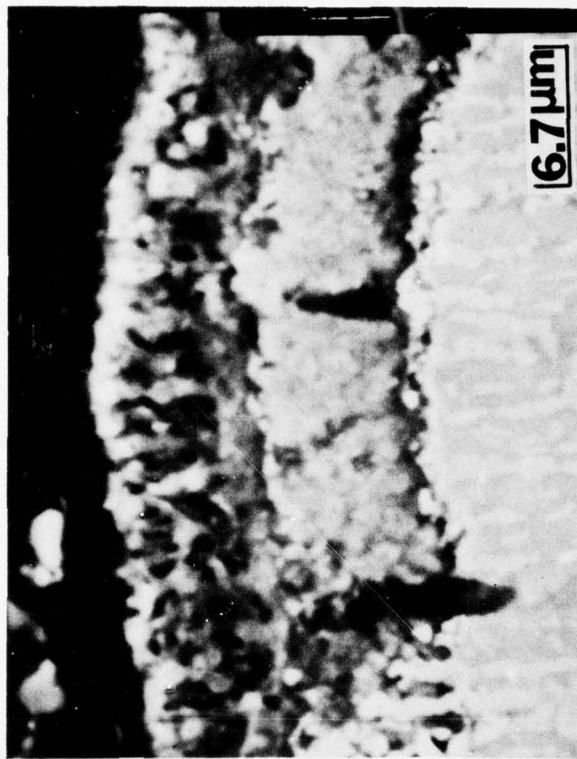
Figure 36. Microstructures of PWA 68 CoCrAlY coating tested at 704C with simultaneous presence of gaseous SO_3 (0.0007 atm) and NaCl vapor (30 ppm). Note characteristic morphology of both SO_3 - and NaCl-induced hot corrosion in randomly selected areas of the attack front.



a. SO_3 -type morphology of attack front (i.e. no diffusion zone or internal oxidation).



b. Sulfur X-ray image of above area

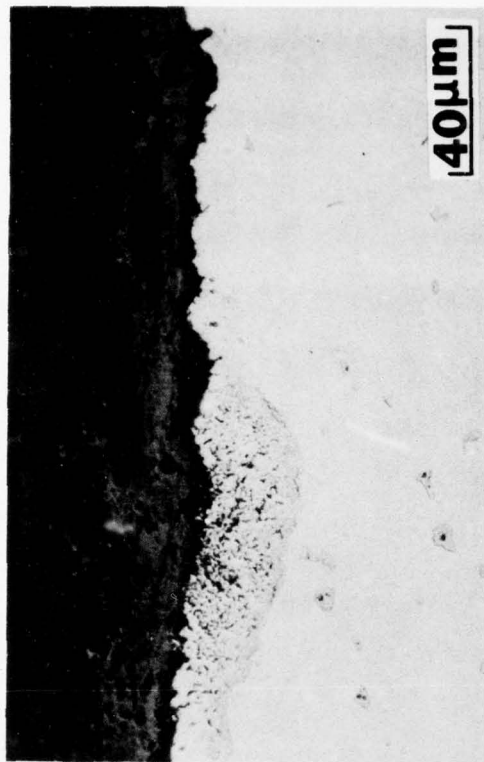


c. Variable composition (indicated by different contrast in back scattered electron image) and morphology of scale

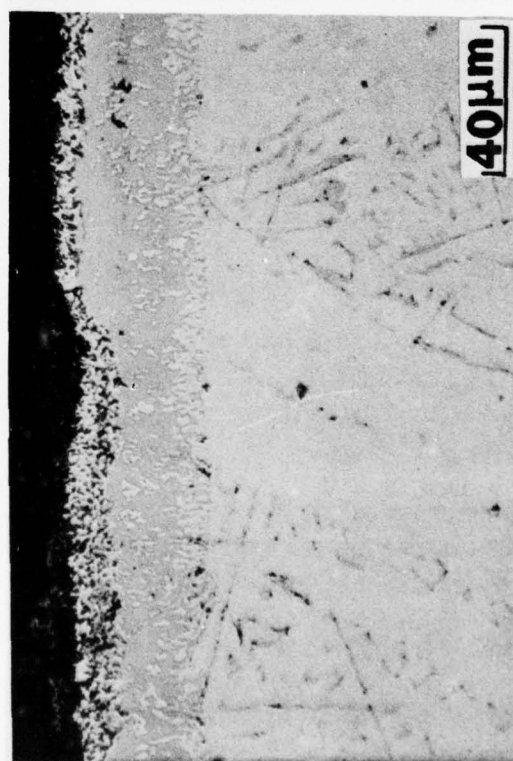
Figure 37. Sulfur-containing scale in area showing SO_3 -type morphology of attack front (a and b); variation in composition and morphology of scale, possibly indicating attack mechanism oscillating between SO_3 - and chloride-type corrosion.



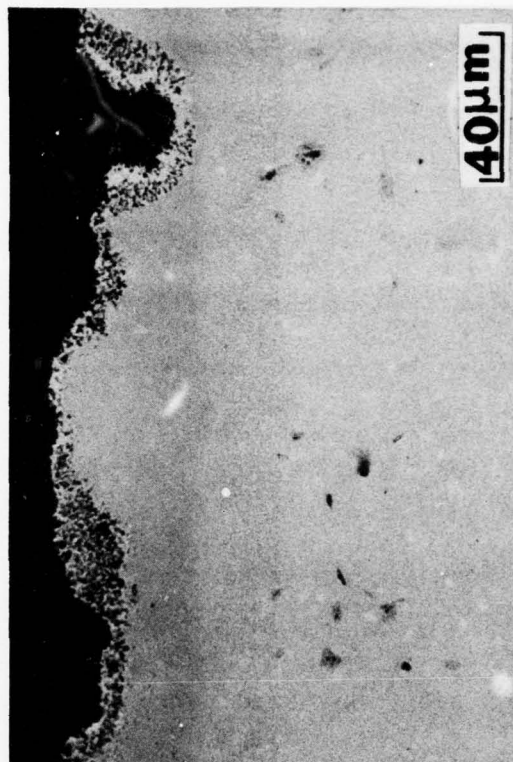
38a. Uncoated Mar-M509



38b. Uncoated IN 792

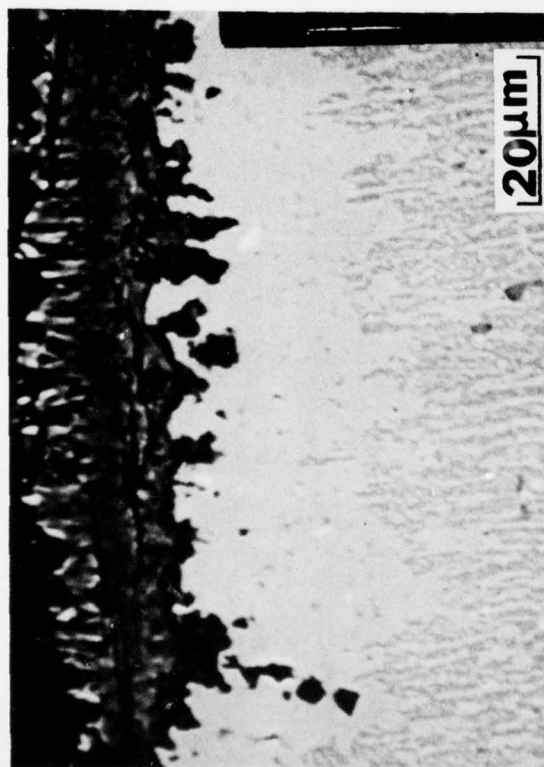


38c. Mar-M509/FWA 28 aluminide

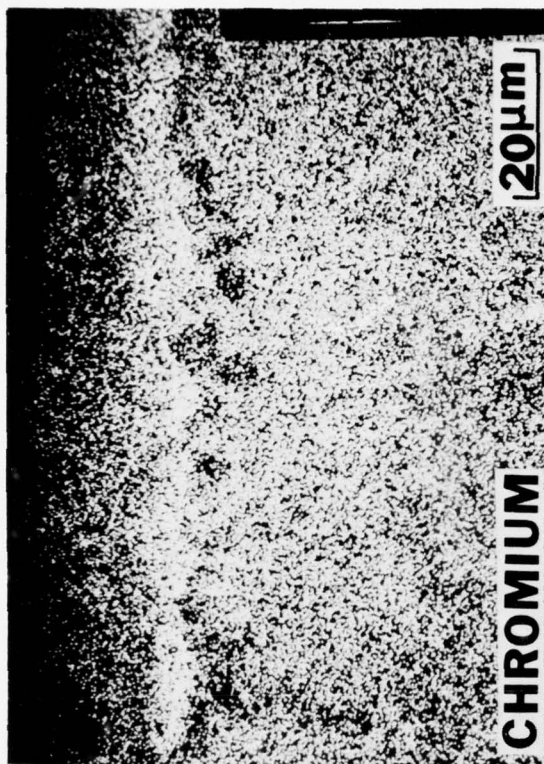


38d. IN 792/FWA 273 aluminide

Figure 38. Uncoated and aluminized alloys tested concurrently with the CoCrAlY coating of Figs. 36 and 37 (i.e. 60 hours at 704C, $PSO_3 = 0.0007$ atm, 30 ppm NaCl vapor)



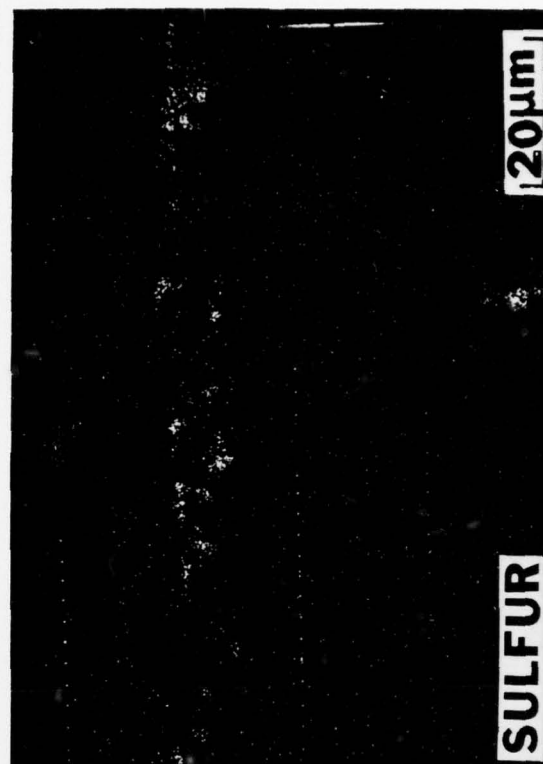
20μm



20μm



20μm

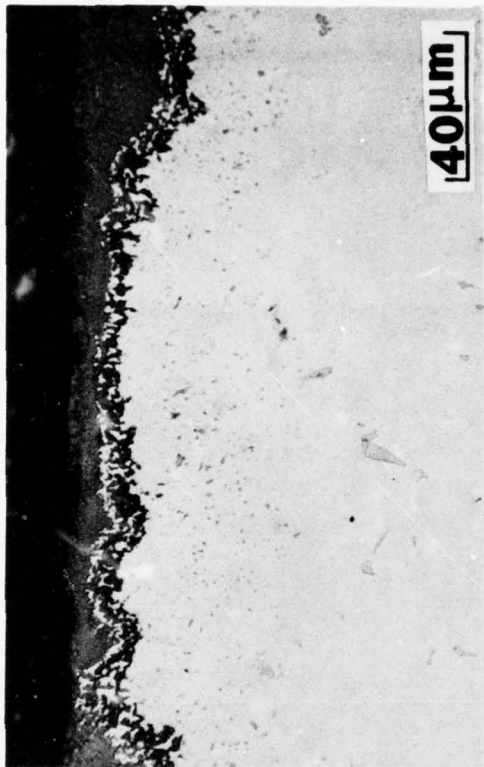


20μm

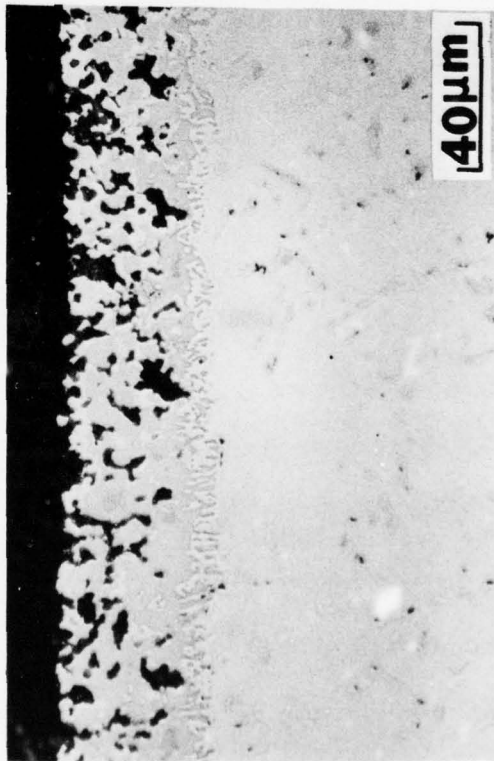
Figure 39. Typical microstructure, depth of attack, and element distribution (Cr, Al, and S) of CoCrAlY coating exposed for 100 hours at 899C with $\text{pSO}_3 = 0.0007$ atm and 30 ppm NaCl vapor.



40a. Uncoated Mar-M509



40b. Uncoated IN 792



40c. Mar-M509/FWA 28 aluminide

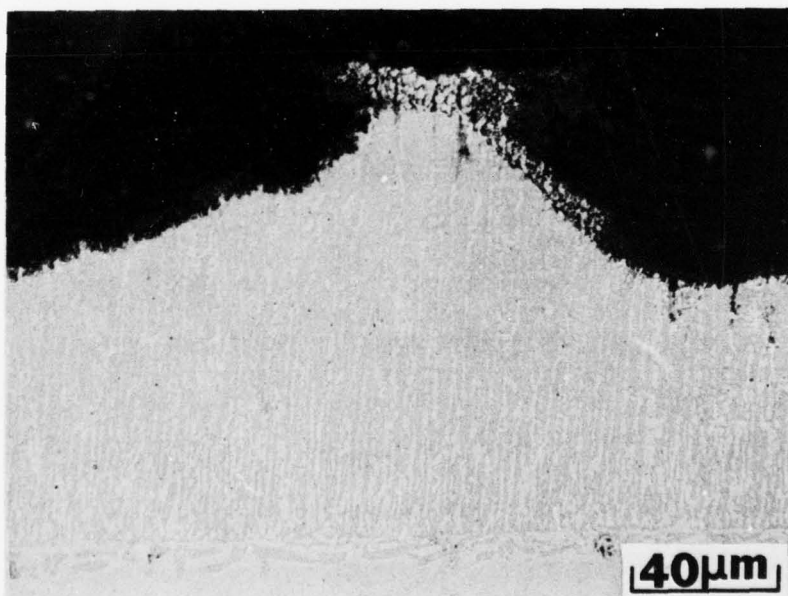


40d. IN 792/FWA 273 aluminide

Figure 40. Uncoated and aluminized alloys tested concurrently with the CoCrAlY coating of Fig. 39 (i.e. 100 hours at 899C, $P_{SO_3} = 0.0007$ atm, 30 ppm NaCl vapor).



a. Na_2SO_4 - 50m% CoSO_4 salt deposit



b. Na_2SO_4 - 50m% ZnSO_4 salt deposit

Figure 41. Typical depth and microstructure of hot corrosion attack produced by 100-hour cyclic exposure of CoCrAlY at 704C with $p_{\text{SO}_3} = 0.0007$ atm and 30 ppm NaCl vapor.

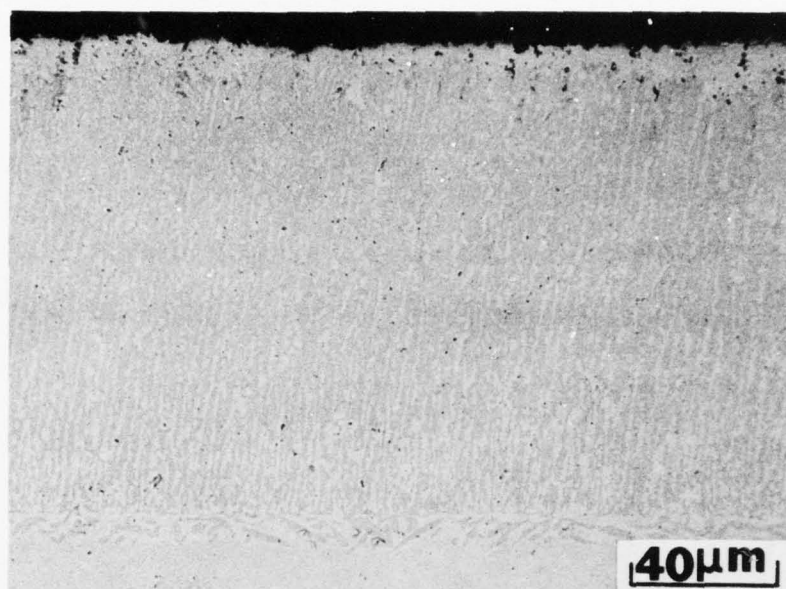


Figure 42. Negligible microstructural degradation of CoCrAlY coating covered with a 2 mg/cm^2 mixture of Na_2SO_4 and CoO and exposed for 100 hours concurrently with the specimens of Fig. 41 (704°C , $p_{\text{SO}_3} = 0.0007 \text{ atm}$, 30 ppm NaCl vapor).

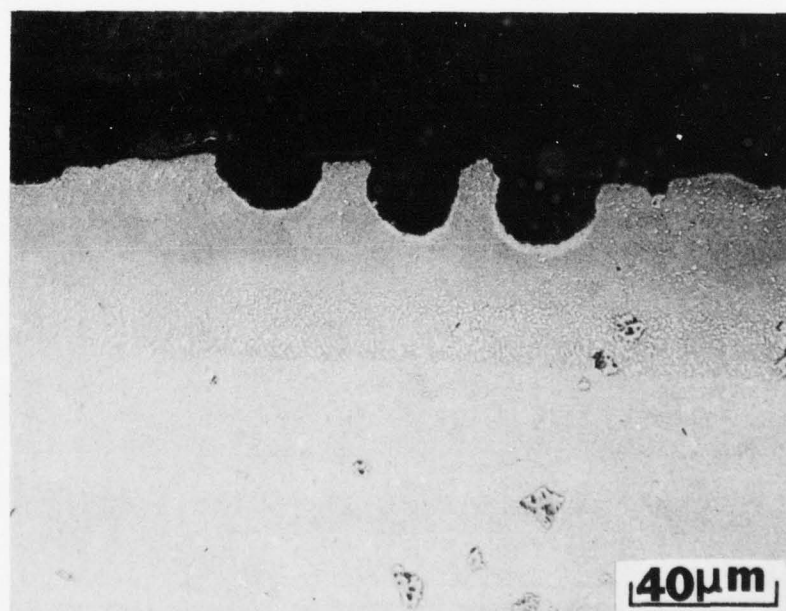
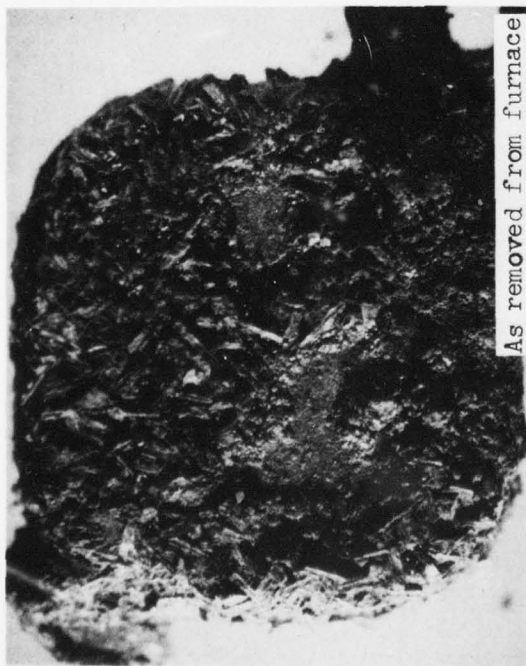
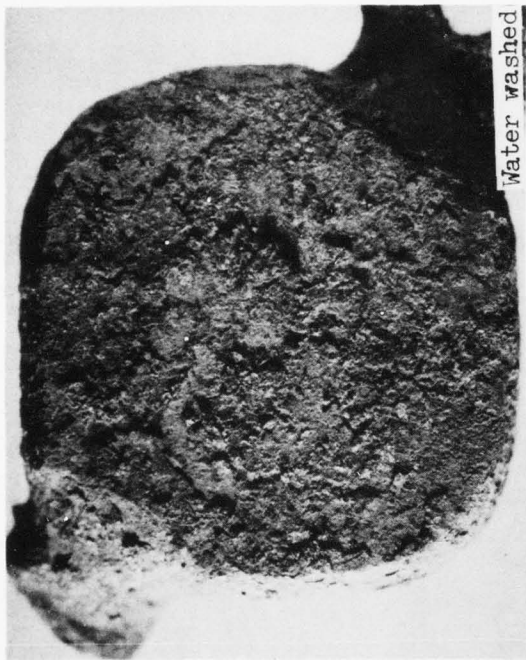


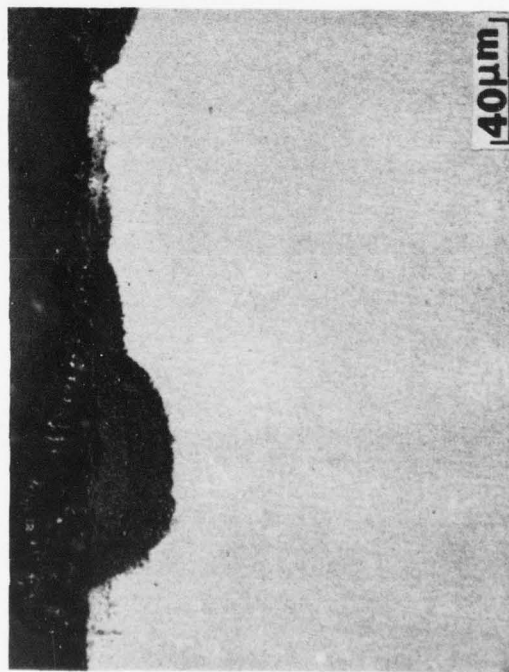
Figure 43. Nodular attack of PWA 273 Ni-base aluminide coating produced by a salt deposit of Na_2SO_4 - 50m% CoSO_4 and cyclic exposure for 100 hours at 704°C , $p_{\text{SO}_3} = 0.0007 \text{ atm}$, and 30 ppm NaCl vapor.



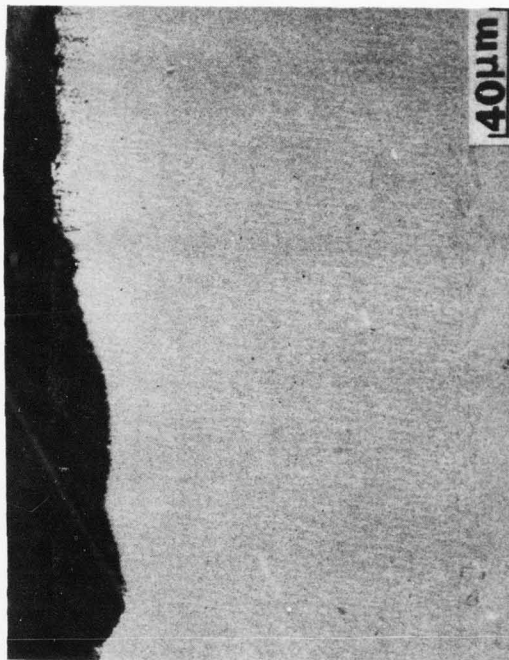
As removed from furnace



Water washed

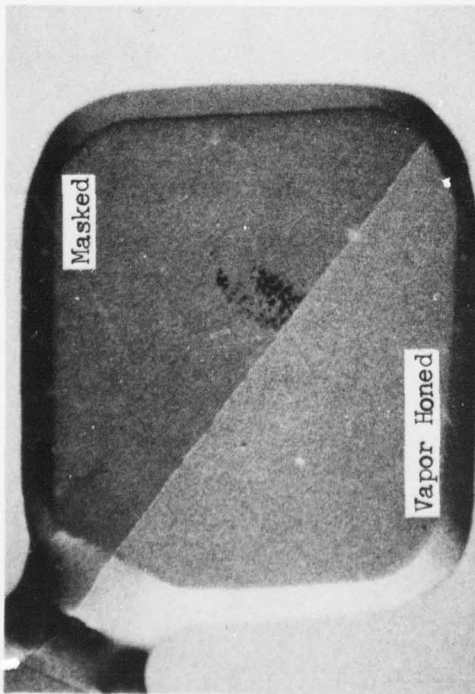


40µm



40µm

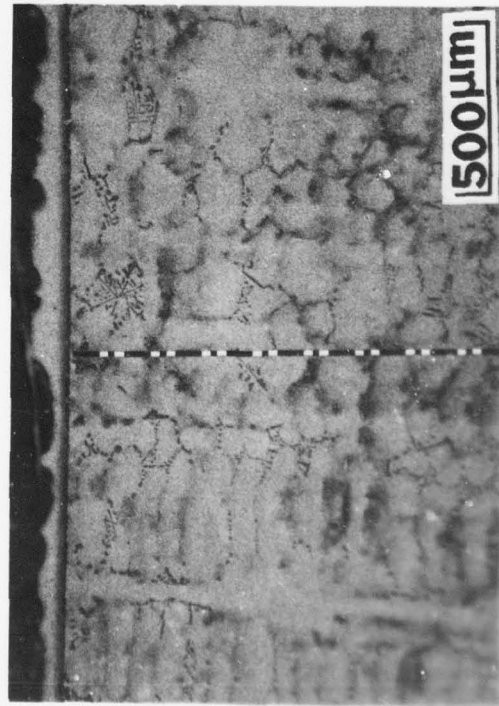
Figure 44. Surface condition and typical depth of attack of CoCrAlY coating produced by 5 mg/cm² salt deposit exposed for 20 hours at 704°C with $\text{PSO}_3 = 0.0007$ and 30 ppm NaCl vapor.



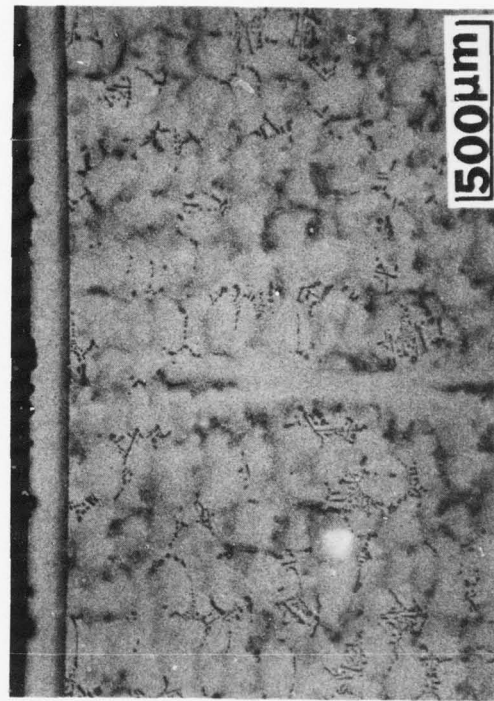
Pre-test condition



Exposed 20 hours; 704C, $\text{pSO}_3 = 0.0007 \text{ atm}$



Transition between masked and vapor honed areas



Typical degradation of masked area

Figure 16. CoCrAlY specimen prepared by masking and vapor honing as described in text.

AD-A071 055

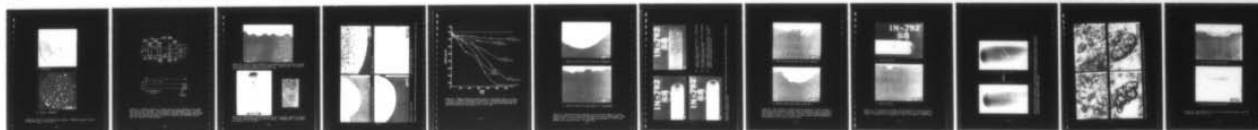
PRATT AND WHITNEY AIRCRAFT GROUP WEST PALM BEACH FL 6--ETC F/G 21/5
MARINE GAS TURBINE HOT CORROSION DEPENDENCE ON INGESTED SALT LE--ETC(U)
APR 79 R H BARKALOW, F S PETTIT N00173-77-C-0206

UNCLASSIFIED

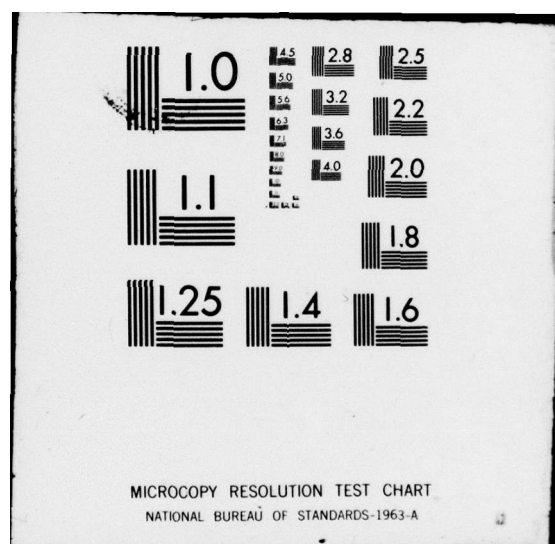
PWA-FR-11544

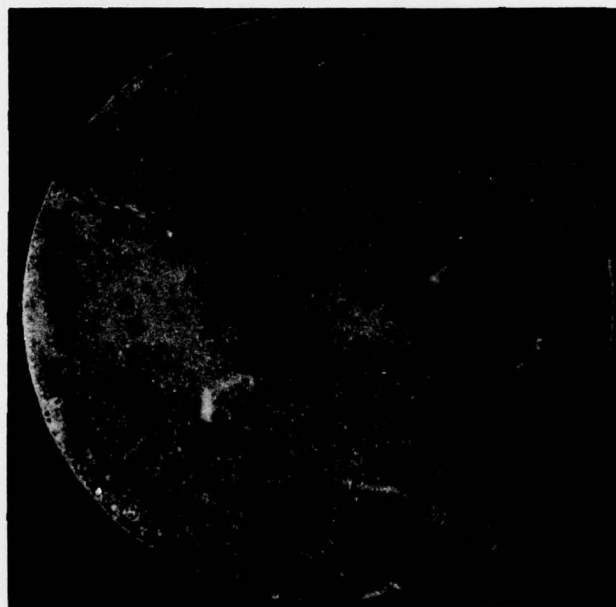
ML

2 OF 2
AD
A071055

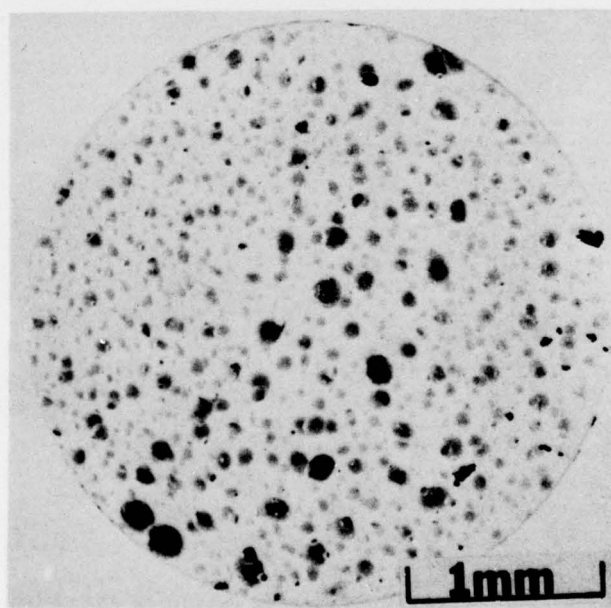


END
DATE
FILMED
8 -79
DDC





a. 100% Na_2SO_4



b. Na_2SO_4 - 50m% CoSO_4

Figure 46. Deposits of 100% Na_2SO_4 and Na_2SO_4 - 50m% CoSO_4 exposed 20 hours at 70°C with $p_{\text{SO}_3} = 0.0007$ atm.

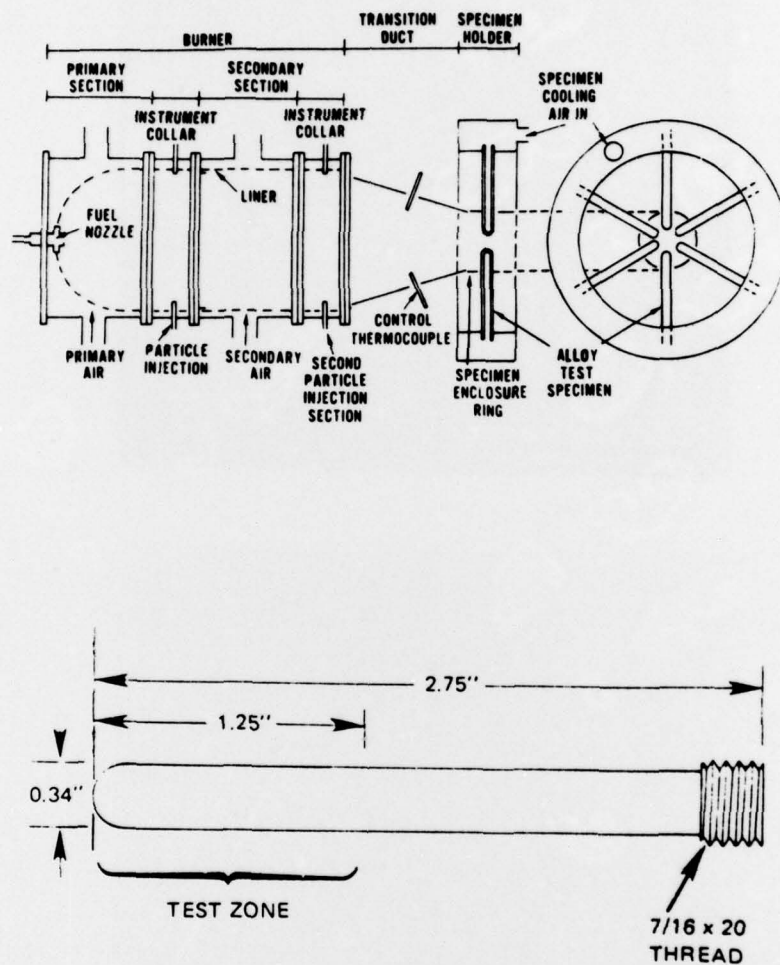


Figure 47. Schematic diagram of ducted burner rig and cylindrical test specimen used for hot corrosion - salt deposition rate dependence tests. (Aqueous salt solution was injected into the primary combustor through hypodermic tubing near the fuel nozzle; provision for particle injection and specimen cooling were not utilized on this program.)

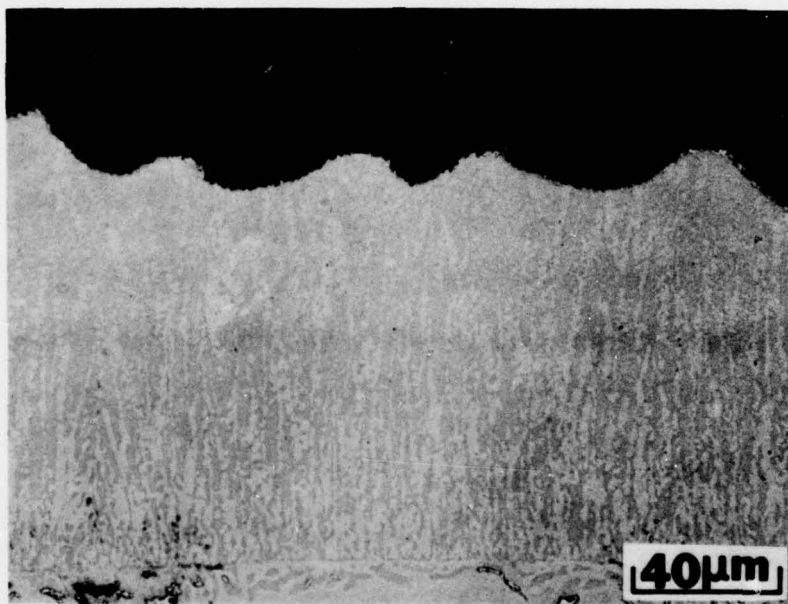


Figure 48. Nodular attack developed in preliminary burner rig test with ASTM sea salt and SO_2 gas mixed with the primary air. Exposure time = 26 hours at 704°C , calculated SO_3 pressure = 5.3×10^{-7} atm.

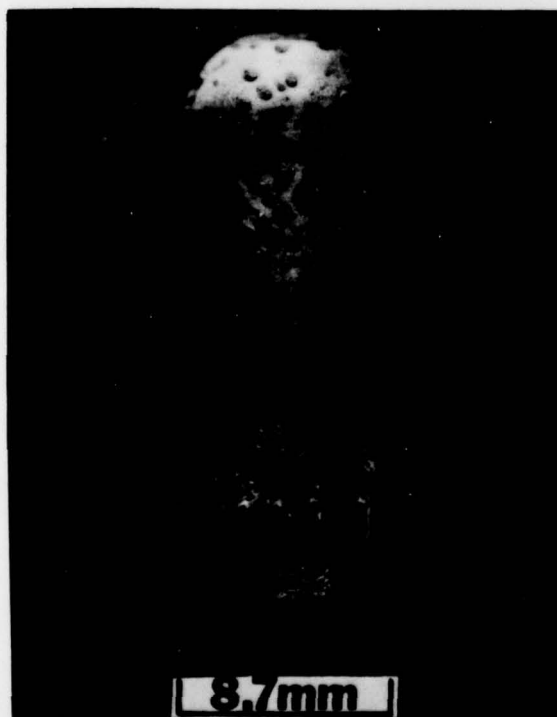
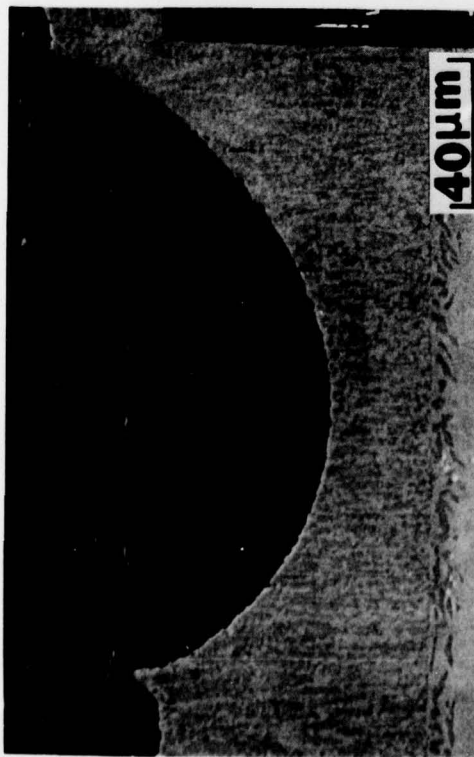
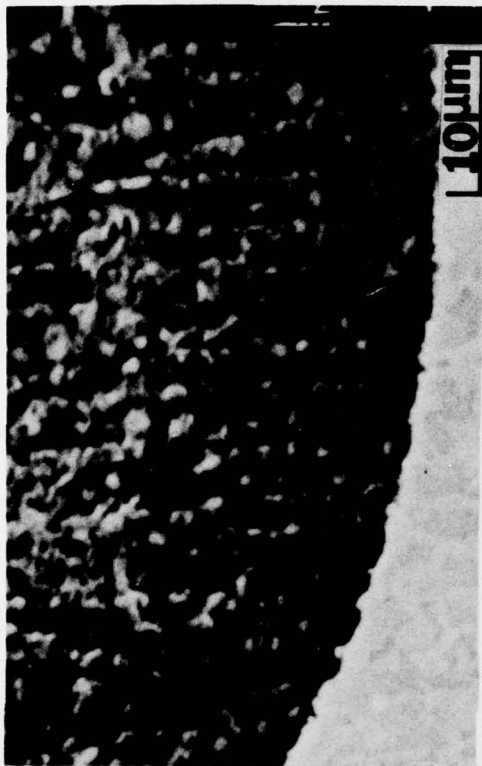


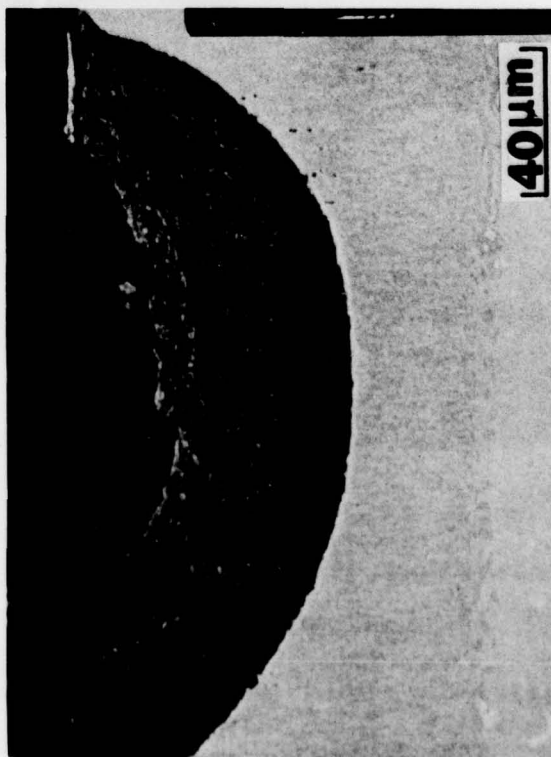
Figure 49. Salt deposit and oxide mounds (inset: pits after removal of mounds) on CoCrAlY specimen exposed 10.5 hours to Na_2SO_4 - 50m% MgSO_4 salt. Calculated SO_3 pressure = 5×10^{-5} atm.



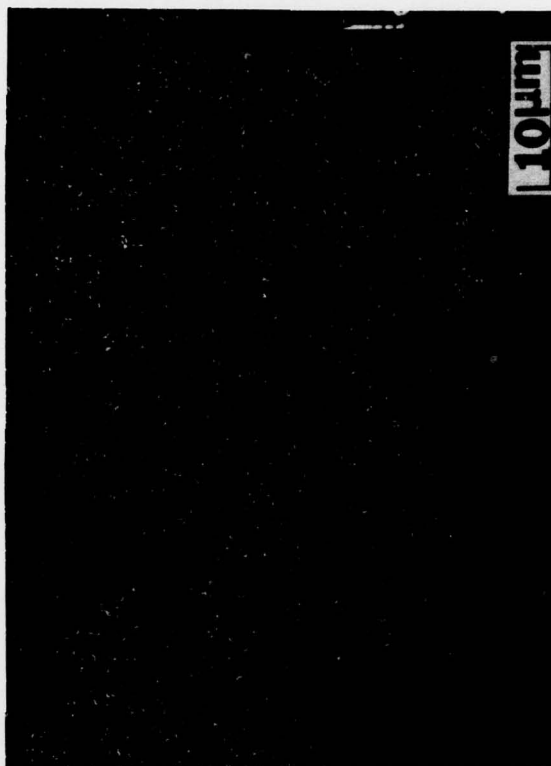
Exposure to show coating microstructure



Ghost image in scale



Exposure to show scale



Sulfur X-rays of above area

Figure 50. Depth and microstructure of pitting attack, as shown by sectioning through the sample of Fig. 49.

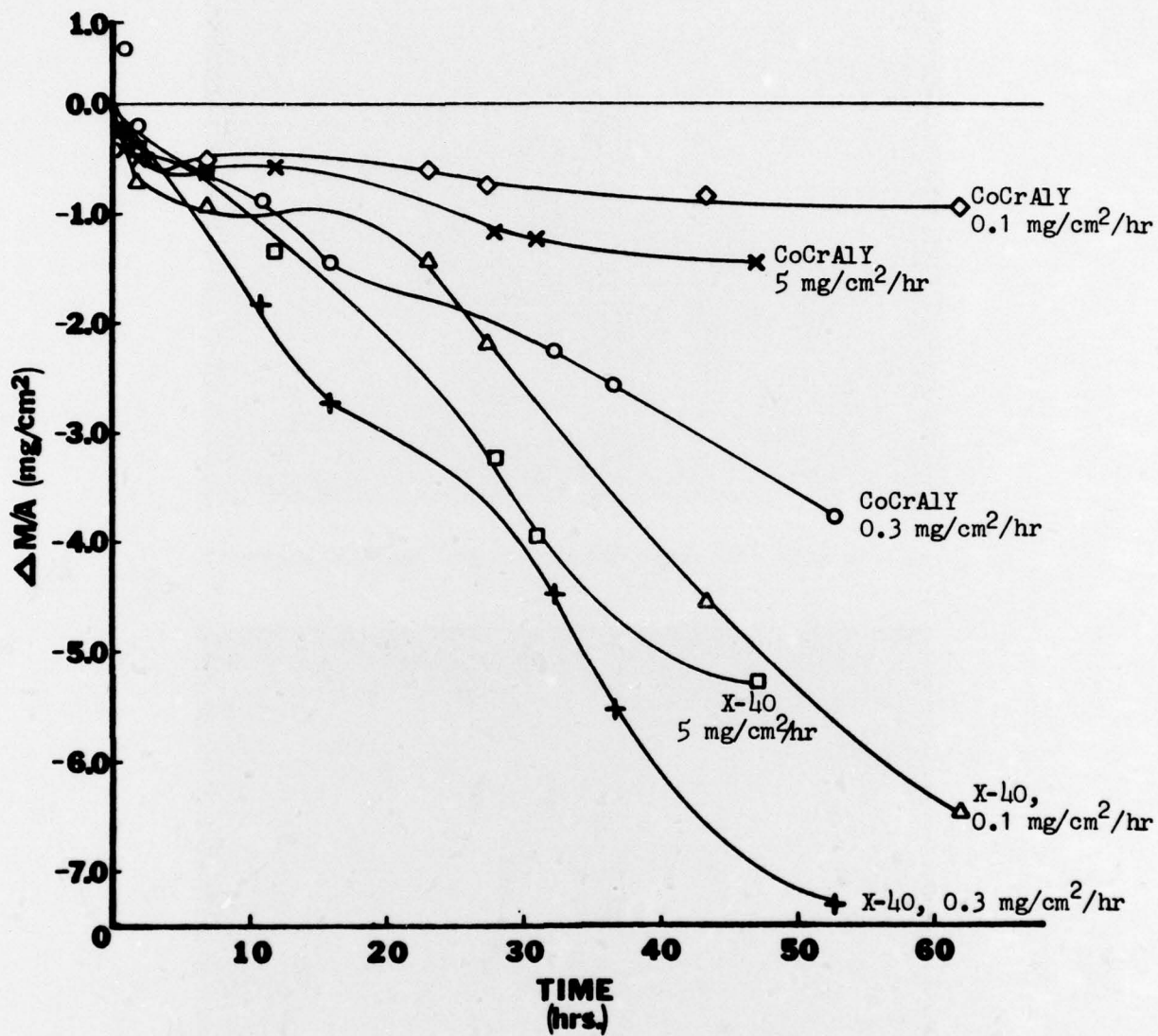
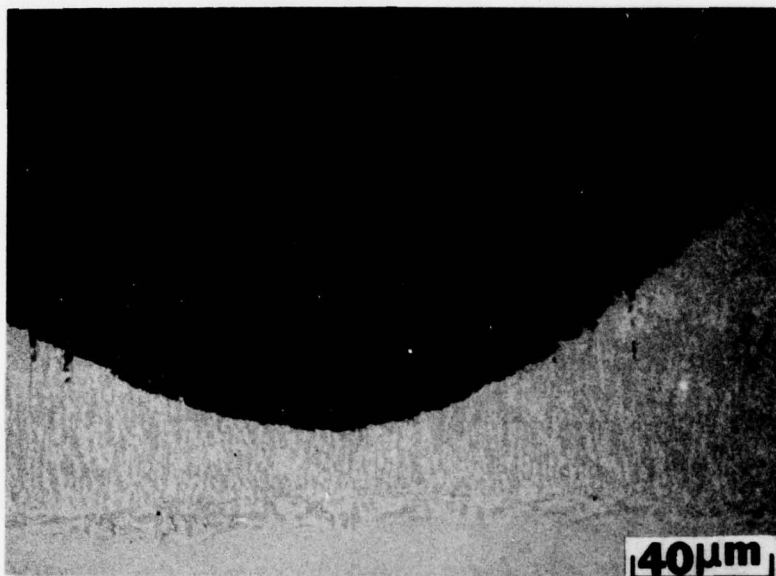
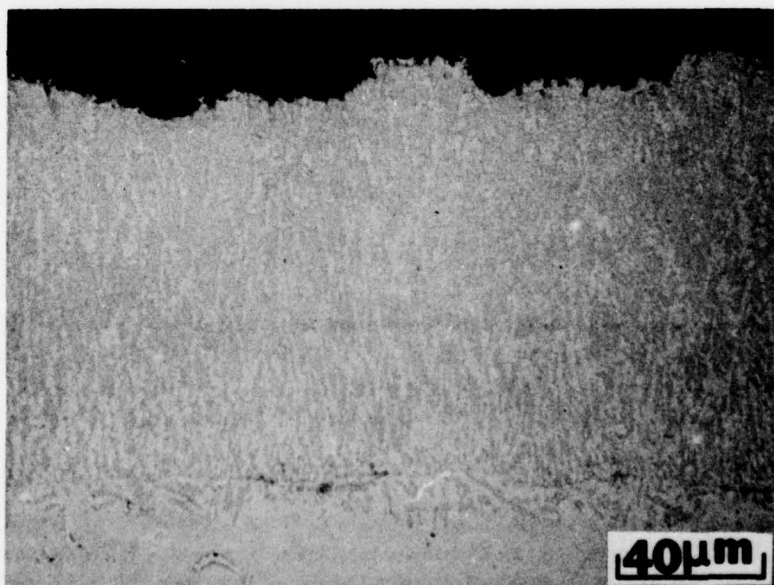


Figure 51. Weight change data showing effect of deposition rate on severity of attack of CoCrAlY coating and uncoated X-40 (concurrently exposed at each deposition rate) in 704C ducted burner rig hot corrosion test with ASTM sea salt and equilibrium SO_3 pressure of 5×10^{-5} atm.

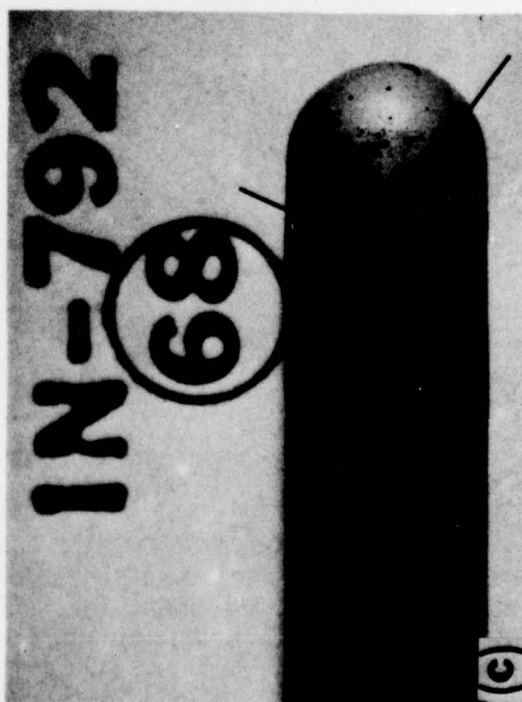


a. Maximum attack at about 70° gas/salt impingement



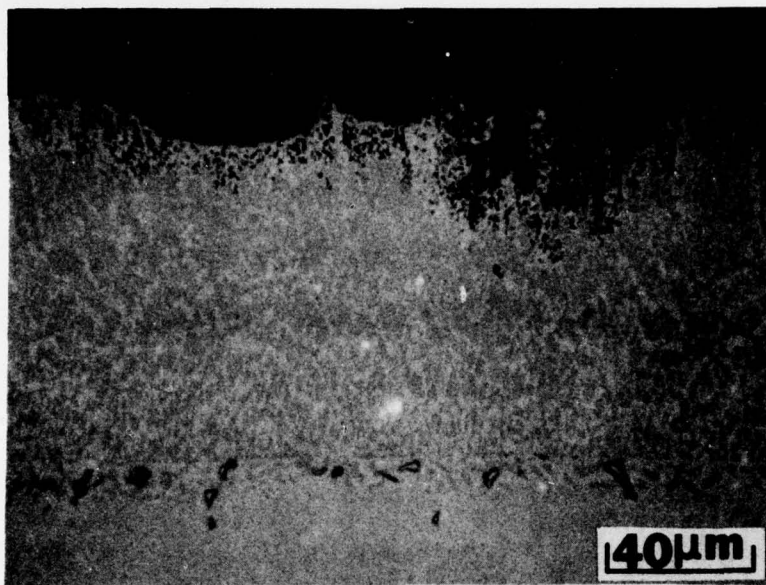
b. Typical structure at approximately 10° impingement

Figure 52. Depth and typical morphology of hot corrosion attack of CoCrAlY coating tested in ducted burner rig with ASTM sea salt and SO_2/SO_3 gas. Total exposure time = 52.7 hours at 704°C; calculated SO_3 pressure = 5×10^{-5} atm; measures salt deposition rate = $0.3 \text{ mg/cm}^2/\text{hr}$.

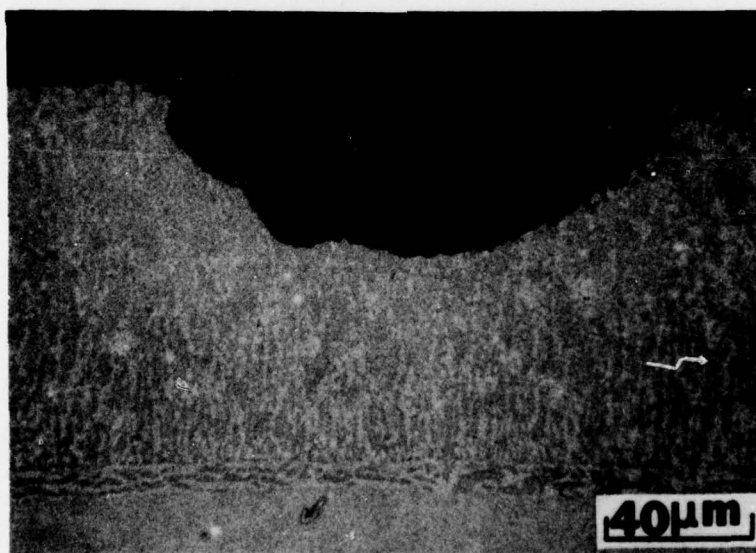


- (a) Surface condition after 28 hours. Arrows mark features visible in (c).
- (b) Salt deposit built up during 19-hour overnight run after taking photo (a).
- (c) Surface condition after 47 hours; i.e. after washing off the salt shown in (b). Arrows point to same features as in (a).

Figure 53. Surface condition of washed CoCrAlY specimen and salt deposit formed in 19-hour exposure at $5 \text{ mg/cm}^2/\text{hr}$ deposition rate.

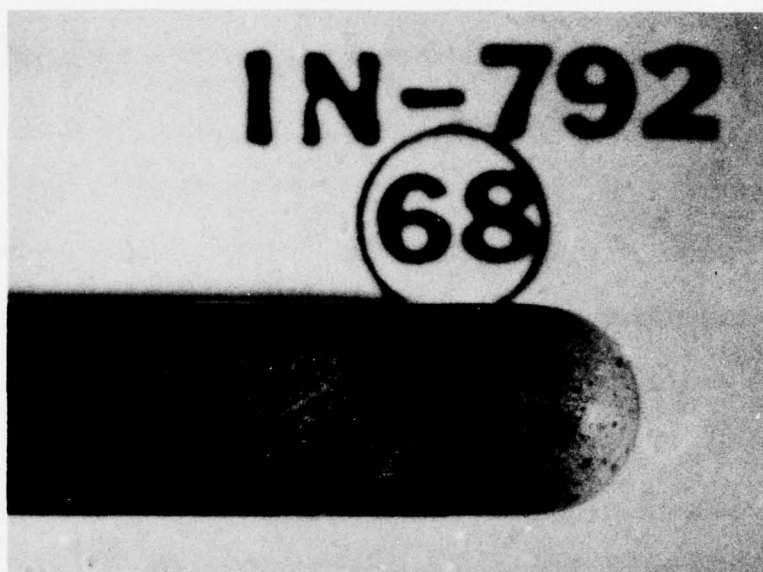


a. Chloride-type morphology near tip of specimen

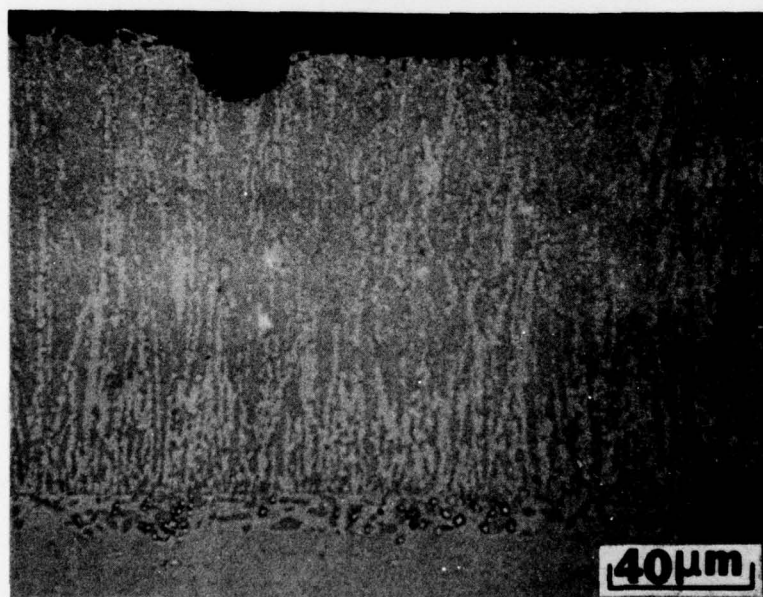


b. Nodular attack near center of hot zone

Figure 54. Hot corrosion of CoCrAlY coating exposed 47.1 hours in ducted burner rig; environmental conditions were as described in Fig. 52 except for salt deposition rate of $5 \text{ mg/cm}^2/\text{hr}$. Extensive chloride-induced dealloying and internal oxidation as in top photo was not common; typical degradation microstructure was SO_3 -type nodular attack.



a. Surface condition



b. Depth of attack

Figure 55. Hot corrosion of CoCrAlY coating exposed 61.1 hours in ducted burner rig; environmental conditions were the same as for the specimens of Figs 52 - 54 except for salt deposition rate of less than $0.1 \text{ mg/cm}^2/\text{hour}$.

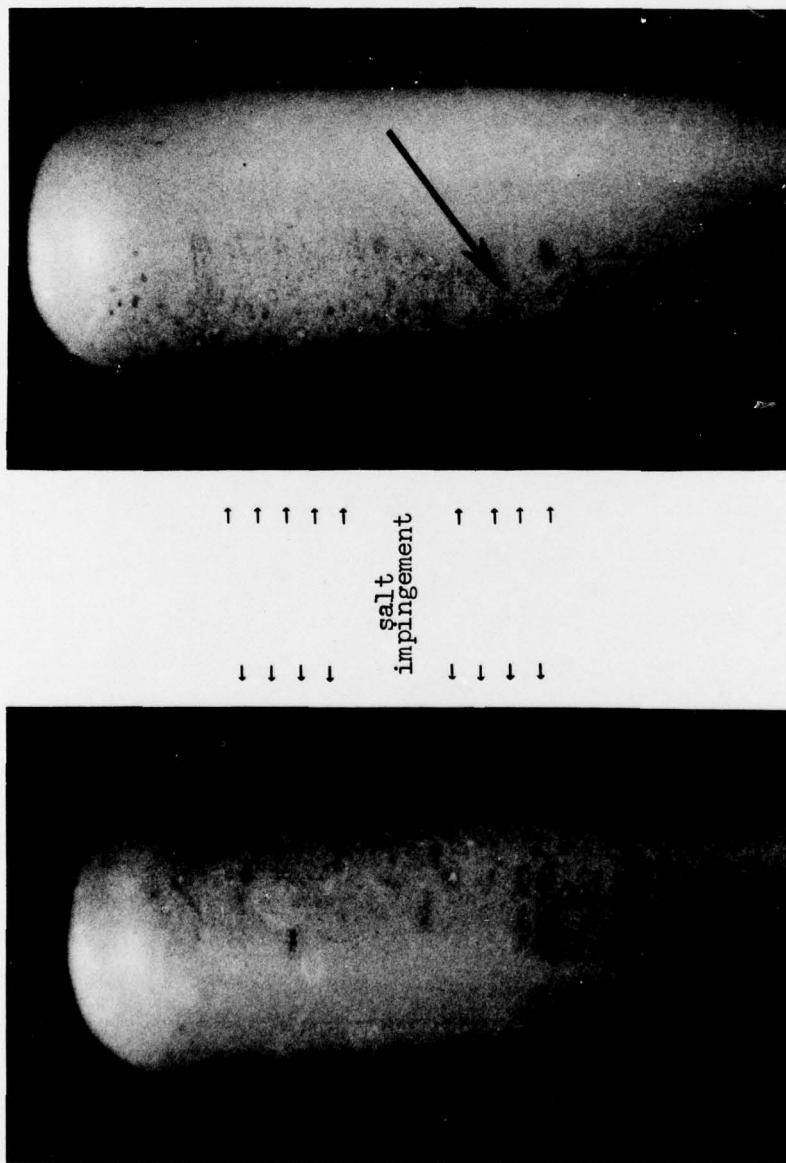


Figure 56. Surface condition of CoCrAlY-coated specimen exposed 6 hours to salt flux of $4 \text{ mg/cm}^2/\text{hour}$. Photos are opposite sides of same specimen, oriented to show difference between leading and trailing edges.

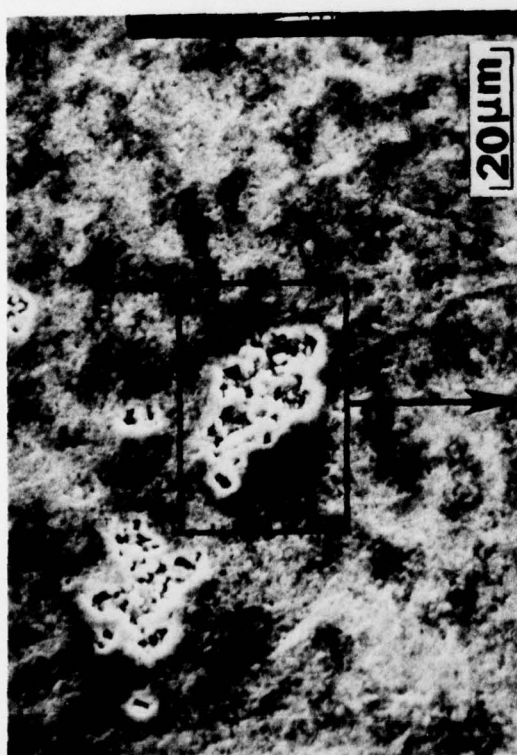
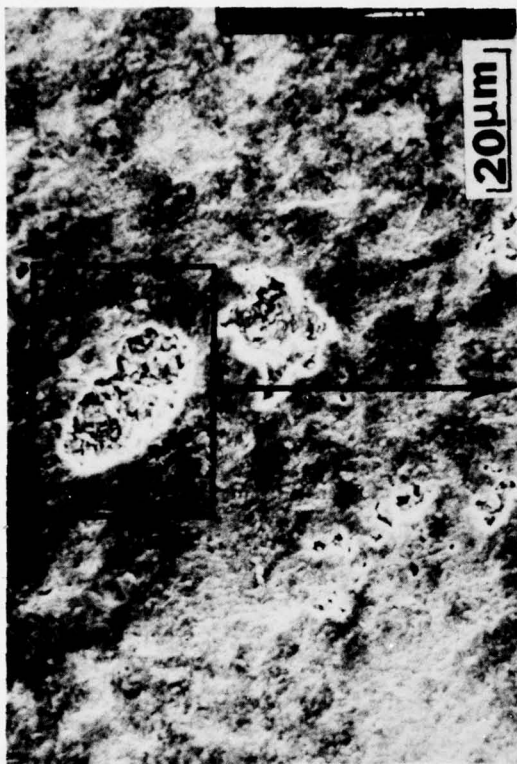
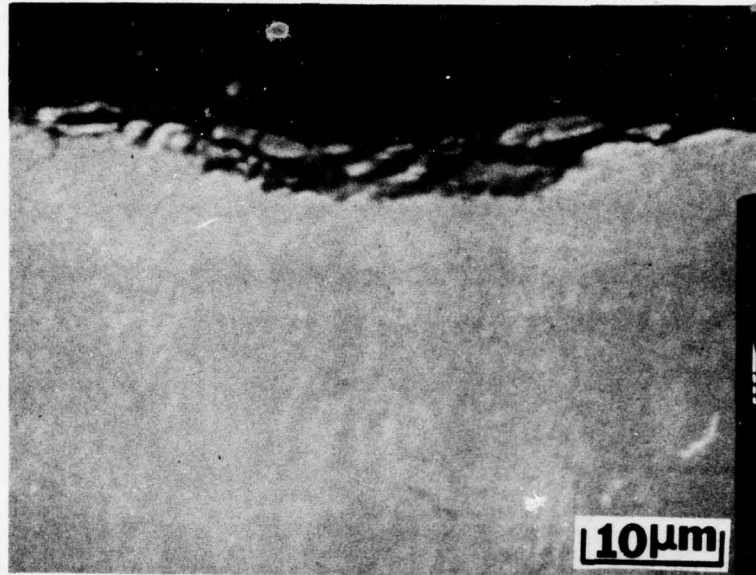
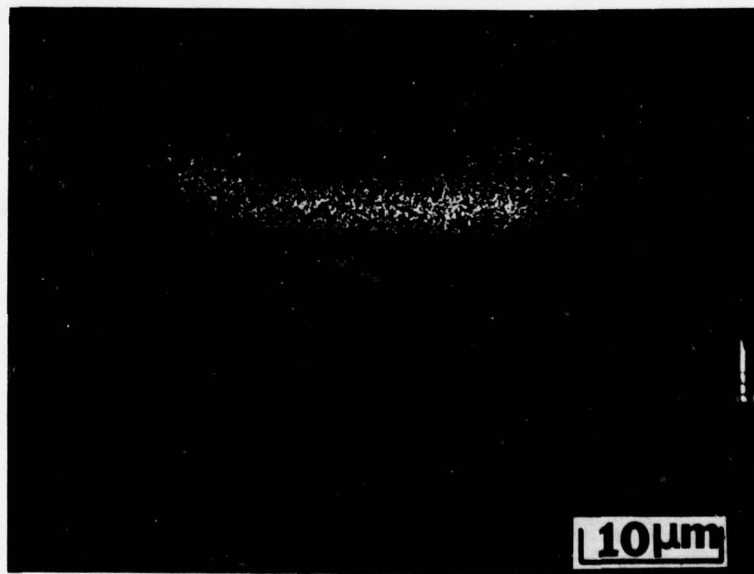


Figure 57. Surface features observed on the leading edge of the specimen described in Fig. 56.

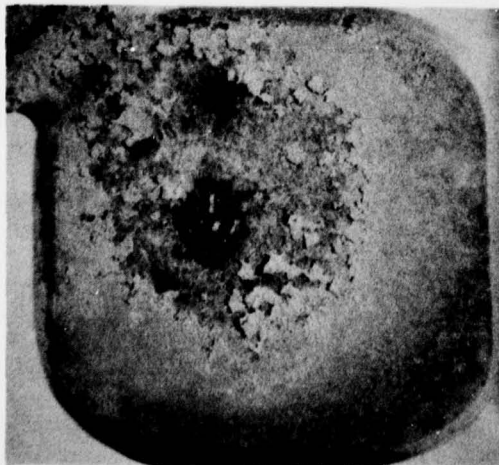


a. Back scattered electron image



b. Sulfur X-rays from above area

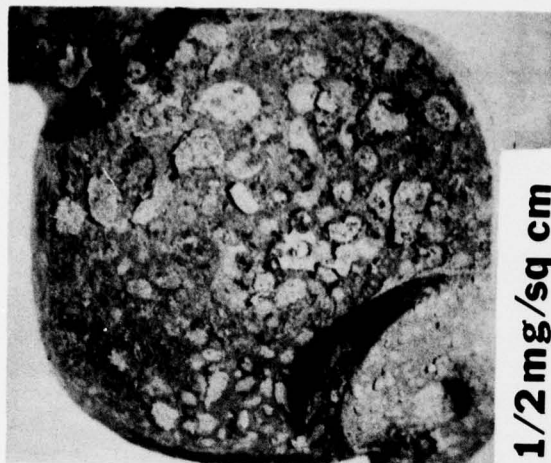
Figure 58. Metallographic cross section presumably through a small pit of the type shown in Fig. 57.



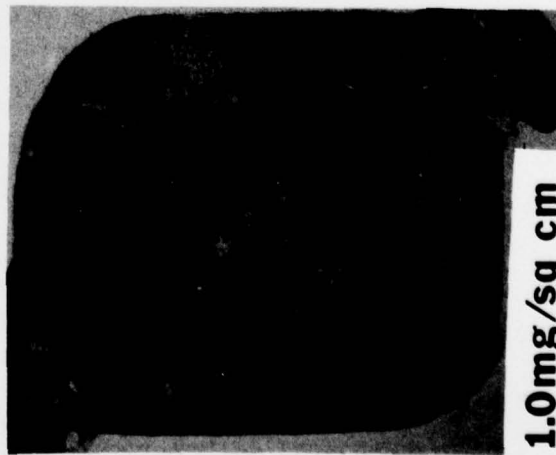
1/8mg/sq cm



1/4mg/sq cm



1/2mg/sq cm



1.0mg/sq cm

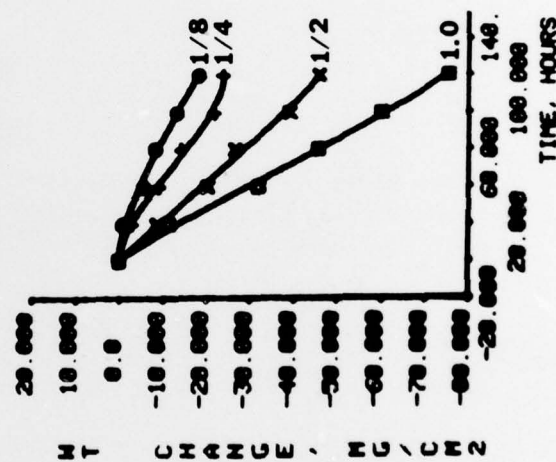


Figure 59. Surface photographs of CoCrAlY-coated coupons with various deposit thicknesses after 20 hours exposure in tube furnace at 704C and $\text{P}_{\text{SO}_3} = 0.0007$ atm; weight change data versus deposit thickness for 100-hour cyclic test.

REFERENCES

1. T. R. Shaw and R. M. Lutje-Schipholt: The Royal Navy's Experience of Blade Corrosion during Engine Tests of Marine Gas Turbines. Proceedings of the 1974 Gas Turbine Materials in the Marine Environment Conference, MCIC Report 75-27, pp. 31 - 38.
2. R. L. Jones: SEM/EDXA Analysis of an LM2500 Stage 1 HPT Blade after Approximately 3000 Hours at 12,000 hp on the GTS Callaghan. NRL Letter Report 6170-324a:RLJ:blr, 16 April 1976.
3. G. Katz and R. Weiss: FT-4C Engines in GTV Asiafreighter - A Test of Gas Turbine Materials. Proceedings of the 3rd Conference on Gas Turbine Materials in the Marine Environment, University of Bath, UK, 20-23 September 1976, Session I, Paper 2.
4. D. J. Wortman, R. E. Fryxell, and I. I. Bessen: A Theory for Accelerated Turbine Corrosion at Intermediate Temperatures. Ibid., Session V, Paper 2.
5. J. Clelland, A. F. Taylor, and L. Wortley: Materials and Coating Developments in Support of Future Marinised Aero Gas Turbines for the Royal Navy. Proceedings of the 1974 Gas Turbine Materials in the Marine Environment Conference, MCIC Report 75-27, pp. 397 - 428.
6. R. H. Barkalow and F. S. Pettit: Degradation of Coating Alloys in Simulated Marine Environments. Report No. FR-10225, Pratt & Whitney Aircraft, West Palm Beach, FL, 15 June 1978.
7. A. F. Taylor, B. A. Wareham, G. C. Booth, and J. F. G. Conde: Low and High Pressure Rig Evaluation of Materials and Coatings. Proceedings of the 3rd Conference on Gas Turbine Materials in the Marine Environment, University of Bath, 20-23 September 1976, Session III, Paper 3.
8. L. F. Aprigliano: Burner Rig Simulation of Low-Temperature Hot Corrosion. Report MAT-77-68, David W. Taylor Naval Ship Research and Development Center, November 1977.
9. R. L. Clarke: Low Temperature Burner Rig Evaluation of Advanced MCrAlY Coating Systems. Report SME-78-28-54, David W. Taylor Naval Ship Research and Development Center, September 1978.
10. R. L. Jones and S. T. Gadomski: Mixed Sulfate/SO₂ Reactions in Low Power Hot Corrosion. NRL Letter Report 6170-773a:RLJ:blr, 1 November 1977.
11. J. A. Goebel and R. J. Hecht: Metallic Coating Development and Evaluation Program. Quarterly Technical Report No. FR-11258, Pratt & Whitney Aircraft, West Palm Beach, FL, 9 February 1979.